SAPIENZA
UNIVERSITÀ DI ROMA

Turbulent dispersion in the Ocean Surface Boundary Layer

Faculty of Civil and Industrial engineering

Department of Civil, Constructional and Environmental engineering
PhD course in Environmental and Hydraulic engineering

XXXV cycle

PhD Thesis of **Simone Zazzini**

Tutor: Prof. Giovanni Leuzzi

A.A. 2021-2022

To Giulia

Table of Contents

Acknowledgments

I would like to thank my supervisor Prof. Giovanni Leuzzi for his invaluable supervision, support and tutelage during the course of my PhD degree. My gratitude extends to the Faculty of Civil and Industrial Engineering for the funding opportunity to undertake my studies at the Department of Civil, Constructional and Environmental Engineering, University of Rome La Sapienza. Additionally, I would like to express gratitude to Dr. Agnese Pini for her treasured support, which was really influential in shaping my research methods and reviewing my results. I also thank Prof. Eric D'Asaro, Prof. Tobias Kukulka, Prof. Angelique Melet and Dr. Leah Johnson for their mentorship. I would like to thank my friends, colleagues and research team Dr. Livia Grandoni and Dr. Paolo Bello for a cherished time spent together in the department and in social settings. My appreciation also goes out to my family and friends for their encouragement and support all through my studies.

Abstract

The Ocean Surface Boundary Layer is where the atmosphere and the ocean interact and where the main exchanges of energy and matter take place. This layer is of considerable interest from an environmental point of view, as it is the area richest in flora and fauna, but in pollutants. In particular, among these, the study of the dispersion of plastic fragments with dimensions smaller than 5 mm defined as microplastics is crucial. In fact, in recent years, the growing consumption of single-use plastics, the low recycling rate and the improper disposal of waste have resulted in a serious threat to the marine ecosystem and to human health. Moreover, considering that there is a large mismatch between the estimates of the amount of plastic that enters the oceans and the total amount of plastic sampled at sea surface, for this particular pollutant, the study cannot be limited to the surface, but must also be extended to the entire water column.

The study of microplastics dispersion in the mixed layer is tackled by the scientific community with numerical models, laboratory experiments and in situ measurement campaigns. Lagrangian models are very commonly used for this purpose, because they can explicitly take into account the different scales of turbulence and they are very often combined with parametric laws directly related to the travel time of the particles.

The aim of this work is to develop a methodology to deduce the marine turbulence, usable for calculating the dispersion of pollutants in the marine environment; in particular, an innovative parameterization of the vertical turbulent diffusivity have been developed with the aim to consider the sub-grid turbulence occurring in the mixed layer, which is not completely resolved by oceanographic models. This similarity law is based on characteristic scales calculated from meteorological and operational oceanographical models. This parametrization of the vertical turbulence has been implemented in a 3D Lagrangian dispersion model (Wiener3D v6).

The model has been validated by comparison with microplastics sampling data deriving from marine monitoring campaigns.

With this Lagrangian model, long-term simulations have been conducted in a domain comprising the Tyrrhenian Sea. The simulations allowed investigating the role of mean currents, sub-grid turbulence and, along the vertical direction, a rising/settling velocity in the microplastics displacements. Thus, the model allowed the analysis of the vertical distribution of microplastics along the water column as well as of beaches or seafloor zones subjected to accumulation. The results showed that vertical turbulent diffusivity is an essential factor for the vertical dispersion of microplastics within the mixed layer. Finally, it is observed that the settling/rising velocity assumes a key role in determining the accumulation of pollutants on the seafloor or on the surface, respectively.

List of Figures

List of Tables

List of Symbols

α: coefficient of thermal expansion

a: turbulent quantity

$\bar{a}$: turbulent quantity first moment

a': turbulent quantity fluctuation

a_E: parameter (E20)

a_V: parameter (V97)

β: saline contraction coefficient

β_*: wave age

β_K: parameter (OSMOSIS)

β_ρ: parameter (D21)

β_σ: coefficient

β_T: experimental coefficient

b: buoyancy

b_E: parameter (E20)

b_V: parameter (V97)

B_0: surface buoyancy flux

B_1: constant

γ: coefficient (ZPL)

γ_σ: coefficient

c: pollutant (MP) concentration

c_b: MP concentration background value

C_ε, $C_{1\varepsilon}$, $C_{2\varepsilon}$, $C_{3\varepsilon}$: constants

C_e, C_{w_*},C_μ^0: empirical coefficients (ePBL)

C_K: constant

c_p: characteristic phase speed of the surface waves

C_{S1}, C_{S2}: constants

C_v: specific heat

C_S: plastic surface concentration

CF: correction factor (E20)

$cmed$: average microplastic concentration in the mixed layer

δ_{i3}: Kronecker delta

D: molecular diffusivity

$d\mu_j$: random increment with zero mean

$\bar{\varepsilon}$: Turbulent Kinetic Energy dissipation rate

ε_{ijk}: Ricci tensor

$\bar{E}$: Turbulent Kinetic Energy

E_1, E_2: constants

f: Coriolis parameter

g: gravity acceleration

$g_{i,j}$: continuous function

G: Turbulent Kinetic Energy buoyancy production

η: constant (ePBL)

θ: Langmuir circulation enhancement factor

Θ: potential temperature

h_i: continuous function

H: depth of the mixed layer

H_{ml} is the well-mixed layer thickness

H_s: significant wave height

i: turbulence intensity

κ: von Karman constant

k_T: thermal diffusivity coefficient

k_S: diffusivity coefficient for salinity

K^U: turbulent diffusivity, for momentum

K^S: turbulent diffusivity, for salinity

K_z^{surf}: near-surface vertical turbulent diffusivity

K^T: turbulent diffusivity, for temperature

K_{ric}^T: thermal vertical turbulent diffusivity critical value

K_b^T: thermal vertical turbulent diffusivity background value

K_B: vertical turbulent diffusivity background value

K: turbulent diffusivity, for particle mass (scalar)

l: mixing length

l_b: bottom length scale

l_ε: dissipation length scale

L: turbulent length scale

L_E: Eulerian length scale

L_L: Langmuir turbulence length scale

L_Z: distance from the wall

La_t: Langmuir turbulent number

μ: average value of the vertical velocity variance

m: parameter (P&P81)

m_*: mixing coefficient due to the turbulent phenomena generated by the wind action on the sea surface

M_e: potential energy change

ν: kinematic viscosity

ν_*: velocity scale in stable conditions

n: parameter (P&P81)

n_*: buoyancy coefficient

N: Brunt-Vaisala frequency

N^2: production of thermal TKE

Π: probability density function

p: pression

P: Turbulent Kinetic Energy shear production

P_{rt}: Prandtl number

ρ: fluid density

ρ_0: average seawater density

ρ_P: particle density

ρ_L: Lagrangian correlation coefficient

r: radius of the particle

R_{ij}: correlation function

R_L: Lagrangian correlation function

Ri: Richardson number

σ_w^2: vertical velocity variance

σ_G: standard deviation of the Gauss distribution

σ_R: standard deviation of the Rayleigh distribution

s: constant (SWB)

s_i is a stochastic process

S: salinity

S_0: average seawater salinity

S_G: normalized standard deviation of the Gauss distribution

S_l: constant

S_R: normalized standard deviation of the Rayleigh distribution

S^2: production of mechanical TKE

τ: shear stress

τ_P: Stokes time

T: temperature

T_E: Eulerian integral time scale

T_L: Lagrangian integral time scale

t_s: time step

T_0: average seawater temperature

u, v, w: velocity field components

u_{s0}: Stokes drift

u_*: friction velocity

u_{*a}: friction velocity of air

U: turbulent velocity scale

w_b: rise velocity of plastic pieces

w_e: entrainment velocity

$w_{r,s}$: rising/settling velocity

w_{*C}: convective velocity scale

w_{*L}: Langmuir turbulence velocity scale

W: Lagrangian velocity

ϕ: stability function of the Monin–Obukhov boundary layer theory

X, Y: Lagrangian displacement in the horizontal direction

z_0: roughness scale of turbulence

Z: Lagrangian displacement in the vertical direction

ω: turbulence frequency

ω_*: velocity scale in unstable conditions

Ω: components of the Earth's angular velocity in a local coordinate reference

Selected publications and presentations

Zazzini S., M. De Dominicis, G. Leuzzi, R. O'Hara Murray, X. Li and A. Pini, Tidal resource and environmental effects of energy extraction in the Pentland Firth: sensitivity to array layouts and turbulence changes, proceedings of 13th EWTEC 2019, Napoli, Italy, September 2-6, 2019

Zazzini S., M. De Dominicis, A. Pini, G. Leuzzi, P. Monti, R. O'Hara Murray and X. Li, Turbulence changes due to a tidal stream turbine operation in the Pentland Firth (Scotland, UK), 2019, proceedings of IMEKO TC-19 International Workshop on Metrology for the Sea, Genova, Italy, October 3-5, 2019

Pini A., P. Tomassetti, M. Matiddi, G. A. de Lucia, P. Bello, **S. Zazzini**, G. Leuzzi and P. Monti, Microplastic detection and Lagrangian modelling in the Tyrrhenian Sea, 2019, proceedings of IMEKO TC-19 International Workshop on Metrology for the Sea, Genova, Italy, October 3-5, 2019

D'Amico A., Pini A., **Zazzini S.**, D'Alessandro D., Leuzzi G. and Currà E., Modelling VOC Emissions from Building Materials for Healthy Building Design. Sustainability, 2021, 13, 184

Zazzini S., A. Pini, G. Leuzzi, and P. Monti, Stima dei flussi turbolenti nello strato limite superficiale marino, 2020, proceedings of XXXVII Convegno Nazionale di Idraulica e Costruzioni Idrauliche, online

Pini A., **S. Zazzini**, G. Leuzzi, and P. Monti, Modellazione numerica della dispersione di microplastiche nel mar Mediterraneo occidentale, 2020, proceedings of XXXVII Convegno Nazionale di Idraulica e Costruzioni Idrauliche, online

Pini A., **S. Zazzini**, P. Bello, P. Monti and G. Leuzzi, Modellazione numerica della dispersione di microplastiche sulla colonna d'acqua, 2022, proceedings of XXXVIII Convegno Nazionale di Idraulica e Costruzioni Idrauliche, Reggio Calabria, Italy, September 4-7, 2022

Zazzini S., A. Pini, P. Bello, P. Monti and G. Leuzzi, Studio della dispersione verticale di microplastiche in ambiente marino, 2022, proceedings of XXXVIII Convegno Nazionale di Idraulica e Costruzioni Idrauliche, Reggio Calabria, Italy, September 4-7, 2022

Pini A., **S. Zazzini**, P. Bello, P. Monti and G. Leuzzi, Numerical investigation of microplastic dispersion in the water column, 2022, proceedings of 2022 IEEE International workshop on Metrology for the Sea, Milazzo (ME), Italy, October 5-7, 2022

Bello P., A. Pini, **S. Zazzini**, , P. Monti and G. Leuzzi, Discrete multivariate probability distributions of microplastic settling/rising velocity in the marine environment, 2022, proceedings of 2022 IEEE International workshop on Metrology for the Sea, Milazzo (ME), Italy, October 5-7, 2022

1. Introduction

Oceans are the world largest ecosystem and they have a significant role in the regulation of global climate; humans are interested in studying their physical, chemical and biological characteristics in order to exploit their economic potential.

Even though a lot of effort have been put into it, there are still many unknowns about the marine environment. For example, oceans exhibit a huge range of turbulent motions, spanning scales from millimetres to several kilometres (van Sebille et al. 2018) and these turbulent structures are still under investigation.

Nowadays oceans are considerably threatened by human pressure and seriously polluted; therefore, in the last decades the study of the turbulent dynamic of the marine currents gained particular attention, with the intention to investigate the 3D transport of pollutant particles in the marine environment.

This environmental problem is currently faced by means of experimental studies both in laboratories and in situ campaigns, as well as by means of physical based models. Ocean Global Circulation Models (OGCMs) are commonly used to resolve the 3D turbulent field of the sea currents and to model the distribution of density, temperature, salinity or passive tracers, such as pollutant particles. The main advantage of OGCMs is that they can simulate and make predictions relative to the dispersion of pollutants, with a considerably lower cost compared with experimental campaigns.

On the other hand, OGCMs calculate only the main scales of the turbulent dispersion; often, horizontal eddies have a length scale ranging from meters to thousands of kilometres, while the turbulent motions that occur along the vertical evolve in a layer of the order of one hundred meters or so. They have low resolution representation of the Ocean Surface Boundary Layer (OSBL), in fact, vertical turbulent processes act on much smaller scales than those explicitly resolved in OGCMs, but this is the part of the ocean where most of the flora and fauna and pollutants are concentrated.

Therefore, turbulence in the OSBL has a crucial role in the particle dispersion in the marine environment; in fact, pollutants are dispersed in the upper ocean by mixing processes predominantly forced from the state of the atmosphere directly above it; more in detail, the daily and seasonal cycle of heating and cooling, wind, rain and changes in temperature and humidity associated with mesoscale weather features produce a hierarchy of physical processes that interact to stir the upper ocean (Moum and Smyth 2001).

So, Lagrangian Stochastic Models (LSMs) could be an essential tool to study the 3D particles dispersion, because they can simulate sub-grid turbulence by means of stochastic processes and therefore model turbulence mixing in the OSBL; in addition they have a significant advantage: they use the 3D velocity field calculated by OGCMs and subsequently they model the dispersion of pollutant particles offline, with a lower computational cost. Most of the LSMs are dedicated to the calculation of the dispersion due to accidental oil spills, motivated by the events that have caused the greatest environmental disasters in the marine sector (Liu et al. 2011).

Recently, the exponential increase in plastic consumption, especially single-use plastic, and the consequently plastic pollution of the marine ecosystem have caused an even more relevant global environmental damage. A particular concern is the occurrence of smaller pieces of plastic debris including those not visible to the naked eye, referred to as microplastics (MP).

Everyone has seen photographs of the Great Garbage Patch of plastic accumulating on surface of the world oceans, but there is a large mismatch between the estimates of the amount of

municipal solid plastic waste generated on land that enters the oceans (5–12 million tonnes per year (Jambeck et al. 2015)) and the total amount of plastic sampled at sea surface (less than 0.3 million tonnes (Cózar et al. 2014; Eriksen et al. 2014)); in fact, recent estimates suggest that between 70 and 90% of the MPs particles are accumulated into sediment profiles (Uddin et al. 2021). This highlights that this problem is 3D and this could provide a significant reason for the development of specific models, which can investigate the 3D dispersion of MP.

The aim of this work is to study the 3D turbulent dispersion of MP in the marine environment, with a specific attention to the OSBL. For this purpose, an innovative parameterization of the vertical turbulent diffusivity has been developed and it has been implemented in a LSM specifically devoted to the study of the 3D dispersion of MP, developed by the research group headed by Prof. Giovanni Leuzzi (hereinafter Wiener3D v6).

The domain analysed is a sub-basin of the Mediterranean Sea, i.e. the Tyrrhenian Sea; this is a semi-closed and densely populated basin and it has been estimated that the MP concentration in the Mediterranean Sea is comparable with that of the famous Great Garbage Patches (Zambianchi, Trani, and Falco 2017).

Compared to the state of the art, this model is based on important innovative elements.

Currently, MP sources estimation models do not explicitly consider the correlation between the flow rate of the MP emission sources and the inhabitants of the region (Liubartseva et al. 2018). In this work, on the other hand, a proportionality is assumed between the population that discharges into the basin investigated and the flow rate of the MP sources. The proportionality factor is the average per capita plastic leakage in the Tyrrhenian Sea, which has been provided by Boucher and Billard 2020. In order to have a greater accuracy of the method, for each river source the population living in the corresponding water catchment area have been considered; while for the coastal cities, the load of MP is proportional to the number of inhabitants of the cities their self.

A second innovative aspect introduced by this work is represented by the scheme used to model the turbulence of the MP trajectories. In the model Wiener3D v6, assuming that velocities are uncorrelated in time, the instantaneous velocity of the MP particles is calculated as the sum of the average component (obtainable from operational oceanographic models) and the turbulent fluctuation (calculated with a stochastic process), both in the horizontal and in the vertical plane. This approach is commonly known as zeroth-order Markov process (Monti and Leuzzi 2010). In the stochastic process, the vertical turbulent diffusivity has been parameterized, because the measure of this parameter is extremely complicated along the water column. This has been derived with an innovative scheme evaluating other turbulent quantities: the vertical velocity variance and the mixing length. In this work, they are calculated by means of similarity laws based on operational oceanographic or meteorological data, such as the friction velocity and the mixed layer depth. The main advantage of this parameterization is that it is based on the vertical velocity variance and the Lagrangian time scale, which are Lagrangian quantities.

The LSM has been validated comparing the simulated MP concentrations profiles with field data. Considering that in the Mediterranean Sea only MP surface concentration have been sampled, the comparison has been carried out with MP concentration profiles obtained during campaigns in the world oceans.

Furthermore, the comparison with these experimental data gives the opportunity to develop a similarity law, which describe the MP vertical distribution. It allows an estimation of the MP profile by means of the average concentration on the mixed layer and the mixed layer depth. In case of lack of experimental data, this could be a useful tool for the study of the turbulent dispersion of MP in the marine environment, in particular within the water column.

This work is organised in three main parts: in the Background chapter, the theoretical background behind the 3D dispersion of MP in the marine environment will be presented. In particular, an overview on the marine environment, the statistical behaviour of marine turbulence and the state of the art of its parameterizations implemented in OGCMs and LSMs will be introduced. Furthermore, a brief overview of the MP pollution of the marine environment as well as the features of the models currently used to describe that will be presented. The Materials and Methods chapter is devoted to the conceptual scheme of the 3D dispersion of MP in the marine environment and all the information about the domain, the input and output data, as well as the equations that govern the dispersion in the 3D LSM will be introduced; in addition, in this chapter the original parameterization of the vertical turbulent diffusivity will be presented. Finally the Results chapter is dedicated to the main results of the 3D dispersion of MP in the Tyrrhenian Sea presenting MP concentration maps and profiles, with a particular attention to the comparison of the simulated MP concentration with experimental data, with the intention to validate the 3D LSM Wiener 3D v6.

2. Background

In this chapter, the theoretical background behind the 3D dispersion of MP in the marine environment will be presented. In particular, an overview on the marine environment, on the statistical behaviour of the marine turbulence and its parameterizations in OGCMs and LSMs will be introduced; furthermore, a brief review about MP pollution of the marine environment as well as the features of the models currently used to describe that will be presented.

2.1 Marine environment

70% of the Earth surface is covered by water. Oceans are home of 94% of all life on Earth, they are the world's largest living ecosystem. In addition, oceans and seas feed world population, support industry, regulate Earth climate and generate most of the oxygen human breathe. So, human economics and survival depend on it (Mendler de Suarez et al. 2014).

But, nowadays the human exploitation have exposed the marine environment to degradation, pollution and alteration even of the pristine areas; the marine complex ecosystem, has been seriously damaged (Mendler de Suarez et al. 2014).

Oceans are vulnerable, thus, in the environmental research framework, the study of the pollution of the marine environment should be a critical topic for researchers, with the purpose to assess how the various physical and biogeochemical processes have been altered, its relation with climate changes, how flora and fauna interact with pollutants, how these particles disperse and accumulate in this environment; the objective of these researches should be elaborating a strategy to remediate and to prevent further damages.

This specific work is focused on the study of the 3D dispersion of MP in the marine environment.

2.1.1 Global circulation and sea currents

The ocean circulation is largely studied; the movements of the water masses occur over a wide range of spatial and temporal scales, for example, horizontal currents range from large scale to mesoscale, whereas vertical structures could be less than one meter. But, sea currents are partially unpredictable because of turbulent and chaotic motions.

Oceanic currents characteristics depends on the interaction with the atmosphere; in fact, winds, rainfall, evaporation, heat exchange, seasonal and day-night cycles are held responsible for the global circulation, the stratification of the water column, as well as the formation of eddies and other turbulent structures.

Globally, ocean circulation could be distinguished in two types:

- wind-driven circulation forced by wind stress on the sea surface, inducing a momentum exchange;
- thermohaline circulation driven by the variations in water density imposed at the sea surface by exchange of ocean heat and water with the atmosphere, inducing a buoyancy exchange.

These two circulation types are not fully independent.

Wind stress induces a circulation pattern that is similar for each ocean, with specific characteristics at different latitudes.

At the Equator, the currents are mostly directed toward west (Lumpkin and Johnson 2013).

Subtropical gyres extend from the equatorial current system to 50° of latitude; they are anticyclonic structures and the Ekman transport within these gyres forces surface water to sink. Western boundary currents of these gyres, like the Gulf Stream, are narrow geographically, they are fast, about 100 km per day (Schmitz and McCartney 1993), they also have very large transport and a very sharp boundary; in this waters, geostrophic- and eddy-driven upwelling drive increased primary productivity (Todd et al. 2019). On the other hand, eastern boundary currents of these gyres are wide geographically, they are slow, about 10 km per day, they have small transport and a very diffuse boundary not very well defined (Carr 2001); the eastern boundary currents cause a lot of coastal upwelling, so they are very productive (Carr 2001).

Among the western boundary currents, the Kuroshio of the North Pacific is perhaps the most like the Gulf Stream, having a similar transport and array of eddies. The Brazil Current and the East Australian Current are relatively weaker. The Agulhas Current, which flows in the south Indian Ocean, has a transport close to that of the Gulf Stream (Lutjeharms 2007). Their respective eastern boundary currents are the Canary Current, the California Current, the Benguela Current, the Peru Current and the west Australian Current. These currents are represented in Fig. (1).

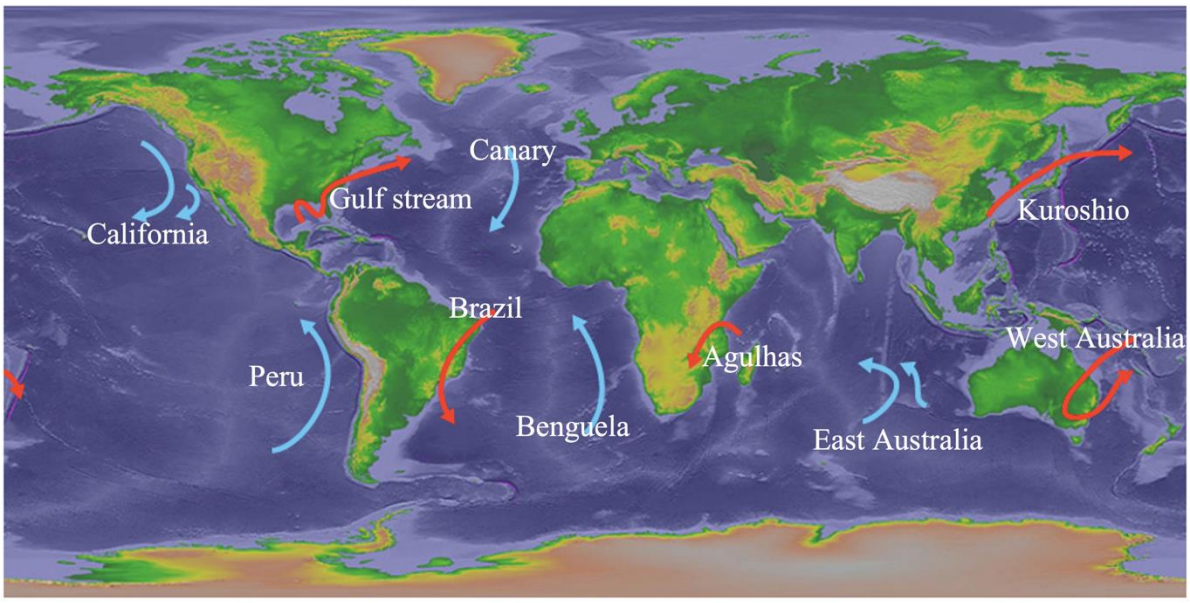

Figure 1. Western and eastern boundary currents of the sub-tropical gyres in global oceans. Source: weather.gov/jetstream/currents_max.

The subpolar gyres extend poleward from the region of the westerlies and they have a cyclonic circulation; so, the Ekman transport within these features forces upwelling and surface water divergence (Koszalka and Stramma 2019).

On the other hand, the thermohaline circulation is largely driven by water density gradients, and thus its temperature and salinity. It acts on the ocean as a whole and has a major influence on the abyssal properties, where wind-driven circulation has no effect. This large-scale circulation is relatively stable on long timescales (Wunsch 2002). At some very specific locations, mainly in the Northern Atlantic and around Antarctica, surface waters become denser and sink. Surface waters are then pulled up to replace the sinking ones. The density increasing of the sea water occurs due to both cooling surface waters and increasing salinity, the latter as a result of the removal of freshwater and the formation of ice (Wunsch 2002).

Moreover, water masses could experience tides because of the interaction of Earth, sun and moon. Tidal currents occur in conjunction with the rise and fall of the tide. The vertical motion

of the tides near the shore causes the water to move horizontally, creating currents, which modify local circulation, particularly in funnel-shaped bays which can dramatically alter tidal current magnitude (Yang, Wang, and Copping 2013).

Finally, it worth mentioning the submesoscale currents, which occur on lateral scales of 100 m–10 km in the ocean and are associated with density fronts and filaments, vortices and topographic wakes at the surface and in the ocean's interior. Recent studies have revealed that horizontal density differences on scales of 0.1–10 km are ubiquitous in the surface mixed layer and play an essential role in its evolution (Chrysagi et al. 2021). In most cases, submesoscale processes do not directly contribute to mixing, however they have an important role in cascading energy and tracer variance from the largely adiabatic mesoscale down to the scales at which diapycnal mixing can occur (Gula et al. 2022). Submesoscale currents re-distribute water properties, including buoyancy, momentum, heat, freshwater, and biogeochemical tracers (Poje et al. 2014).

2.1.2 The Ocean Surface Boundary Layer

The water column, in synthesis, could be described citing Victor Hugo: '*water! Pretending to be pure, thou false friends! Thou art warm at the top and cold at the bottom*'. So, examining the vertical profile of the temperature, see Fig. (2), it has its maximum value on the top, and then below the sea surface it decreases slowly until a strong gradient occurs.

In fact, it has been observed that the first layer of the water column is characterized by an almost homogeneous trend of temperature, salinity and, therefore, density due to the effective mixing action; for this reason it takes the name of mixed layer.

Furthermore, below the mixed layer, there is a layer, which extends up to about 500 m, established by strong vertical gradients of temperature and/or salinity. It is called thermocline if it is considered the gradient of temperature, halocline for salinity or pycnocline for density.

This layer separates efficiently the OSBL from the deep ocean. In fact, below about 500 m, the temperature decreases slightly until it reaches low values, while the density increases.

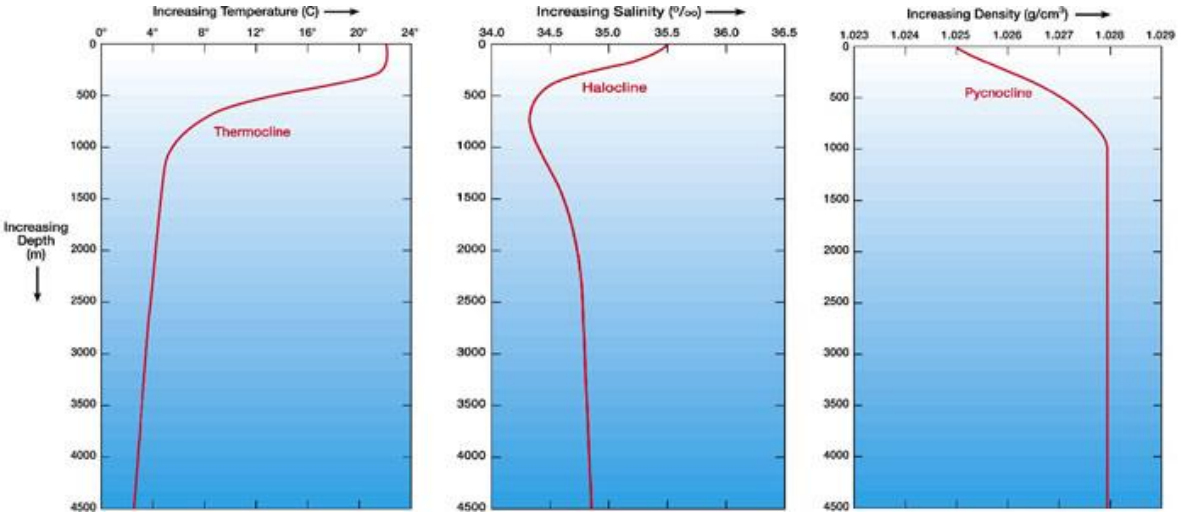

Figure 2. Typical water properties in the open ocean. Source: hurricanescience.org/science/basic/water.

It is worth to notice that the first tens of meters of the water column have a significant role in the regulation of the global climate; in addition, they worth a particular attention in the framework of the dispersion of pollutants in the marine environment; in fact, in this layer of

the ocean, there are high light levels, so it's populated by most of flora and fauna species living in the oceans, as well as nowadays by pollutants.

Oceanographers use loosely this term to describe the region of the ocean that responds most directly to surface processes. Late in the day or following periods of strong heating from the atmosphere, the mixed layer may be quite shallow, a few meters or less. During the cold season or following series of strong winds and storms, the mixed layer may extend vertically to hundreds of meters, marking the depth of the seasonal thermo-cline at midlatitudes (Moum and Smyth 2001).

Thus, the OSBL could be considered a quasi-homogeneous region in the upper ocean where there is little variation in temperature or density with depth (Kara, Rochford, and Hurlburt 2000). In addition, in situ data have been clearly revealed the presence of approximately uniform vertical regions of temperature, salinity and, therefore, density starting at the ocean surfaces (Moum and Smyth 2001).

For this particular reason, the mixed layer depth is defined as the water column depth where the density increases at least by 0.01 kg/m^3 (de Boyer Montégut et al. 2004).

The vertical uniformity of the OSBL owes its existence to turbulent mixing generated from the energy input by the action of wind stress and heat fluxes at the ocean surface.

In fact, pollutants are dispersed in the upper ocean by mixing processes predominantly forced from the state of the atmosphere directly above it, see Fig. (3). In brief, turbulence in the OSBL is produced either by the mean shear (loss of mean-flow kinetic energy) or by unstable stratification (loss of potential energy) (Burchard et al. 2008). More in detail, the daily and seasonal cycle of heating and cooling, wind, rain and changes in temperature and humidity associated with mesoscale weather features produce a hierarchy of physical processes that interact to stir the upper ocean (Moum and Smyth 2001).

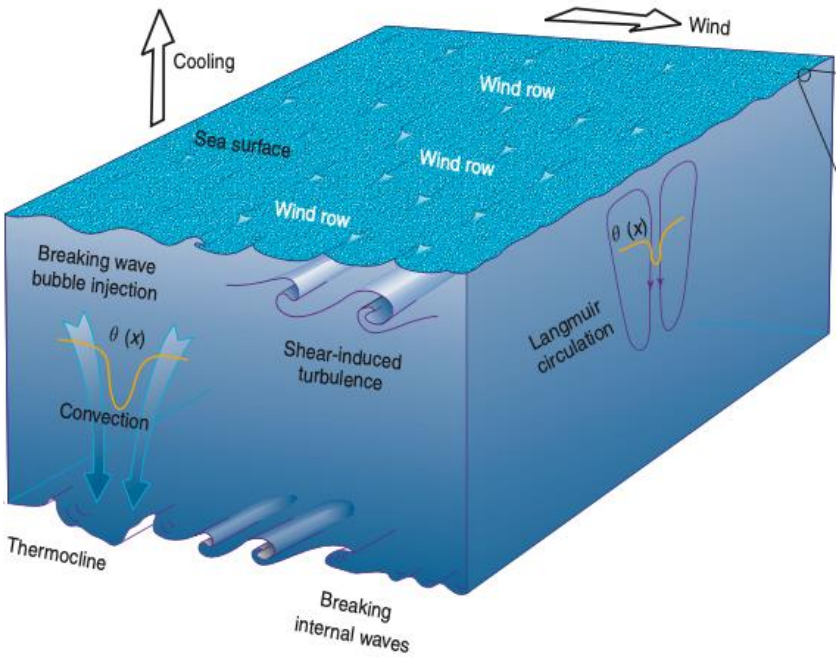

Figure 3. Turbulent processes that contribute to mixing the upper ocean in association with surface cooling and winds. Source: Moum and Smyth 2001.

Winds produce a surface stress and a sheared current profile; this profile, if the sea surface was solid, could be described with a classic wall-layer law, but the ocean's upper boundary is free

to support waves, ranging from centimetre-scale capillary waves to tens of meters in case of swell.

At the sea surface, there is a thin skin layer of a few millimetre thickness that is controlled by molecular viscosity and diffusivity (Burchard et al. 2008). This isolating skin layer is disrupted by breaking surface waves. At low to moderate wind speeds this occurs mainly in form of micro-breaking; while at strong wind speeds, the wave breaking is evidenced at the surface by whitecapping and surface foam; this process disrupts the ocean's cool skin and enhances the injection of bubbles and particles beneath the sea surface (Moum and Smyth 2001).

Winds could provoke also Langmuir circulation (LC); this turbulent process has been parameterized and described for the first time by Craik and Leibovich 1976, then it has been further investigated in many studies, see Belcher et al. 2012, McWilliams, Sullivan, and Moeng 1997, Sullivan and McWilliams 2010. LC is triggered when the Stokes drift interacts with the wind-driven currents and the surface mixed layer is not too deep. LC is constituted by coherent structures within the mixed layer that produce counterrotating vortices with axes aligned parallel to the wind; LC is visible as characteristic surface windrows that are caused by bubble clouds in horizontal.

As mentioned before, turbulence in the OSBL could be generated by mechanical and/or thermal processes; thus, the cooling at the sea surface creates parcels of cool, dense fluid, which later sink to a depth determined by the local stratification in a process known as convection (Moum and Smyth 2001). Cooling occurs almost every night and also sometimes in daytime in association with weather systems such as cold air outbreaks from continental landmasses, every cold season, depending on the latitude and it is enhanced by the formation of ice. Convection may also be caused by an excess of evaporation over precipitation, which increases salinity, and hence density, at the surface; moreover, winds aid convection disrupting the viscous sub-layer and permitting a rapid transfer of heat through the surface. Therefore, convection is a turbulent process which acts to increase the mixed layer depth in particular during night time or cold seasons; on the other hand, when the water column is heated from above, stratification rules.

In addition, it has been found by means of field measurements that submesoscale features can restratify the water column (Boccaletti, Ferrari, and Fox-Kemper 2007) and shallow the depth of the mixed layer. In fact, submesoscale restratification tends to counteract the destratification effect caused by atmospheric forcing, yielding stably stratified patches (Chrysagi et al. 2021).

So, the interaction of all these turbulent processes modify the depth of the OSBL; but, close to the shores its lower boundary is the seabed, on the other hand, offshore, it is a pycnocline established by vertical gradients of temperature and/or salinity.

In case of a pycnocline, internal waves may be generated. So, at the bottom of the OSBL there is a turbulent zone where underwater oscillations with an amplitude from 10 to 100 m (Klemas 2012) are triggered by a disturbance of the interface between water layers of different density.

The turbulent processes mentioned in this paragraph have been widely investigated by means of sampling campaigns and many schemes have been tested to model them (e.g. Kraus and Turner 1967; Large, McWilliams, and Doney 1994; Li et al. 2019; Pacanowski and Philander 1981), a detailed description of the mixing in the OSBL is fundamental for the study of the 3D dispersion of pollutants in the marine environment.

2.2 Marine turbulence

Winds and marine currents are turbulent, nearly all environmental flows are turbulent. As mentioned before, within the Earth's ocean and atmosphere, turbulence sets the mass, momentum and heat transfer rates involved in pollutant dispersion and climate regulation.

Turbulence is a state of the flows, it involves fluctuations that are generally unpredictable and not yet full described by OGCMs. Therefore, it is not easy to define precisely, but since the last century, physical intuition, dimensional arguments, direct numerical simulations, or empirical models and computational schemes have been carried out by researchers and their findings will be briefly reported in the next chapters.

Following Kundu and Cohen 2008, the generic characteristics of turbulence are:

- fluctuations: turbulent flows contain fluctuations of velocity, pressure, temperature and other quantities; they appear to be irregular, chaotic and unpredictable;
- non-linearity: turbulence occurs when the Reynolds number, Re, exceeds a critical value. Once the critical parametric value is exceeded small perturbations can grow spontaneously and may equilibrate as finite amplitude disturbances. However, the new equilibrium state can become unstable to more complicated disturbances, and so on;
- vorticity: turbulence is characterized by fluctuating vorticity. A turbulent flow is constituted by streaks, strain regions and swirls constantly moving and evolving. Identifiable structures in a turbulent flow are called eddies; it involves a range of eddy sizes and the size range increases with increasing Reynolds number. The characteristic size of the largest eddies is the width of the turbulent region; in the Ocean Surface Boundary Layer, this is the thickness of the layer;
- dissipation: in a turbulent flow, energy is transferred to smaller and smaller scales via non-linear interactions, until velocity gradients become so large that the energy is converted into heat and dissipated by the action of viscosity and the motion of the smallest eddies;
- diffusivity: due to the presence of eddies, turbulent flows are characterized by a rapid rate of mixing and diffusion of species, momentum, and heat.

A useful and common approach in the study of the turbulent flows is to analyse and describe, for example, the velocity components of the sea currents, pressure, temperature and the other variables using the theory of stochastic processes and random variables. In particular, following the Reynolds decomposition, a turbulent field quantity a is expressed as the sum of its first moment, $\bar{a}$, and its fluctuation, a', which have zero mean:

$$a = \bar{a} + a' \tag{1}$$

The moments of a random variable are important to describe its behaviour, but they do not give information about the temporal duration or spatial extent of fluctuations, or about the relationships between one or more variables at different places and times. So, in the study of turbulence, correlations and spectra are commonly used to further characterize fluctuations.

Assuming for simplicity a temporally stationary random variable a_i sampled at the same point in space, or a spatially stationary random variable sampled at different points at the same time; in 3D, the correlation function of a_i at location $\boldsymbol{x_1}$ and time t_1 with the random variable a_j at location $\boldsymbol{x_2}$ and time t_2 is:

$$R_{ij}(\boldsymbol{x_1}, t_1, \boldsymbol{x_2}, t_2) = \overline{a_i(\boldsymbol{x_1}, t_1) a_j(\boldsymbol{x_2}, t_2)} \tag{2}$$

Eq. (2) specifies how similar are $a_i(\boldsymbol{x_1}, t_1)$ and $a_j(\boldsymbol{x_2}, t_2)$ to each other. If $R_{ij} = 0$, these variables are uncorrelated; R_{ij} could be either positive or negative, if $R_{ij} \approx 1$, the variables are correlated, while if $R_{ij} \approx -1$, the variables are anticorrelated. When $i = j$ in Eq. (2), the function is called autocorrelation function, while if $i \neq j$ the function is called cross-correlation.

For statistically stationary processes that are sampled at the same point in space, the statistics are independent of the time origin, so, defining $t_s = t_2 - t_1$, Eq. (2) can be rewritten as:

$$R_{ij}(t_s) = \overline{a_i(t) a_j(t + t_s)} \tag{3}$$

The integral time scale is determined from the autocorrelation function. The integral time scale, T_L, is a generic specification of the time over which a turbulent fluctuation is correlated with itself. In other words, T_L is a measure of the memory of the turbulence and it can be expressed as in the following equation, with $i = j$:

$$T_L = \frac{1}{R_{ij}(0)} \int_0^\infty R_{ij}(t_s)\, dt_s \tag{4}$$

2.3 Modelling turbulent dispersion in the marine environment

The study of the dispersion of pollutants in the marine environment is generally divided into two phases: the first is the calculation of the velocity field, the other is constituted by the evaluation of the pollutant concentrations. This is possible, i.e. the two problems could be decoupled, if the presence of the pollutant does not perturb the fluid dynamics.

The velocity field of the marine currents is commonly calculated by hydrodynamic models, which could integrate the experimental data or make predictions.

2.3.1 Hydrodynamic models: estimation of the velocity field

The governing principles in fluid mechanics are the conservation laws for mass, momentum and energy and the fundamental equations describing the fluid motions have been derived from these principles.

In the hydrodynamic models, the 3D marine velocity field and the other hydrodynamic variables are calculated by means of a set of non-linear partial differential equations: the Navier–Stokes equations, which are a statement of the budget law for momentum in a viscous fluid on the rotating earth, together with conservation laws for mass, heat and salt.

These equations are usually simplified considering the following hypothesis:

- Spherical Earth approximation: the geopotential surfaces are approximated by spheres;
- Thin-shell approximation: the ocean depth is neglected compared to the Earth's radius;
- Turbulent closure hypothesis: the effects of smaller scale motions are represented in terms of large-scale patterns to close the equations, as presented in paragraph (2.3.1.2);
- Boussinesq hypothesis: only the direct effect of density differences on buoyancy term are considered; see Eq. (5);
- Hydrostatic hypothesis: the vertical momentum equation is reduced to a balance between the vertical pressure gradient and the buoyancy force, see Eq. (8);

- Incompressibility hypothesis: the three dimensional divergence of the velocity field $\boldsymbol{u}$ is assumed to be zero, see Eq. (12);
- Neglect of additional Coriolis terms: the Coriolis terms that vary with the cosine of latitude are neglected.

Thus, considering the 'incompressibility hypothesis', which imply that the density of fluid particles does not change, the conservation of mass or '*continuity equation*' becomes:

$$\boldsymbol{\nabla} \cdot \boldsymbol{u} = 0 \tag{5}$$

The conservation of momentum equation is derived from the Newton's second law. It states that the rate of change of momentum, per unit volume, for a fluid particle is equal to the sum of the surface and volume forces. In the horizontal plane, it is:

$$\frac{Du}{Dt} = -\frac{1}{\rho_0}\frac{\partial p}{\partial x} + fv + \nu\nabla^2 u \tag{6}$$

$$\frac{Dv}{Dt} = -\frac{1}{\rho_0}\frac{\partial p}{\partial y} - fu + \nu\nabla^2 v \tag{7}$$

where u, v, w are the component of the sea currents along the three directions x, y, z; ρ_0 is the reference density, p is the pressure, and ν is the kinematic viscosity; $f = 2\Omega$ is the Coriolis acceleration, Ω represents the components of the Earth's angular velocity in a local coordinate reference.

While in the vertical direction, considering the hydrostatic hypothesis, the conservation of momentum equation becomes:

$$\frac{\partial p}{\partial z} = -\rho g \tag{8}$$

where g is the gravity acceleration. In addition, the heat conservation equation is:

$$\frac{DT}{Dt} = \frac{k_T}{\rho C_v}\nabla^2 T \tag{9}$$

where T is the temperature, C_v is the specific heat and k_T is the thermal diffusivity coefficient.

Considering the Boussinesq hypothesis, the constitutive equation for seawater is expressed in the following way:

$$\rho = \rho_0[1 - \alpha(T - T_0) + \beta(S - S_0)] \tag{10}$$

where $\rho_0 = 1028$ kg/m^3, $T_0 = 10$°C is the average seawater temperature, S is the salinity, $S_0 = 34.7$ g/kg is the average seawater salinity, $\alpha = 1.7 * 10^{-1}$ K^{-1} is the coefficient of thermal expansion and $\beta = 7.6 * 10^{-1}$ kg/g is the saline contraction coefficient (IOC and IAPSO 2010).

Finally, the salt conservation equation is expressed in the following way:

$$\frac{DS}{Dt} = k_S\nabla^2 S \tag{11}$$

where k_S is the diffusivity coefficient for salinity.

Eq. (5-11) form a set of 7 equations and 7 unknowns, they are commonly known as the governing equations for moving fluids. In fact, the turbulent motions in the ocean are fully described by this system of equations.

2.3.1.1 Averaged equations of motion (RANS equations)

As it has been said in paragraph (2.2), the environmental flows are turbulent, so even the marine currents are. Thus, considering that turbulent motions are non-stationary, 3D and highly random, a statistical approach is necessary. In this paragraph, starting from the Eq. (5-11) presented in the previous paragraph, the equations of motion for the mean state in a turbulent flow are derived.

To obtain that, the state variables, such as velocity, pressure and salinity, are decomposed by means of the Reynolds decomposition: $\rho = \bar{\rho} + \rho'$, $u = \bar{u} + u'$, $v = \bar{v} + v'$, $w = \bar{w} + w'$, $p = \bar{p} + p'$, $T = \bar{T} + T'$ and $S = \bar{S} + S'$. Thus, the equations for the mean state are derived by formal substitution of the Reynolds decomposition into the governing equations, and ensemble averaging the result. Following these steps, the next equations have been obtained:

$$\frac{\partial \bar{u}}{\partial x} + \frac{\partial \bar{v}}{\partial x} + \frac{\partial \bar{w}}{\partial x} = 0 \tag{12}$$

$$\frac{\partial \bar{u}}{\partial t} + \bar{u}\frac{\partial \bar{u}}{\partial x} + \bar{v}\frac{\partial \bar{u}}{\partial y} = -\frac{1}{\bar{\rho}}\frac{\partial \bar{p}}{\partial x} + f\bar{v} + \nu\left(\frac{\partial^2 \bar{u}}{\partial x^2} + \frac{\partial^2 \bar{u}}{\partial y^2} + \frac{\partial^2 \bar{u}}{\partial z^2}\right) - \left(\frac{\partial \overline{u'u'}}{\partial x} + \frac{\partial \overline{u'v'}}{\partial y} + \frac{\partial \overline{u'w'}}{\partial z}\right) \tag{13}$$

$$\frac{\partial \bar{v}}{\partial t} + \bar{v}\frac{\partial \bar{v}}{\partial y} + \bar{u}\frac{\partial \bar{v}}{\partial x} = -\frac{1}{\bar{\rho}}\frac{\partial \bar{p}}{\partial y} - f\bar{u} + \nu\left(\frac{\partial^2 \bar{v}}{\partial x^2} + \frac{\partial^2 \bar{v}}{\partial y^2} + \frac{\partial^2 \bar{v}}{\partial z^2}\right) - \left(\frac{\partial \overline{u'v'}}{\partial x} + \frac{\partial \overline{v'v'}}{\partial y} + \frac{\partial \overline{v'w'}}{\partial z}\right) \tag{14}$$

$$\frac{\partial \bar{p}}{\partial z} = -\bar{\rho}g \tag{15}$$

$$\frac{D\bar{\theta}}{Dt} = \frac{k_T}{\rho C_v}\frac{\partial^2 \bar{\theta}}{\partial y^2} - \left(\frac{\partial \overline{u'\theta'}}{\partial x} + \frac{\partial \overline{v'\theta'}}{\partial y} + \frac{\partial \overline{w'\theta'}}{\partial z}\right) \tag{16}$$

$$\bar{\rho} = \rho_0[1 - \alpha(\bar{\Theta} - \Theta_0) + \beta(\bar{S} - S_0)] \tag{17}$$

$$\frac{D\bar{S}}{Dt} = k_S\frac{\partial^2 \bar{S}}{\partial y^2} - \left(\frac{\partial \overline{u'S'}}{\partial x} + \frac{\partial \overline{v'S'}}{\partial y} + \frac{\partial \overline{w'S'}}{\partial z}\right) \tag{18}$$

where $\Theta = T(p_0/p)$ is the potential temperature.

The new set of Eq. (12-18) is commonly known as the Reynolds Averaged Navier-Stokes (RANS) equations and it is formally equivalent to the Navier–Stokes equations, but contains now several new unknowns, such as $\overline{u'v'}$, $\overline{v'\Theta'}$and $\overline{v'S'}$. These unknowns represent the turbulent fluxes of the corresponding quantity.

At this point, the number of unknowns is higher than the number of the equations. In order to solve this problem, there are three approaches (Kundu and Cohen 2008). The first involves additional equations (closures) developed from dimensional analysis, intuition, symmetry requirements and experimental results; this approach will be further discussed in the next paragraph. The second, known as direct numerical simulations (DNS) involves numerically

solving the time-dependent equations of motion and then Reynolds averaging the computational output to determine mean-flow quantities. The third, known as large-eddy simulation (LES), involves some modelling and some numerical simulation of large-scale turbulent fluctuations.

2.3.1.2 Turbulence modelling

The aforementioned Eq. (12-18) are usually solved at larger scales: the specified grid spacing and time step of the OGCMs. The effects of smaller scale motions (coming from the advective terms in the Navier-Stokes equations) must be represented entirely in terms of large-scale patterns to close the equations. Thus, the turbulent fluxes of momentum, temperature and salinity respectively, are solved by means of a closure scheme. In fact, assuming an analogy between molecular-motion-based laminar momentum and scalar transport and eddy-motion-based turbulent momentum and scalar transport, the purpose of a turbulent-mean-flow closure model is to relate the turbulent fluxes to the mean field of the turbulent quantity by means of a coefficient, i.e. the eddy or turbulent diffusivity.

For instance, the vertical turbulent closures for momentum, temperature and salinity could be expressed as in the following equation:

$$\overline{u'w'} = -K_Z^U \frac{\partial \bar{U}}{\partial z};\ \overline{w'\Theta'} = -K_Z^T \frac{\partial \bar{\Theta}}{\partial z};\ \overline{w'S'} = -K_Z^S \frac{\partial \bar{S}}{\partial z} \tag{19}$$

where K^U is the turbulent diffusivity for momentum, K^T for temperature and K^S for salinity, and the subscripts X, Y, Z indicate the direction.

Unfortunately, the molecular-dynamics-to-eddy-dynamics analogy is imperfect. In fact, molecular sizes are typically much less than fluid-flow gradient length scales while turbulent eddy sizes are typically comparable to fluid-flow gradient length scales. So, averages over eddies may be unsuccessful because turbulent eddies are so much larger than molecules (Kundu and Cohen 2008).

In Eq. (19), K^U is not a property of the fluid, but of the flow. So, from dimensional considerations, it is m^2/s and it should be proportional to the product of a characteristic turbulent length scale L and a characteristic turbulent velocity U:

$$K^U \propto L * U \tag{20}$$

A very common approach in turbulence modelling contemplates that the random character of turbulence is represented with a statistical method; so, the RANS equations are solved using additional equations or parameterizations.

Horizontal turbulence can be roughly divided into a mesoscale turbulence associated with eddies, which can be solved explicitly if the resolution is sufficient since their underlying physics are included in the primitive equations, and a sub-mesoscale turbulence which is never explicitly solved even partially, but always parameterized. Gent and McWilliams 1990 proposed a parameterisation of mesoscale eddy-induced turbulence which associates an eddy-induced velocity to the isoneutral diffusion. The main ones sub-mesoscale parameterisations are: Laplacian and bilaplacian operators acting along geopotential or iso-neutral surfaces and various slightly diffusive advection schemes (Gent and McWilliams 1990).

Considering vertical turbulence, the model resolution is often not sufficient to solve all the eddy structures. The simplest-level closure model for vertical turbulence is known as ‘zero-

equation model'. This approach was firstly introduced by Taylor 1915, but fully developed by Prandtl 1925. In this case, the turbulent diffusivity could be derived considering the length scale, L, as the mixing length, $l(z)$, which is the cross-stream distance travelled by a fluid particle before it gives up its momentum and loses its identity. For a wall-bounded flow, $l(z) = \kappa * z$, where $\kappa = 0.4$ is the von Karman constant, and the horizontal velocity, $\bar{u}$, is described by a logarithmic profile:

$$\frac{\bar{u}}{u_*} = \frac{1}{\kappa}\ln(z/z_0) \tag{21}$$

where z_0 is the roughness length.

In this case, no balance equation is solved, but the unknowns are expressed directly as semi-empirical functions of time and space.

Alternatively, the turbulent diffusivity could be obtained from an algebraic specification of the turbulent length scale and the determination of the velocity scale from the Turbulent Kinetic Energy (TKE) transport equation, as Kolmogorov and Prandtl suggested. The TKE equation is one additional second-order partial differential equation, hence this approach is named 'one-equation model'.

In this case, the dissipation rate, $\bar{\varepsilon}$, could be modelled in the following way:

$$\bar{\varepsilon} = C_\varepsilon \bar{E}^{3/2}/l_\varepsilon \tag{22}$$

where C_ε is a constant, $\bar{E} = \frac{1}{2}\overline{(u'^2 + v'^2 + w'^2)}$ is the Turbulent Kinetic Energy and l_ε is the dissipation length scale.

In the oceanic case, Gaspar, Grégoris, and Lefevre 1990 developed a model based on these assumptions and it is an option for the calculation of the turbulent diffusivity used in NEMO model (Madec et al. 2019). The time evolution of $\bar{E}$ is described in the following equation and it is the result of the production of $\bar{E}$ through vertical shear, its destruction through stratification, its vertical diffusion and its dissipation:

$$\frac{D\bar{E}}{Dt} = K_Z^U\left(\left(\frac{\partial\bar{u}}{\partial z}\right)^2 + \left(\frac{\partial\bar{v}}{\partial z}\right)^2\right) - \frac{K_Z^U}{P_{rt}}N^2 + \frac{\partial}{\partial z}\left(K_Z^U\frac{\partial\bar{E}}{\partial z}\right) - \bar{\varepsilon} \tag{23}$$

where $K_z = C_K * \bar{E}^{\frac{1}{2}} * l(z)$ is the vertical turbulent diffusivity, $C_K = 0.1$ and $C_\varepsilon = 0.7$, N^2 is the Brunt-Vaisala frequency; P_{rt} is the Prandtl number and it can be set to unity or be a function of the Richardson number.

Furthermore, the 'two-equation models' calculate the turbulent length scale by means of two additional partial differential equations.

The first additional partial-differential equation is for TKE, see Eq. (23). In the framework of the 'k - ε model' (Jones and Launder 1972), further developed by many other researchers such as Rodi 1987, the second additional partial-differential equation is an empirical construction for the dissipation:

$$\frac{D\bar{\varepsilon}}{\partial t} = \frac{\partial}{\partial z}\left(K_Z^U\frac{\partial\bar{\varepsilon}}{\partial z}\right) + C_{1\varepsilon}\frac{\bar{\varepsilon}}{\bar{E}}(P + C_{1\varepsilon}G) - C_{2\varepsilon}\frac{\bar{\varepsilon}^2}{\bar{E}} \tag{24}$$

where $P = K_Z^U \left(\frac{\partial \bar{u}}{\partial z} + \frac{\partial \bar{w}}{\partial x}\right)\frac{\partial \bar{u}}{\partial z}$ is the shear production and $G = \alpha g K_Z^U \frac{\partial \bar{\theta}}{\partial z}$ is the buoyancy production, $C_{1\varepsilon} = 1.44$, $C_{2\varepsilon} = 1.92$ and $C_{3\varepsilon} = 0 \div 1$, which depends on the state of the flow, are empirical constants.

On the other hand, Mellor and Yamada 1982 have criticized the use of Eq. (24), because they believe that $\bar{\varepsilon}$ is a quantity describing small-scale turbulence; so, they have developed a '$k - kL$ model', which was further modified by Galperin et al. 1988, and it is widely used in oceanography. In this model, the second additional transport equation is for the variable $\overline{EL}$, which is the product of the Turbulent Kinetic Energy and the turbulent length scale, and it is expressed in the following way:

$$\frac{D\overline{EL}}{Dt} = \frac{\partial}{\partial z}\left(\sqrt{2}S_l\sqrt{\bar{E}}L\frac{\partial \overline{EL}}{\partial z}\right) + \frac{E_1}{2}L(P+G) - \frac{\sqrt{2}\bar{E}^{\frac{3}{2}}}{B_1}(1 + E_2\left(\frac{L}{\kappa L_Z}\right)^2) \qquad (25)$$

where $S_l = 0.2$, $E_1 = 1.8$, $E_2 = 1.33$ and $B_1 = 16.6$ are empirical constant and L_Z is a measure of the distance from the wall.

Another length-scale related quantity is the turbulence frequency $\omega = \bar{\varepsilon}/\bar{E}$ used in the 'k - ω model' (Wilcox 1988), which has been extended for geophysical applications by Umlauf, Burchard, and Hutter 2003.

In the framework of the second moment closure models, to reduce the number of transport equations, a local equilibrium is assumed for the second moments, so any non-local processes are neglected, such as counter-gradient fluxes that may occur in convective boundary layers. Furthermore, the effect of the earth's rotation on turbulent motions is neglected, leading to some inaccuracies for deep oceanic convection (Burchard et al. 2008).

Besides, parameterizations based entirely on empirical knowledge, are a useful alternative for statistical turbulence models. In fact, large-scale ocean and climate models are incapable of explicitly resolving the complex physics of the upper ocean, and it will remain so for the near future.

This approach allows to represent physical processes without the use of additional transport equations; on the other hand, the main drawback in using the empirical models is that they depends on the quality of the observations used to parameterize the turbulent fluxes.

The earliest empirical models have treated the boundary layer as a slab, one of them is the Well-Mixed boundary layer model (WMBL) implemented by Kraus and Turner 1967.

In this scheme, the transported scalar is assumed homogeneous in the mixed layer. Following the analytical approach of Niiler & Kraus (1977) presented in Gaspar 1988, the turbulent flux of a generic scalar a at the base of the mixed layer can be expressed with the following relation:

$$\overline{a'w'} = -w_e \Delta a \qquad (26)$$

where w_e is the entrainment velocity, i.e. the growth rate of the mixed layer, and Δa denotes the variation of the scalar across the base of the mixed layer. The surface fluxes of temperature and salinity are derived from the heat fluxes and precipitation and evaporation rates, respectively.

The velocity w_e is the only turbulent quantity that requires a closure and it can be obtained by integrating the TKE equation, written in the case of horizontal homogeneity; after the

integration along the vertical direction and the parametrization of its terms, the TKE equation leads to the following algebraic equation (Reichl and Hallberg 2018):

$$\frac{H}{2} w_e \Delta b = m_* u_*^3 - n_* \frac{H}{2} B_0 \tag{27}$$

where H is the depth of the mixed layer, $u_* = \sqrt{\tau/\rho}$ is the friction velocity, τ is the shear stress, b is the buoyancy, m_* is a mixing coefficient due to the turbulent phenomena generated by the wind action on the sea surface, n_* is a buoyancy coefficient and B_0 is the surface buoyancy flux. n_* assumes a unitary value in the case of a stratified water column, alternatively, in the case of convection, it is less than one (Schumann and Gerz 1995); while m_*, in the presence of wind-forced turbulent structures and stratification, can be parameterized with $m_* = C_{S1}(B_0^2 h/u_*^5 |f|)^{C_{S2}}$, where $|f|$ is the Coriolis parameter, $C_{S1} = 0.2$ and $C_{S2} = 0.4$ are parameters (Reichl and Hallberg 2018).

Another well-known scheme is the K-Profile Parameterization (KPP) developed by Large et al. 1994, which is distinguished from other empirical models by the inclusion of non-local fluxes, as in the next equation:

$$\overline{a'w'} = \overline{a'w_L'} + \overline{a'w_N'} \tag{28}$$

The local component, $\overline{a'w_L'}$, is given by the gradient closure, as in Eq. (19); where, following Onink, van Sebille, and Laufkötter 2022, $K_Z^U(z)$ is calculated with the next equation:

$$K_Z^U(z) = \left(\frac{\kappa u_*}{\phi}\theta\right)(|z| + z_0)\left(1 - \frac{|z|}{H}\right) + K_B \tag{29}$$

where $\phi = 0.9$ is the stability function of the Monin–Obukhov boundary layer theory; $z_0 = 0.1 * H_s$ is the roughness scale of turbulence, where $H_s = 0.96 g^{-1} \beta_*^{3/2} u_{*a}^2$ is the significant wave height, which is defined as the average height of the highest third of surface displacement maxima, a few meters is generally regarded as a large value; $\beta_* = c_p/u_{*a}$ is the wave age, c_p is the characteristic phase speed of the surface waves and u_{*a} is the friction velocity of air; following Kukulka et al. 2012, in a fully developed sea state $\beta_* = 35$. Finally, below the mixed layer, $K_Z^U(z) = K_B = 3 * 10^{-5}$ m^2/s. In addition, θ is a Langmuir circulation enhancement factor and different values have been tested: Boufadel et al. 2020 examined a case where LC-driven turbulence was considered negligible and thus $\theta = 1$. However, the presence of LC can increase turbulent mixing by a factor $\theta = 3 \div 4$ (McWilliams and Sullivan 2000) and it has been shown to strongly affect the vertical concentration profiles of buoyant microplastic particles in LES experiments (Brunner et al. 2015; Kukulka and Brunner 2015).

Moreover, non-local fluxes, $\overline{a'w_N'}$, may be written in terms of local variables by making various approximations to the flux budget, in fact they depends only on surface fluxes and on the mixed layer depth. Large et al. 1994 established the parameter values for non-local fluxes of heat and salt. Parameterization of non-local momentum fluxes has been undertaken more recently by Smyth et al. 2002.

A further approach to close the turbulent fluxes is the OSMOSIS scheme (Li et al. 2019), which combines a bulk model of the surface boundary layer (e.g. WMBL) with a turbulence model based on non-local flux-gradient relationships (e.g. KPP). The bulk model is used to determine the evolution of the depth of the boundary layer, while the turbulence model determines the mean profiles within the boundary layer (Damerell et al. 2020). In addition, this

parameterization allows considering Langmuir turbulence. In this scheme, the turbulent flux of a generic scalar a can be expressed with the following relation:

$$\overline{a'w'} = -K_Z^U \frac{\partial \bar{a}}{\partial z} + N_s + N_b + N_t \tag{30}$$

where N_s, N_b and N_t are the non-gradient terms: N_s represents the effects that the Stokes shear, N_b the effect of buoyancy and N_t the effect of the turbulent transport.

In unstable conditions, the boundary layer is assumed to deepen through entrainment due to the combination of Langmuir turbulence and convection. The vertical turbulent diffusivity is parameterized in the following way:

$$K_Z^U(z) = 0.3\omega_* z(1 - \beta_K \frac{z}{H_{ml}})(1 - \frac{1}{2}\left(\frac{z}{H_{ml}}\right)^2) \tag{31}$$

where β_K is a parameter, $\omega_* = (\nu_*^3 + 0.5w_{*C}^3)^{1/3}$ is the velocity scale in unstable conditions, where $\nu_* = (u_*^3\left(1 - e^{-0.5La_t^2}\right)) + w_{*L}^3)^{1/3}$ is the velocity scale in stable conditions, $La_t = u_*/u_{s0}$ is the Langmuir turbulent number, which is the ratio between the friction velocity and the stokes drift, u_{s0}; the Langmuir turbulence velocity scale is $w_{*L} = (u_*^2 u_{s0})^{1/3}$ and the convective velocity scale is $w_{*C} = (B_0 H_{ml})^{1/3}$. Finally, H_{ml} is the well-mixed layer thickness, i.e. the mixed layer depth, H, without the pycnocline layer.

The prognostic equation for the mixed layer depth is given by:

$$\frac{\partial H}{\partial t} = \bar{w} - \frac{\overline{w'b'_{ent}}}{\Delta B} \tag{32}$$

where $\overline{w'b'_{ent}}$ is the buoyancy entrainment flux and ΔB is the difference between the buoyancy averaged over the depth of the mixed layer and the buoyancy just below the base of the mixed layer.

In stable conditions, the turbulent diffusivity is:

$$K_Z^U(z) = 0.375\nu_* z e^{\left(-2.8(H/L_L)^2\right)}\left(1 - \frac{z}{H_{ml}}\right)(1 - \frac{1}{2}\left(\frac{z}{H_{ml}}\right)^2) \tag{33}$$

In Eq. (33), $K_Z^U(z)$ depends on the Langmuir turbulence, in fact L_L is its length scale.

In this case, the prognostic equation for the mixed layer depth is given by:

$$\max\left(\Delta B, \frac{w_{*L}^2}{H}\right)\frac{\partial H}{\partial t} = \left(0.06 + 0.52\frac{H}{L_L}\right)\frac{w_{*L}^3}{H} + \langle\overline{w'b'}\rangle_L \tag{34}$$

where $\langle\overline{w'b'}\rangle_L$ is the mean turbulent buoyancy flux averaged over the mixed layer.

A recent parameterization has been proposed by Reichl and Hallberg 2018 and it is called energetic based Planetary Boundary Layer (ePBL). In this scheme, the turbulent mixing has a relatively weak dependence on model vertical resolution and time step, because the integral of the vertical turbulence buoyancy flux, that describes potential energy change associated with turbulent mixing, i.e. the mixing coefficient and the depth of the boundary layer are explicitly

constrained to satisfy the potential energy change due to turbulent mixing imposed, using the next equation:

$$M_e = m_* u_*^3 - n_* \int_{-H}^{0} K_Z^U \min(N^2, 0)\, dz \tag{35}$$

where the turbulent diffusivity profile $K_Z^U(z) = C_e U(z) L(z)$ is the product of a turbulent velocity scale, $U(z)$, and a length scale, $L(z)$; C_e is a coefficient.

In this scheme, the scales are defined as it follows:

$$\begin{aligned} U(z) &= C_{w_*} \left(\int_z^0 \overline{w'b'} \right)^{\frac{1}{3}} + \left(C_\mu^0\right)^{\frac{1}{3}} u_* \left(1 - a * \min\left(1, \frac{|z|}{H}\right)\right) \\ L(z) &= (z_0 + |z|) * \max\left(\frac{l_b}{H}, \left(\frac{H - |z|}{H}\right)^\eta\right) \end{aligned} \tag{36}$$

where C_{w_*} and C_μ^0 are empirical coefficients; with $\eta = 2$ providing a similar shape to KPP and l_b being a bottom length scale, which is dependent on bottom roughness or interior stratification and prevents $L(z)$ from becoming zero at the base of the OSBL (Li et al. 2019).

Further parameterizations of the turbulent diffusivity have been yielded essentially from empirical quantities and similarity laws.

For instance, the Richardson number, Ri, can be considered as a valuable parameter to assess turbulence in the water column, because it expresses the ratio of the buoyancy term (N^2) to the flow shear term (S^2), i.e. the ratio between the production of the thermal Turbulent Kinetic Energy and the mechanical Turbulent Kinetic Energy:

$$Ri = \frac{\frac{-g}{\rho}\frac{d\rho}{dz}}{\left(\frac{\partial u}{\partial z}\right)^2 + \left(\frac{\partial v}{\partial z}\right)^2} = \frac{N^2}{S^2} \tag{37}$$

Considering that, Pacanowski and Philander 1981 (hereinafter P&P81) developed a parameterization where $K_Z^U(z)$ essentially depends on Ri, as it follows:

$$K_Z^U(z) = \frac{K^T}{(1 + mRi)} + K_B \tag{38}$$

where K^T is the thermal vertical turbulent diffusivity and it is given by:

$$K^T = \frac{K_{ric}^T}{(1 + mRi)^n} + K_B^T \tag{39}$$

where $K_{ric}^T = 10^{-4}$ m^2/s is its critical value and $K_B^T = 1.2 * 10^{-5}$ m^2/s is its background value; $K_B = 1.2 * 10^{-4}$ m^2/s is the vertical turbulent diffusivity background value and $m = 5$ and $n = 2$ are parameters.

Another parametric law aiming to estimate the vertical turbulence diffusivity has been proposed by Kukulka et al. 2012 and it has been extended by Poulain et al. 2019 (hereinafter SWB). Following Onink et al. 2022, SWB estimates $K_Z^U(z)$ in this way:

$$K_Z^U(z) = \begin{cases} K_z^{surf} + K_B, & z < sH_S \\ K_z^{surf}(sH_s)^{3/2}|z|^{3/2} + K_B, & z > sH_S \end{cases} \quad (40)$$

where $K_z^{surf} = 1.5u_*\kappa H_S$ is the near-surface vertical diffusivity as in Kukulka et al. 2012, and different values of s have been tested, which is a multiple of H_S that sets the depth to which $K_Z^U(z)$ is constant; this increases $K_Z^U(z)$ for $z \approx 0$ and allows to investigate the influence which the higher near-surface mixing would have on the vertical turbulent dispersion. $K_B = 3 * 10^{-5}$ m^2/s is the diffusivity background value. This parameterization defines a constant $K_Z^U(z)$ in the first meters of the water column in order to consider turbulence generated by breaking surface waves; after that $K_Z^U(z)$ decreases with $|z|^{3/2}$. SWB does not provide any information about the stratification of the water column.

Furthermore, in random walk simulations, Visser 1997 implemented the next parameterization of $K_Z^U(z)$:

$$K_Z^U(z) = a_V * z * e^{-b_V z} \quad (41)$$

where $a_V = 6 * 10^{-3}$ m/s and $b_V = 0.5$ m^{-1} are parameters. In this parameterization, $K_Z^U(z)$ behaves as an exponential function.

An estimation of the turbulent diffusivity coefficient related to Lagrangian statistics has been carried out by Yamazaki and Kamykowski 1991; in this scheme, $K_Z^U(z)$ is expressed in the following way:

$$K_Z^U(z) = 2.7\frac{\sqrt{\bar{\varepsilon}(z)\nu}}{N} \quad (42)$$

Even if $K_Z^U(z)$ is a function of the same quantities, i.e. dissipation and Brunt-Vaisala frequency, this parameterization is considerably different from the empirical one suggested by Osborn 1980, because it starts from Eulerian assumptions. In this, $K_Z^U(z)$ is expressed as:

$$K_Z^U(z) = 0.2\frac{\bar{\varepsilon}(z)}{N^2} \quad (43)$$

Finally, as it has been pointed out in this paragraph, the turbulent closure schemes are various, but the choice will depend on the application.

2.3.2 Dispersion models: estimation of the particle concentration

Once the velocity field has been obtained from the RANS equations combined with one of the turbulence closure schemes presented in the previous paragraph, the study of the dispersion of pollutants in the marine environment continues with the definition of the pollutant concentrations.

Thus, estimating pollutant pathways and accumulation zone in the marine environment is possible by means of in situ campaigns with tracers; besides, another and more feasible approach involves the use of models, Eulerian or Lagrangian.

In the Eulerian framework, the values of the particle velocities, $u(\boldsymbol{x}, t)$, in fixed points of the field at the same instant t are determined. However, the Eulerian study of dispersion permits to solve the problem completely by determining both the velocity field and the concentration.

On the other hand, the Lagrangian models employ an ensemble of virtual passive particles whose trajectories are determined by a mean velocity field and a stochastic process. The velocity fields that are used to move the particles often come from OGCMs, or rarely from observational-based velocities. The trajectories of the virtual particles follow the path lines of the velocity field, often including the effect of sub-grid scale diffusion. Then, the statistics of the trajectories define the particle pathways and their associated time scales.

These models are based on the pollutant mass balance equation, written for a fixed reference system with respect to the Earth. This can be obtained by equating the Lagrangian derivative of the mass of pollutant, contained in a volume of moving fluid, to the molecular flow through the boundary surface and the result is:

$$\frac{Dc}{Dt} = \frac{\partial}{\partial x_i}\left(D\frac{\partial c}{\partial x_i}\right) \tag{44}$$

where c is the pollutant concentration and D is the molecular diffusivity.

2.3.2.1 Eulerian models

In the marine environment, fluxes are very often turbulent; so, using the Reynolds decomposition for the pollutant concentration, $c = \bar{c} + c'$ has been imposed and considering that molecular diffusion is far weaker than turbulent diffusion, Eq. (44) can be updated as:

$$\frac{\partial \bar{c}}{\partial t} + \overline{u_i}\frac{\partial \bar{c}}{\partial x_i} = -\frac{\partial \overline{u_i{}'c'}}{\partial x_i} \tag{45}$$

In the Eulerian framework, the classical '*k*-model' have been developed, where a gradient closure could be adopted for the turbulent flux; so, using explicit notation, Eq. (45) can be rewritten as:

$$\frac{\partial \bar{c}}{\partial t} + \bar{u}\frac{\partial \bar{c}}{\partial x} + \bar{v}\frac{\partial \bar{c}}{\partial y} + \bar{w}\frac{\partial \bar{c}}{\partial z} = \frac{\partial}{\partial x}\left(K_x\frac{\partial \bar{c}}{\partial x}\right) + \frac{\partial}{\partial y}\left(K_y\frac{\partial \bar{c}}{\partial y}\right) + \frac{\partial}{\partial z}\left(K_z\frac{\partial \bar{c}}{\partial z}\right) \tag{46}$$

Eq. (46) is called '*diffusion equation*' and in order to get the particles concentration, it could be solved with a finite-differences method.

In Eq. (46), K_x, K_y are the horizontal turbulent diffusivities and K_z is the vertical turbulent diffusivity. It is worth mentioning that these turbulent diffusivities have been calculated from Eq. (45), so they are calculated for the particle mass, which is a scalar. K^U and K have different origins, but they have the same dimension, i.e. m^2/s. They are related by means of the turbulent Schmidt number, which is a property of the flow defined as the ratio of the eddy diffusivity of momentum to the eddy diffusivity of mass (Di Bernardino et al. 2020). The Schmidt number is $o(1)$; in the mixed layer, K^U and K are similar, while they differ mostly at the interface.

2.3.2.2 Lagrangian models

In the Lagrangian framework, the attention is on the pollutant particles trajectories.

Taylor 1921 studied the turbulent dispersion using Lagrangian coordinates and he calculated the rate at which a particle moves away from its initial location. He assumed that the particles are emitted into a stationary and homogeneous turbulent medium in which the mean velocity

is zero; with this hypothesis, the Lagrangian velocity variance is equal to the Eulerian velocity variance: $\overline{W^2} = \overline{w^2}$, where $W(t) = \partial Z(t)/\partial t$ is the Lagrangian velocity and $Z(t)$ is the Lagrangian displacement of a particles.

The Lagrangian correlation function, $R_L(\tau)$, can be expressed in the following way:

$$R_L(\tau) = \overline{W(t)W(t-\tau)} \tag{47}$$

and its correlation coefficient is:

$$\rho_L(\tau) = R_L(\tau)/\overline{W^2} \tag{48}$$

So, the average rate at which the magnitude of $Z(t)$ increases, i.e. the particle displacement variance $\overline{Z^2(t)}$, can be calculated from the next equation:

$$\frac{1}{2}\frac{d}{dt}\overline{Z^2(t)} = \overline{W(t)Z(t)} = \overline{W^2}\int_0^t \rho_L(\tau)d\tau \tag{49}$$

Integrating by parts, it has been obtained:

$$\overline{Z^2(t)} = 2\overline{W^2}\int_0^t (t-\tau)\rho_L(\tau)d\tau \tag{50}$$

From Eq. (50) it is possible to examine two limiting cases:

$$\begin{cases} \overline{Z^2(t)} = \overline{W^2}t^2, & t \to 0 \\ \overline{Z^2(t)} = 2\overline{W^2}T_L(t-t_1), & t \to \infty \end{cases} \tag{51}$$

where $t_1 = \int_0^\infty \tau\rho_L(\tau)d\tau/T_L$.

So, as highlighted in Eq. (51), the plume generated by a pollutant source in a homogeneous and stationary turbulent flow with mean horizontal velocities will have a conical shape close to the source and will approximate a paraboloid at large distances. In addition, the plume behaviour at longer time is similar to the behaviour in a random walk with uncorrelated velocities. This similarity is due to the fact that, far from the source, the fluid particles have forgotten their initial behaviour.

Thus, the particle trajectories can be simulated by means of stochastic processes which have statistical properties analogous to the fluid motion; the more statistical parameters that are reproduced, the more realistic are the trajectories generated. These stochastic processes can describe the motion of particles, i.e. of ensembles of particles independently launched in different realizations of the turbulent flow (Griffa 1996), and the particles concentration corresponds to the ensemble average concentration of them.

Some models based on these assumptions have been developed and they have a hierarchy of increasingly detailed descriptions of particle motion. These models are Markovian, i.e. they describe processes whose conditional probability density at time t_n depends only on the process value at the earlier time t_{n-1}.

These models are based on the following non-linear equation:

$$ds_i = h_i(\boldsymbol{x}, t)dt + g_{i,j}(\boldsymbol{x}, t)d\mu_j \tag{52}$$

where s_i is a stochastic process, with $i = 1, N$; $d\mu_j$ is a random increment with zero mean, h_i and $g_{i,j}$ are continuous functions. Eq. (52) states that the behaviour of stochastic processes depends both on a deterministic and a random contribution. Furthermore, the behaviour of stochastic processes such as s_i is characterized by their probability density function Π. The evolution equation for the probability density, Π, of a Markovian process as Eq. (52) is called the Fokker-Planck equation.

A zeroth-order Markov model corresponds to the classic random walk model and it assumes that the particle position is a Markov variable; it is also known as Wiener process. This model assumes also that the correlation scales of the turbulence velocity are infinitesimal and it is equivalent to the advection-diffusion description.

In this model, the equations that describe the particle motion in the *z*-direction can be written, in incremental form, as:

$$dz = \left(\overline{w} + \frac{dK_z}{dz}\right)dt + \sqrt{K_z}d\mu_z \tag{53}$$

where, according to Taylor 1921, the turbulent diffusivity in the *z*-direction, K_z, can be calculated as the product of the vertical velocity variance, σ_w^2, and the Lagrangian integral time scale, T_L, as in the following equation:

$$K_z(z) = \sigma_w^2(z) * T_L(z) \tag{54}$$

The drift term, dK_z/dz, in Eq. (50), can be obtained by comparing the Fokker Plank equation with the diffusion equation. This term ensures the well-mixed condition, when the diffusivity tensor is not spatially uniform.

This scheme is reusable for the other directions.

Physically, Eq. (53) describe the displacement of a particle as resulting from two contributions: the mean flow, represented deterministically by the term $\overline{w}dt$, and the turbulence, which is represented as a stochastic process uncorrelated from one time step to the next. This means that the particle moving through the fluid receives at each time step a random impulse due to the action of the incoherent turbulent motions and it loses memory of its previous turbulent momentum.

The Fokker-Planck equation associated with a zeroth-order Markov model is:

$$\frac{\partial \Pi(z,t)}{\partial t} + \frac{\partial(\overline{w}(z)\Pi(z,t))}{\partial z} = \frac{\partial^2\left(K_z(z)\Pi(z,t)\right)}{\partial z^2} \tag{55}$$

where $\Pi(z,t) = \int \Pi(z - dZ, t - dt)d\Pi(dZ|z - dZ)$ is the probability density function, where $d\Pi(dZ|z - dZ)$ gives the probability that a particle moves to z from $z - dZ$.

Eq. (55) is equivalent to:

$$\frac{\partial \Pi(z,t)}{\partial t} + \frac{\partial}{\partial z}\left(\left(\overline{w}(z) - \frac{\partial K_z(z)}{\partial z}\right)\Pi(z,t)\right) = \frac{\partial}{\partial z}\left(K_z(z)\frac{\partial \Pi(z,t)}{\partial z}\right) \tag{56}$$

A first-order Markov model, which is sometimes referred to as a '*random flight*' model, assumes that the particle position and the turbulent velocity are jointly Markovian; it is also

known as Langevin process. In this model, the equations that describe the particle motion in the *z*-direction can be written, in incremental form, as:

$$dz = (\overline{w} + w')dt \tag{57}$$

$$dw' = -\left(\frac{1}{T_L}w' + \frac{d\sigma_w^2(z)}{dz}\right)dt + \sqrt{2\frac{\sigma_w^2(z)}{T_L}}d\mu_w \tag{58}$$

The deterministic part of this equation consists of two terms: the first ensures an exponential decay in the autocorrelation of the particle's velocity, regulated through the Lagrangian integral time scale, T_L, and a drift correction which ensures the well-mixed condition. The stochastic forcing term consists of the Wiener increment, $d\mu_w$, related to the ratio of the turbulent velocity variance and the Lagrangian integral time scale.

The first-order Markov model differs from the zeroth-order in the treatment of the turbulent velocity, which is not assumed to be uncorrelated from one time step to another. Rather, at each time step the particle loses only a fraction of its momentum, and in turn receives a random impulse. As a consequence, the particle conserves the memory of its initial turbulence velocity during a finite time of order of T_L (Griffa 1996).

The zeroth-order and the first-order Markov model have been compared in Lagrangian simulation of the MP dispersion in the marine environment (Onink et al. 2022; Reijnders, Deleersnijder, and van Sebille 2022). In this comparison, it has been obtained that the zeroth-order Markov models provide good model performance, while first-order Markov models do not consistently improve model performance relative to zeroth-order Markov models and require an additional parameter that is poorly constrained.

Finally, a second-order Markov model assumes that the position, the velocity and the turbulent acceleration are jointly Markovian.

2.4 Plastic pollution of the marine environment

Plastic pollution is a worldwide issue; no landscape or seascape, not even the mountain peaks or remote islands, has escaped (Boucher and Billard 2020). This problem is known since long time, but it has gained considerable attention in the recent decades.

It has been confirmed that the plastic contamination of the marine environment is closely linked to anthropic activities; so, it is widely assumed that most plastic debris derives from land-based sources, mainly from densely populated continental areas, although sea-based sources, related to the fishing industry or transportation, play an important role too (Boucher et al. 2020).

The widespread nature of plastics in the marine environment is generally believed to result from their longevity in the environment and relatively high buoyancy, which facilitates long-distance transport from source areas (Andrady 2011).

Nevertheless, there is a large mismatch between the estimates of the amount of municipal solid plastic waste generated on land that enters the oceans (5–12 million tonnes per year (Jambeck et al. 2015) and the total amount of plastic sampled at sea surface (less than 0.3 million tonnes (Cózar et al. 2014; Eriksen et al. 2014)); in fact, recent estimates suggest between 70 and 90% of the MP particles are accumulated into sediment profiles (Uddin et al. 2021).

At this moment, the knowledge about the processes involved in the plastic pollution of the marine environment is still incomplete; in order to fill this gap, physical processes that govern

the dispersion, biological processes, fragmentation, beaching, sedimentation and particles characteristics need a more detailed description.

In particular, for a complete analysis of the phenomena involved, the first step consists in a correct estimation of the plastic sources and the load of the pollutant particles discharged. It is recognized that they come from coastal and inland mismanaged waste or fishing activities; also, plastic debris already in microformat can come from cosmetics, tyre dust or road and ship paintings. It has been estimated that 12 million tonnes per year is the global yearly marine plastic leakage (Boucher et al. 2020).

The particles entering the oceans can also be transported at great distances by the turbulent marine currents and they can accumulate in particular areas, such as beaches or ocean canyons. Nowadays, they also accumulate in correspondence of the sub-tropical gyres, presented in par. (2.1.1), forming the famous Great Garbage Patches.

As it is visible in Fig. (4), during their journey, the plastic debris are subjected to fragmentation due to UV-radiation, oxidation and higher temperatures or embrittling (Kaandorp, Dijkstra, and van Sebille 2021); their sedimentation rate can be enhanced because can aggregate and form bigger objects or because they are subjected to biofouling (algal growth on a substrate) (Lobelle et al. 2021). Furthermore, seabirds or other aquatic organisms can ingest plastic particles and so they enter the food chain, exposing even humans.

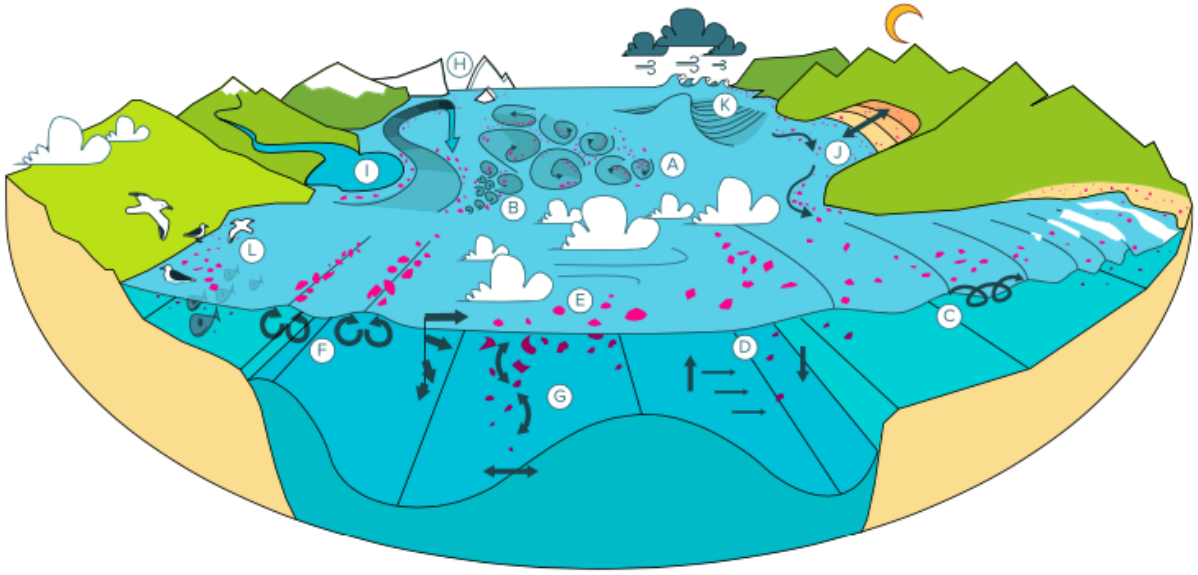

Figure 4. Physical processes that affect the transport of plastic (pink items) in the ocean. Source: van Sebille et al. 2020

2.4.1 Physical properties of the plastic debris

Plastic debris entering the marine environment in various size and shapes and they are made by different polymers.

Erni-Cassola et al. 2019 established that the most abundant plastic polymers discharged into water bodies are PE (polyethylene), which have density between $850 \div 920$ kg/m^3, and PP (polypropylene), which have density between $890 \div 980$ kg/m^3, so they are both positively buoyant polymers; but, also polyesters, polyamide and acrylics have been found in the marine environment, on the other hand all of them have a density greater than seawater.

While considering the size of the particles, it is possible to have a range from μm to m.

In particular, microplastics are the particles with dimensions less than 5 mm. Moreover, they can be distinguished between primary microplastics, which are plastic fragments entering the ocean already in micro format, and secondary microplastics, which result from the fragmentation of bigger plastic objects.

Furthermore, plastic debris are commonly founded in a wide range of shapes, such as fragments, spheres, films, filaments and fibres.

2.4.2 Modelling of the 3D microplastic dispersion

The complexity of this phenomenon can be investigated both by means of experimental campaigns and modelling. But given the sparsity of observations, numerical simulations can both fill in the gaps between these observations and test hypotheses about how plastic particles behave in the marine environment (van Sebille et al. 2020). Lagrangian stochastic models are commonly used in oceanography for modelling both the 3D transport of seawater and the pathways and distribution of plastic particles in the ocean (Lebreton, Greer, and Borrero 2012).

In the framework of the modelling of the 3D microplastic dispersion, on the horizontal plane particles are advected by mean currents and transported far from sources; while how microplastics behave within the water column needs a further attention, because turbulent mixing processes, physical and biological phenomena could modify sedimentation rates and they are not immediate to understand and model.

In general, there are not many numerical models developed exactly for the study of the dispersion of MP, but very often models developed for other applications and re-adapted for MP dispersion being used to investigate this environmental problem.

An exhaustive review is presented in van Sebille et al. 2018.

Recently, the Ariane 3D model (Blanke and Raynaud 1997) has been employed in the works of Durgadoo et al. 2019, van Gennip et al. 2019 and Maes and Blanke 2015 for the study of MP dispersion in the marine environment; this model provides only an advection scheme for the dispersion of pollutant particles, so no diffusion is modelled.

The Connectivity Modelling System model (Paris et al. 2013), for the study of MP dispersion, proposes a series of modules to describe the vertical movements of the particles, also taking into consideration the biological phenomena, the interactions with the benthic layer of the bottom and the beaching.

The OpenDrift model (Dagestad et al. 2018) describes the phenomenon of dispersion using a random walk scheme, so velocities are considered uncorrelated and turbulence is modelled with the scheme developed by Visser 1997. This model was used in the study of Röhrs et al. 2018 to analyse the role of vertical mixing in oil dispersion, but it could be borrowed to investigate how the mixing processes affect MP vertical distribution.

The Parcels model (Delandmeter and van Sebille 2019) has recently been used by Onink et al. 2019 to study the role of Ekman currents, geostrophic currents and Stokes drift in MP dispersion in the North Atlantic Ocean and North Pacific Ocean. This model uses a zeroth-order Markov process to close turbulent fluxes.

Finally, the TRACMASS model (Döös, Jönsson, and Kjellsson 2017) is also based on a zeroth-order Markov process and is has been widely used to study marine turbulence.

2.4.2.1 Microplastic vertical distribution

Considering that the seabed is the destiny for many plastic debris entering the marine environment from the sea surface, negatively buoyant particles imminently start to settle upon entering the ocean, but there is substantial evidence of positively buoyant particles in the water column and in marine sediments (Song et al. 2018).

In particular, the sedimentation of microplastics particles is due to various processes, such as entrapment with organic detritus to form sinking aggregates, incorporation into sinking faecal pellets from plankton, fishes, seabirds and marine mammals, carriage by giant larvaceans, zooplankton and mesopelagic fishes, aggregation with suspended inorganic particles and biofouling. The relative importance of all these processes is generally unclear in different regions of the ocean.

For example, De La Fuente et al. 2021 investigating the sinking of microplastics in the water column evaluated the importance of inertia, Coriolis force, sub-grid turbulence and variable density of the particles. A standard modelling approach for the transport of noninteracting sinking particles has been used in this recent study, in which the vertical velocity of the particle results from the combination of the ambient fluid flow and a rising/settling velocity, $w_{r,s}$, characteristic of the particles, as in the following equation:

$$w_{r,s} = \left(1 - \beta_\rho\right)\boldsymbol{g}\tau_P \tag{59}$$

where $\beta_\rho = 3\rho/(2\rho_P + \rho)$ is a parameter depending on the fluid density and the particle density, ρ_P; so, particles heavier than seawater have $\beta_\rho < 1$, $\beta_\rho = 1$ in the case of neutrally buoyant particles, while positively buoyant particles have $\beta_\rho < 1$. In addition, $\tau_P = r^2/3\beta_\rho\nu$ is the Stokes time, i.e., the characteristic response time of the particle to changes in the flow, where r is the radius of the particle, assuming spherical particles.

Another, but very significant tool to investigate the vertical distribution of MP are similarity laws based on observational data. For instance, Kukulka et al. 2012 developed the following one-dimensional model, accounting for wind-driven mixing of buoyant plastics at the sea surface, so the vertical distribution of the MP concentration can be expressed as:

$$c(z) = C_s * \exp\left(zw_b/K_z^{surf}\right) \tag{60}$$

where C_s is the surface concentration, $w_b = 0.01$ m/s is the rise velocity of plastic pieces which depends on plastic size, shape and density and $K_z^{surf} = 1.5u_*\kappa H_S$ is the near-surface vertical turbulent diffusivity as in Eq. (40).

Another similarity law has been proposed by Egger, Sulu-Gambari, and Lebreton 2020, the vertical plastic concentration is calculated as a function of the water depth, according to:

$$c(z) = 10^{(a_E * \log(z) + b_E)} * CF \tag{61}$$

where a_E and b_E are parameters derived from the comparison between experimental data and simulations, CF is a correction factor.

2.4.3 Microplastic pollution in the Mediterranean Sea

The Mediterranean Sea, which is a semi-enclosed basin, is under significant pressure due to plastic pollution, as a result of high population densities, lack of consistent waste-

management schemes and large influxes of tourists and strategic merchant navigation (Boucher and Billard 2020).

The total plastic accumulated in the Mediterranean Sea is estimated in the order of magnitude of one million tonnes. Boucher and Billard 2020 estimates also an annual plastic leakage of two hundred thousand tonnes, made up 94% macroplastics and 6% microplastics. Moreover, according to the same report, the top three countries contributing to plastic leakage are Egypt, Italy and Turkey.

This basin has been subject of many oceanographic field studies and plastic sampling campaigns, their main characteristics are summarized in Tab. 1. These investigations are often focused on a particular sub basin of the Mediterranean Sea. The period analysed spans from 2010 to 2020. The most common instrument used is the manta trawl with a 0.333 mm mesh size, but this can be used only to sample the surface particles.

Table 1. MP sampling campaigns in the Mediterranean Sea.

Source	Domain	Period	Measurement approach
Collignon et al. 2012	Western basin	July - August 2010	manta trawl net (0.333 mm mesh size)
Fossi et al. 2012	Tyrrhenian Sea (Pelagos Sanctuary)	June - July 2011	WP2 standard net (0.2 mm mesh size)
Collignon et al. 2014	Bay of Calvi (Corsica)	August 2011 - August 2012	floating WP2 net (0.2 mm mesh size)
de Lucia et al. 2014	Gulf of Oristano (Sardinia)	July 2012 - July 2013	manta trawl (0.5 mm mesh size)
Suaria and Aliani 2014	Western basin	May - October 2013	visual survey
Faure et al. 2015	Western basin	September 2011 and August 2012	manta trawl (0.333 mm mesh size)
Cózar et al. 2015	Mediterranean Sea	May 2013	neuston net (0.2 mm mesh size)
Panti et al. 2015	Tyrrhenian Sea (Pelagos Sanctuary)	July 2012-2013	WP2 standard ring net (0.2 mm mesh size)
Pedrotti et al. 2016	Tyrrhenian Sea (Pelagos Sanctuary)	July - August 2013	manta trawl (0.333 mm mesh size)
Suaria et al. 2016	Western basin	May - June 2013	neuston net (0.2 mm mesh size)
Gajšt et al. 2016	Adriatic Sea	December 2012 - August 2014	epineuston net (0.3 mm mesh size)
Gündoğdu 2017	Bay of Iskenderun (Turkey)	February 2017	manta trawl (0.333 mm mesh size)
Gündoğdu and Çevik 2017	Bay of Iskenderun and Mersin (Turkey)	October - November 2016	manta trawl (0.333 mm mesh size)
Güven et al. 2017	Levantine basin	July - August 2015	manta net (0.333 mm mesh size)
van der Hal, Ariel, and Angel 2017	Levantine basin	Summer 2013 - Spring 2015	manta net (0.333 mm mesh size)
Fossi et al. 2017	Tyrrhenian Sea (Pelagos Sanctuary)	September 2014	High Speed Manta Trawl (0.33 mm mesh size)
Di-Méglio and Campana 2017	Western basin	2006 - 2015	visual survey
Vianello et al. 2018	Adriatic Sea	March - April 2014	manta trawl (0.333 mm mesh size)
Baini et al. 2018	Tyrrhenian Sea	November 2013 – May 2014	manta trawl (0.333 mm mesh size) and standard ring net (0.2 mm mesh size)
Ruiz-Orejón, Sardá, and Ramis-Pujol 2018	Balearic Islands	Summer 2014	manta trawl net (0.333 mm mesh size)

Schmidt et al. 2018	Gulf of Lyon	February 2014 - April 2016	manta trawl (0.78 mm mesh size)
de Lucia et al. 2018	Tyrrhenian Sea and Adriatic Sea	July - September 2015	manta trawl and plankton net (0.333 mm mesh size)
Zeri et al. 2018	Adriatic Sea	Autumn - Winter 2014-2015; Spring - Summer 2015	visual survey and manta net (0.333 mm mesh size)
Arcangeli et al. 2018	Western basin	October 2013 - September 2016	visual survey
de Haan, Sanchez-Vidal, and Canals 2019	Western basin	March - June 2015	manta trawl net (0.335 mm mesh size)
Palatinus et al. 2019	Adriatic Sea	April 2015	visual survey and manta net (0.308 mm mesh size)
Caldwell et al. 2019	Tyrrhenian Sea	May - June 2018	manta trawl net (0.333 mm mesh size)
Jemaa et al. 2021	Levantine basin	Spring - Autumn 2019	manta net (0.2 mm mesh size)
Adamopoulou et al. 2021	Levantine basin	2014-2020	manta net (0.333 mm mesh size)
Sayed et al. 2021	Levantine basin	September – October 2020	-
Fagiano et al. 2022	Western basin	Summer 2019	manta net (0.335 mm mesh size)
Pedrotti et al. 2022	Mediterranean Sea	June – November 2014	manta net (0.333 mm mesh size)

Furthermore, this basin has been investigated by means of many modelling studies; their main characteristics are summarized in Tab. 2. Most of them analysed the all Mediterranean Sea, while very few are focalised on a particular sub basin, such as the Adriatic or the Tyrrhenian Sea. Most of these studies examined only the surface dispersion of plastic debris; the studies of Coppini et al. 2018; Kaandorp, Dijkstra, and van Sebille 2020; Soto-Navarro et al. 2020 and Tsiaras et al. 2021 have tried to investigate even the particles dispersion in the vertical direction. The modelling framework is based on a hydrodynamic model, very often currents data are provided by the Copernicus Marine Environment Monitoring Service (CMEMS), which have been calculate by means of NEMO (Nucleus for European Modelling of the Ocean) (Madec et al. 2019), and a dispersion model. Moreover, for a more accurate analysis, some of these works have compared the numerical simulation results with experimental data.

Table 2. MP dispersion in the Mediterranean Sea. Modelling studies.

Source	Domain		Hydrodynamic model	Dispersion model	Comparison with experimental data
Eriksen et al. 2014	world oceans	2D	HYCOM	Pol3DD	yes
Mansui, Molcard, and Ourmières 2015	Mediterranean Sea	2D	NEMO	Ariane	no
Fossi et al. 2017	Ligurian & Sardinian Sea	2D	ROMS	generic LSM	yes
Carlson et al. 2017	Adriatic Sea	2D	ROMS	PaTATO	yes
Zambianchi, Trani, and Falco 2017	Mediterranean Sea	2D	-	-	no
Liubartseva et al. 2018	Mediterranean Sea	2D	NEMO	generic LSM	no
Coppini et al. 2018	Mediterranean Sea	3D	NEMO	generic LSM	no
Shchekinova and Kumkar 2018	Sicily Channel	2D	NEMO	LEEWAY	no
Guerrini, Mari, and Casagrandi 2019	Ligurian & Sardinian Sea	2D	NEMO	generic LSM	no

Macias et al. 2019	Mediterranean Sea	2D	GETM	Ichthyop	no
Pini et al. 2019	Tyrrhenian Sea	2D	NEMO	generic LSM	yes
Politikos et al. 2020	Ionian Sea	2D	POM	generic LSM	no
Soto-Navarro et al. 2020	Mediterranean Sea	3D	NEMO (MED36)	Ichthyop	no
Kaandorp et al. 2020	Mediterranean Sea	3D	NEMO	Ocean Parcels	yes
Mansui et al. 2020	Mediterranean Sea	2D	NEMO (MED12)	Ariane	yes
Guerrini, Mari, and Casagrandi 2021	Mediterranean Sea	2D	NEMO	generic LSM	no
Tsiaras et al. 2021	Mediterranean Sea	3D	POM	Pollani01	yes
Baudena et al. 2022	Mediterranean Sea	2D	NEMO	TrackMPD	yes

3. Materials & Methods

In this chapter, the conceptual scheme adopted to study the 3D dispersion of MP in the marine environment will be presented; in addition, all the information about the domain investigated, the input and output data, as well as the equations that govern the dispersion in the 3D LSM Wiener3D v6 and the original parameterization of the vertical turbulent diffusivity will be introduced.

3.1 Domain

The domain studied is the Tyrrhenian Sea (TYS) (longitude from 7.79° E to 16.5° E; latitude from 36.18° N to 44.81°N), which is a sub-basin of the Mediterranean Sea (see Fig. 5).

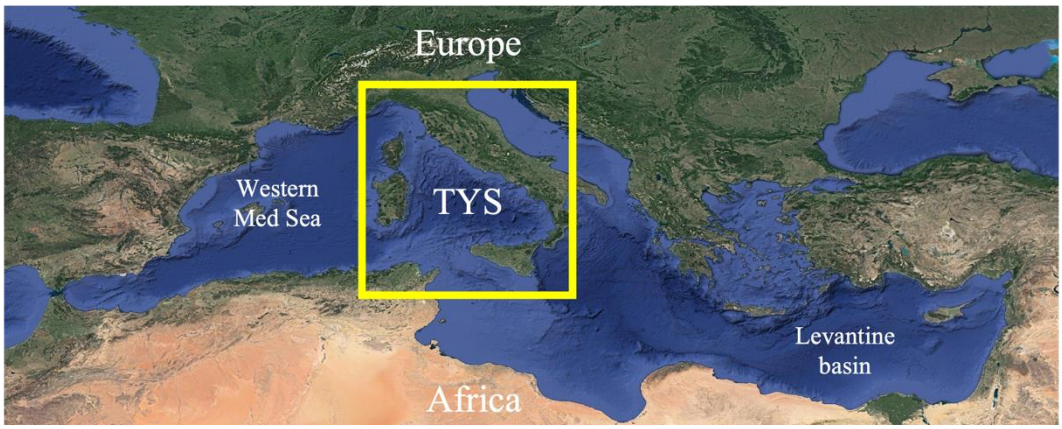

Figure 5. Mediterranean Sea. The Tyrrhenian Sea is highlighted in the yellow box.

It has a delicate coastal and marine ecosystem, considering that it is a densely populated basin which washes the western shores of the Italian peninsula as well as Sardinia, Sicily and Corsica Islands. The complex bathymetry of the Tyrrhenian Sea is displayed in Fig. (6).

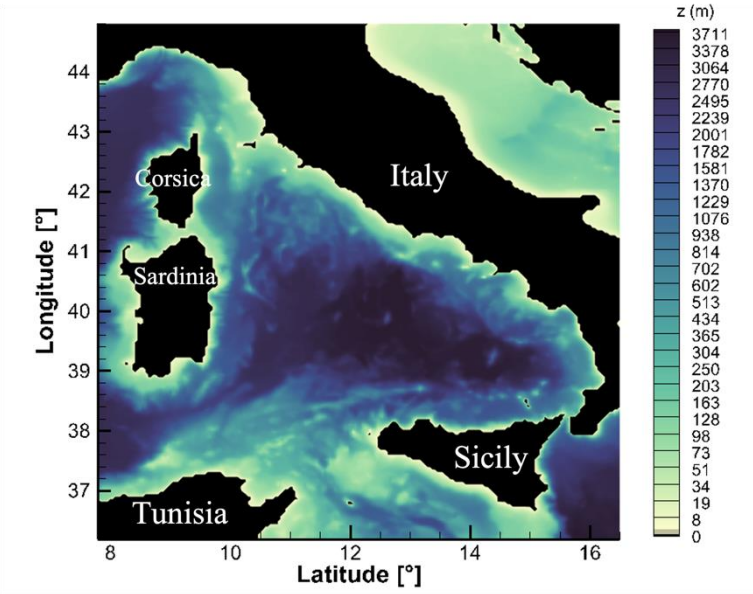

Figure 6. Bathymetry of the Tyrrhenian Sea.

The detailed physical characteristics and the circulation of this basin are extremely well described in Iacono et al. 2021. In synthesis, the Corsica and Sardinia Channels (to the North and southwest, respectively), connect the Tyrrhenian Sea to the westernmost part of the western

Mediterranean, while the Strait of Sicily (to the South), allows the communication between the western Mediterranean and the eastern sub-basin, i.e. Levantine basin.

The surface water mass of the Tyrrhenian Sea results from the inflow of Atlantic waters in the South-western part of the Mediterranean basin, through the Strait of Gibraltar: these currents after following the African coastline, crosses the southern part of the Sardinia Channel and bifurcates twice before reaching Sicily, the remaining current, from late Autumn to the beginning of Spring, enters the Tyrrhenian Sea; this stream then makes a wide cyclonic path along the Sicilian and Italian coasts, and finally outflows into the Ligurian Sea through the Corsica Channel; only a small fraction of it recirculates towards the South, exiting through the northern part of the Sardinia Channel. In the transition between Winter and Spring, the presence of an instability leads to the formation of anticyclones along the coast and cyclones on the offshore side of the current. During Summer, the region between the northern end of Corsica and the Elba Islands is now occupied by an anticyclone, denoted as the Ligurian anticyclone, which appears to separate the Tyrrhenian Sea circulation from that of the Ligurian Sea. At the same time, in the southern Tyrrhenian Sea, the Atlantic water stream is very weak, this allows the anticyclonic eddies formed near the coast in Spring to grow, becoming dominant elements of the local circulation, also sustained by the strengthening of the negative wind-stress curl pole present to the North of Sicily. The sea surface circulation in the Tyrrhenian sea described above is visible in Fig. (7).

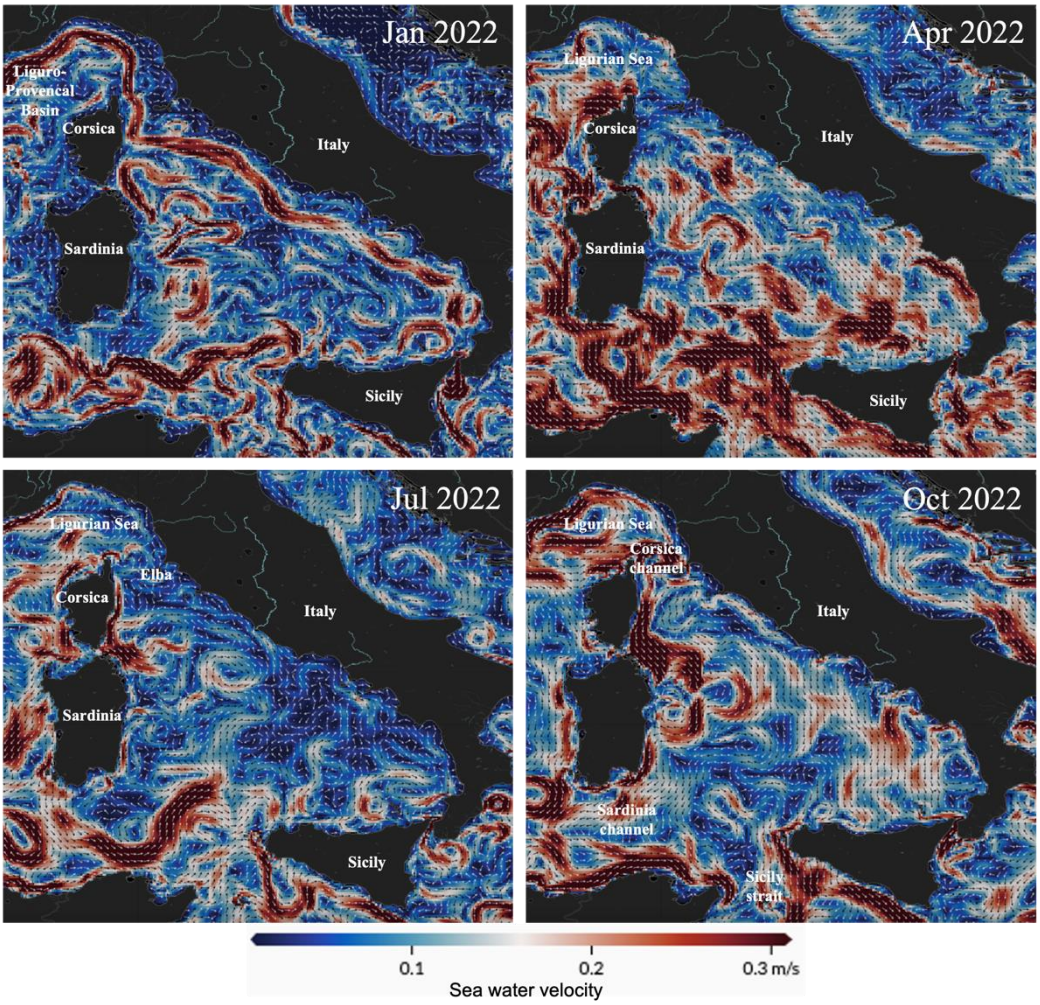

Figure 7. Sea surface currents circulation in the Tyrrhenian Sea during 2022.

The intermediate water masses have different origins: the Tyrrhenian Intermediate Water is of local origin from local Winter convection processes and it is found between 100 and 200 m; the Levantine Intermediate Water comes from the Levantine basin, enters the Tyrrhenian Sea through the Sicily Channel and occupies a deeper and wider layer (200-700 m).

Below 1000–1500 m, deep waters are formed during the processes of deep convection in the Gulf of Lion, and more generally in the Liguro-Provençal basin, and enter the Tyrrhenian Sea after crossing the Sardinia Channel. Little is known about the deep circulation, the scheme of the deep circulation is similar to that for the intermediate circulation, characterized by a cyclonic path along the coasts of the basin, controlled by the topography.

This basin has been chosen as test case, but the conceptual scheme adopted in this work for the simulation of the dispersion of MP could be extended to other basins, to the Mediterranean Sea or even in different world seas or oceans.

3.2 Input data

The inputs to the 3D LSM, used in this study, are: the bathymetry, the 3D daily velocity fields of the sea currents, the mixed layer depth and the friction velocity. They are provided by the CMEMS and by the European Centre for Medium-Range Weather Forecasts (ECMWF) and they are calculated by means of operational oceanographic and meteorological models. More in detail, three databases have been used in this study.

The 3D daily velocity fields of the marine currents and the mixed layer depth have been extracted from the MEDSEA_ANALYSISFORECAST_PHY_006_013 database (Clementi et al. 2021), with 1/24° (~4.5 km) horizontal resolution, 141 vertical levels and with a temporal coverage ranging from 01/05/2019 to present. This database allows short-term simulations.

The variables included in this database are: potential temperature, salinity, zonal and meridional velocity, sea surface height, mixed layer depth, seabed temperature. These oceanographic variables are calculated with the model NEMO version 3.6 (Madec et al. 2019). The model covers the whole Mediterranean Sea.

Following the quality information document of this database, the advection scheme for active tracers, temperature and salinity is a mixed up-stream/MUSCL (van Leer 1979). The vertical diffusion and viscosity terms are parameterized as function of the Richardson number as in Pacanowski and Philander 1981. The model iteratively computes air-surface fluxes of momentum, mass, and heat. The vertical background viscosity and diffusivity values are set to $1.2 * 10^{-6}$ m^2/s and $1.0 * 10^{-7}$ m^2/s, respectively. A quadratic bottom drag coefficient with a logarithmic formulation has been used. Tidal waves have been included. The model is forced by momentum, water and heat fluxes interactively computed by bulk formulae using the 1/10° horizontal-resolution operational analysis and forecast fields from ECMWF and the model sea surface temperature. The water balance is computed as Evaporation minus Precipitation and Runoff. The evaporation is derived from the latent heat flux, precipitation is provided by ECMWF as daily averages, while the runoff of the 39 rivers implemented is provided by monthly datasets.

The wave dynamic is solved by a Mediterranean implementation of the WaveWatch-III (WW3) code version 3.14 (Tolman 2009), which is coupled with NEMO v3.6.

The data assimilation system is based on the 3D variational ocean data assimilation scheme OceanVar, developed by Dobricic and Pinardi 2008 and later upgraded by Storto, Masina, and Navarra 2016. The observations that are assimilated are: along-track sea level anomaly from CLS SEALEVEL-TAC and in-situ vertical temperature and salinity profiles from Voluntary

Observing Ship-eXpandable Bathythermograph and ARGO floats.

Alternatively, the 3D daily velocity fields of the marine currents and the mixed layer depth have been extracted from the MEDSEA_MULTIYEAR_PHY_006_004 database (Escudier et al. 2020), with the same spatial resolution and coverage of MEDSEA_ANALYSISFORECAST_PHY_006_013 database, but it has a different temporal coverage ranging from 1987 to 2019. This database allows long-term simulations.

The variables included are: temperature, salinity, sea surface height, currents, mixed layer depth and eddy kinetic energy. These oceanographic variables are calculated with NEMO v3.6 and assimilated with OceanVar.

Moreover, the friction velocity has been extracted from the ECMWF 'ERA5 hourly data on single levels from 1959 to present, Copernicus Climate Change Service (C3S) Climate Data Store (CDS)' database (Hersbach et al. 2020). ERA5 data is available from 1950. The reanalysis combines model data with observations from across the world into a globally complete and consistent dataset. ERA5 provides hourly estimates for a large number of atmospheric, ocean-wave and land-surface quantities. Data has been regridded to a regular latitude-longitude grid of 0.25° for the reanalysis and 0.5° for the uncertainty estimate (0.5° and 1° respectively for ocean waves). There are four main sub sets: hourly and monthly products, both on pressure levels (upper air fields) and single levels (atmospheric, ocean-wave and land surface quantities).

3.3 MP sources estimation method

As explained in the paragraph (2.4.1), MP could be distinguished between primary or secondary, depending on their generation process. Primary MP are plastic pieces entering oceans already in microformat, such as fibres of synthetic clothes, tyres, city dust or pellets from cosmetics; on the other hand, secondary MP result from the fragmentation of bigger debris (Boucher and Friot 2017).

MP generation is directly related to human daily activities. Thus, in this study, the definition of MP sources has been carried out through an estimation method (Pini et al. 2020), that considers the population as a main factor.

Two types of sources have been considered: rivers and coastal cities.

The river contribution is proportional to the amount of the population resident in the entire water catchment basin, so even people living inland could contribute to MP discharge in the sea. This contribution has been calculated by overlapping the map of the main hydrographic basins, provided by the Institute for Environmental Protection and Research (ISPRA), with that of the resident population, provided by the Italian National Statistical Institute (ISTAT); the mouth of the rivers has been considered as the source point. On the other hand, coastal cities have been treated as direct inputs, also adding the contribution of the population living in smaller towns nearby.

The output of this estimation method is an unevenly spaced distribution of the MP sources along the Italian shores. In the Mediterranean Sea, 135 sources have been estimated, as it is visible in Fig. (8), between rivers and coastal cities, to which a load of 0.06 kg of MP per person per year (Boucher and Billard 2020) have been assigned.

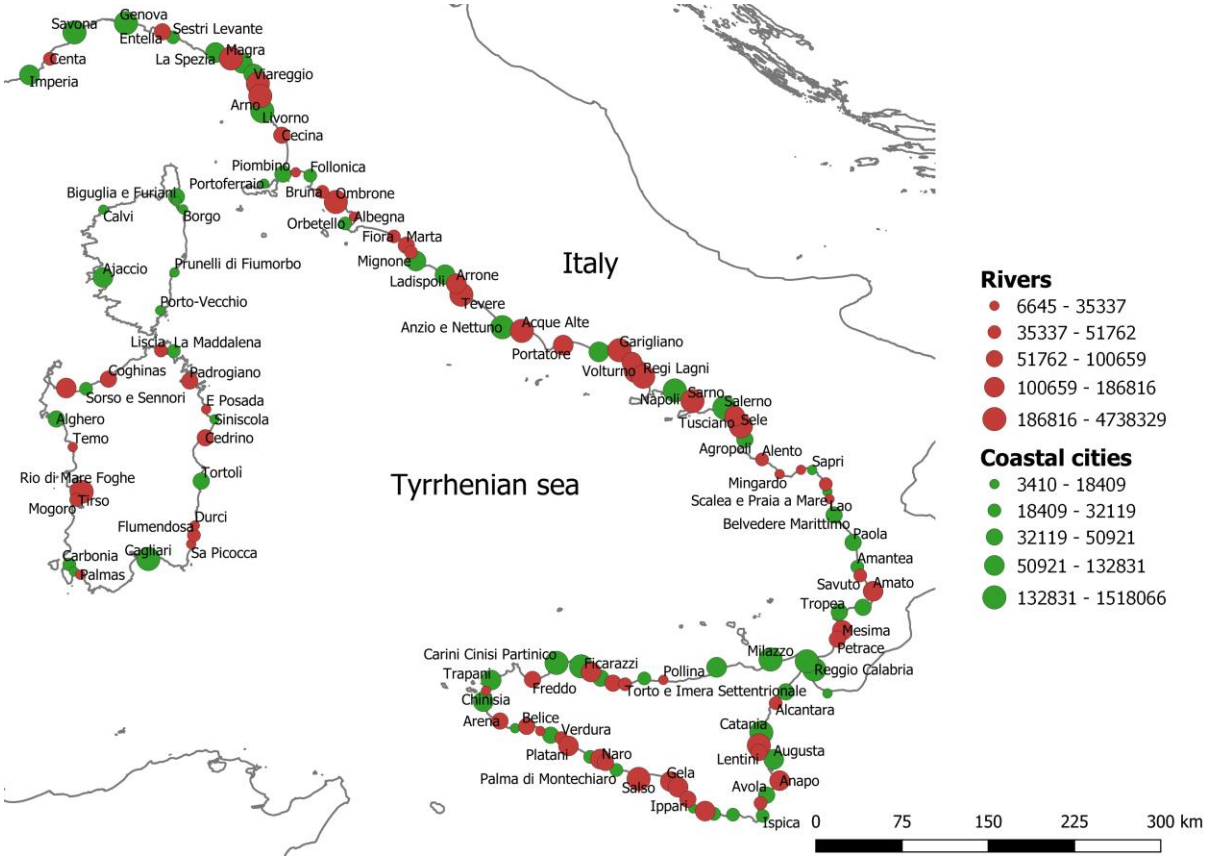

Figure 8. MP sources estimated in the Tyrrhenian Sea.

3.4 3D Lagrangian Stochastic Model

The 3D Lagrangian Stochastic Model Wiener3D v6 faces the MP dispersion in the marine environment calculating pathways, concentration fields and accumulation zones of MP. It needs as input the mean field of the sea currents, the mixed layer depth and the friction velocity and it gives back the MP concentration.

As presented in paragraph (2.3.2), this model is based on the mass balance equation. It calculates the concentration of the particles, $\bar{c}$, (which in this case study are microplastics, but they could be any passive pollutant) by integrating the number of particles in a cell.

Along the three directions, particle trajectories are due to contribution of the mean field of the sea currents and the sub-grid turbulence, which is represented by a stochastic process; in addition, the physical characteristics of the particles have a role in the vertical dispersion.

More in detail, the displacement of the particles in the domain is described by the Wiener process, which is a zeroth-order Markov model. Among the various possible Markov processes presented in paragraph (2.3.2.2), it has been chosen because it provides a good model performance (Onink et al. 2022); in fact, many LSMs use this approach to describe the 3D dispersion of MP in the marine environment, e.g. Parcels (Delandmeter and van Sebille 2019; Lange and van Sebille 2017), TRACMASS (Döös et al. 2017), OpenDrift (Dagestad et al. 2018).

Developing Eq. (52), the displacement of the MP in the 3D is described by the Wiener equation in the following way:

$$dX = \bar{u}dt + \sqrt{2K_X}d\mu_X \tag{62}$$

$$dY = \bar{v}dt + \sqrt{2K_Y}d\mu_Y \tag{63}$$

$$dZ = \left(\bar{w} + \frac{dK_z}{dz}\right)dt + \sqrt{2K_z}d\mu_Z + w_{r,s} \tag{64}$$

where $\bar{u}$, $\bar{v}$ and $\bar{w}$ are the components of the mean currents; K_X and K_Y are the horizontal turbulent diffusivity coefficients and they are set equal to 30 m^2/s (Pini et al. 2018), K_Z is the vertical turbulent diffusivity, it is variable and it is parameterized as in the next paragraph; $d\mu$ is a random variable, uncorrelated over time, with zero mean and variance equal to dt.

In the Eq. (62-64), the first term on the right describes the mean field of the sea currents and it is provided by CMEMS, as described in paragraph (3.2). In particular, the vertical component, $\bar{w}$, has been obtained by the continuity equation.

The second term is a stochastic process which represents the sub-grid turbulence.

Furthermore, in the vertical direction, to ensure mixing, the equation also provides a drift term, $(dK_z/dz)\,dt$, to avoid anomalous accumulations in areas of low turbulence. On the other hand, in the horizontal direction the drift term is null because the turbulent diffusivity has been assumed constant.

As pointed out in Pini et al. 2018, in the horizontal direction a variable turbulent diffusivity is necessary only in the first steps of the dispersion and close to the source; for longer time steps and far away in the domain, as in this case, the mean field of the sea currents have the major contribute in the dispersion, so it is possible to use a constant horizontal turbulent diffusivity. In the framework of the study of the MP dispersion in the marine environment, other works have uses a costant horizontal turbulent diffusivity, e.g. Liubartseva et al. 2018.

Moreover, to study the MP dispersion in the water column, it is important to take also into account the characteristics of the MP, such as density, size and shape, so in the vertical direction a rising/settling velocity term, $w_{r,s}$, has been added.

As described in paragraph (3.3), each MP source is identified by its position and the number of inhabitants which determines its contribution. MP particles, released in the TYS from the anthropogenic sources, all have the same mass (i.e. 560 g), but they are released in a number proportional to the less populated source.

The releasing of MP during the simulation is continuous, with a time step of $600s$.

In addition, some MP removal processes have been modelled: beaching and sedimentation on the bottom; in fact, the 10% of the MP particles hitting the shores or the bottom remain trapped on the coasts of Italy or lie definitely on the sea floor. This value has been chosen considering that MP lying on the beaches or on the bottom could also be washed away or resuspended. The biofouling process have not been modelled yet.

As output, the model gives the 3D concentration fields of microplastics.

The simulated MP concentrations have been studied analysing their statistical moments and by means of surface maps, vertical sections, temporal series and profiles. In particular, MP concentration profiles have been analysed in 60 points unevenly spaced in the simulated basin, i.e. the Tyrrhenian Sea, and they are shown in Fig. (9).

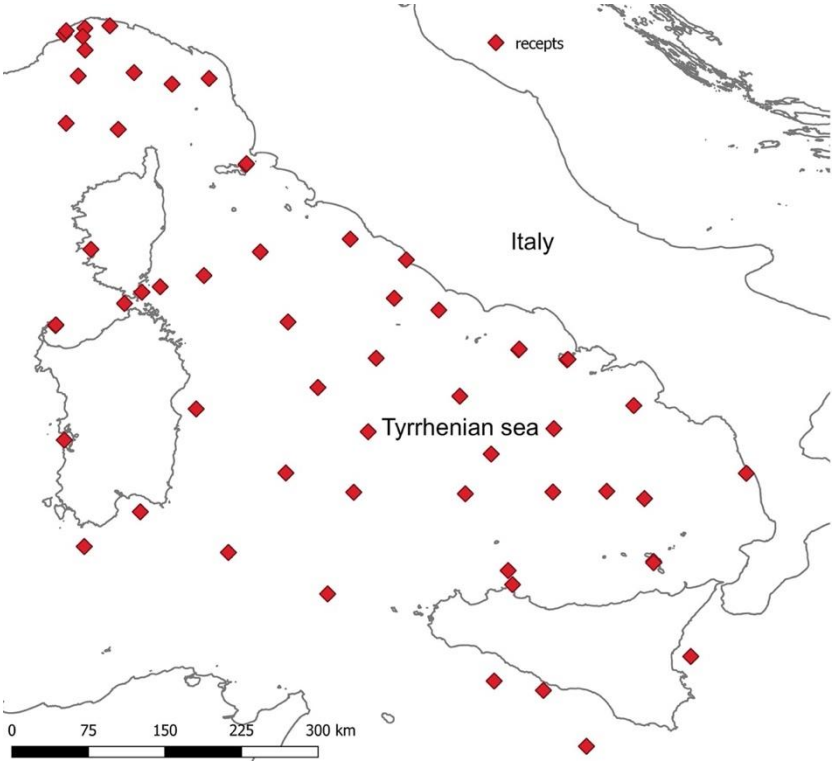

Figure 9. Unevenly spaced points investigated in the Tyrrhenian Sea.

3.4.1 Vertical turbulent diffusivity parameterization

In this work, to face the problem of choosing the vertical turbulent diffusivity parameterization as accurate as possible for the representation of the vertical turbulence and as suitable as possible for LSMs, different possibilities have been tested.

As first attempt, it has been assumed $K_z(z) = 0$ m^2/s, but it means that no turbulence occurs within the water column; this disagrees with the experimental evidences: as it has been pointed out in the paragraph (2.1.2), many turbulent phenomena affect the dispersion in the marine environment, especially in the OSBL, so it is mandatory to model them. The 3D LSM Ariane (Blanke and Raynaud 1997) uses a null vertical turbulent diffusivity.

As second attempt, it has been assumed $K_z(z)$ as constant. More specifically, it has been set $K_z(z) = 1.2 * 10^{-4}$ m^2/s, which is the background value of the parameterization developed by Pacanowski and Philander 1981. Considering that means that the vertical turbulence has not a seasonal variability; actually, the vertical turbulent phenomena during the cold season, due to stronger winds blowing on the sea surface or due to the cooling of the water masses from the atmosphere, are more intense than in the warm season, where on the contrary the water column is stratified. In addition, a diurnal, but weaker, cycle happens because the sea water is warmed during the day enhancing the stratification of the water column, while during the night it loses its heat in favour of the atmosphere, so convection and mixing start. Therefore, the different atmospheric conditions depending on the period of the year directly affect the mixing or the stratification of the water column.

So, assuming $K_z(z)$ as constant is not a realistic option, but in order to obtain a more physically based parameterization for the vertical turbulent diffusivity, the physical characteristics of the sea water have been analysed: temperature, salinity and density. These results are presented in paragraph (4.1).

Since the mixed layer depth varies as the density varies, Ri can be considered as a valuable parameter to assess turbulence in the water column, as third attempt, it has been assumed that $K_z(z)$ essentially depends on Ri, as in the parameterization of Pacanowski and Philander 1981, as it has been described in paragraph (2.3.1.2) by Eq. (38).

This parameterization is implemented in NEMO v3.6 and it has been used to calculate the oceanographic data provided in the MEDSEA_ANALYSISFORECAST_PHY_006_013 database.

In Fig. (10), it is possible to notice that $K_z(z)$ calculated with the P&P81 parameterization is of the order of magnitude of 10^{-4} m^2/s, it has its maximum value close to the surface, but in general $K_z(z)$ has a very low variability in the mixed layer; below the mixed layer $K_z(z) = 1.2 * 10^{-4}$ m^2/s. These characteristics are not able to represent adequately the vertical turbulence in the mixed layer: first of all, close to the surface it has been expected a non-zero value, but not the maximum value, because turbulent eddies do not have enough space to develop (Wang et al. 2016); furthermore, the very low variability of $K_z(z)$ within the water column cannot describe mixing in this boundary layer, in fact measurements carried out by Sloyan 2005 in the southern hemisphere oceans have shown that turbulent mixing is vertically and spatially non-uniform.

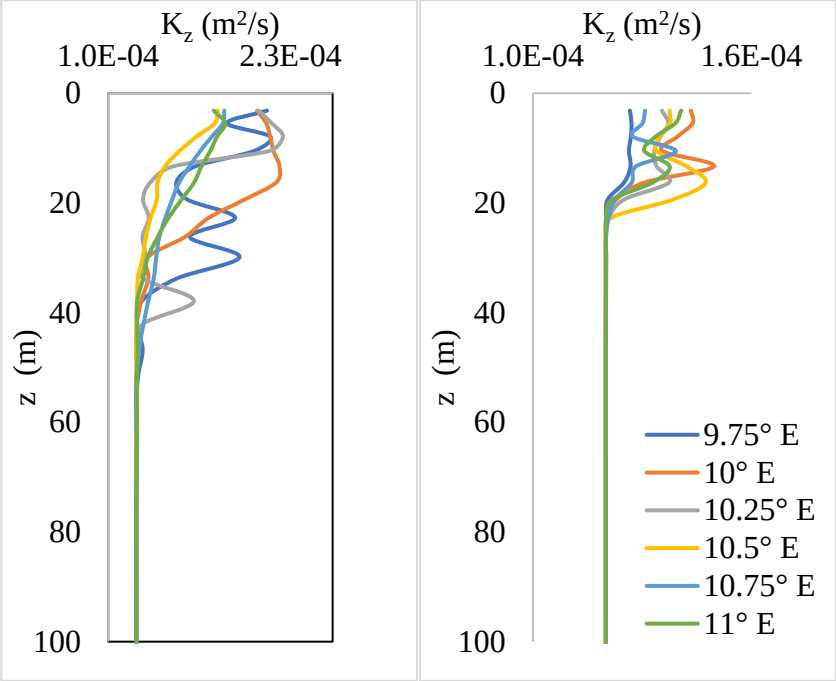

Figure 10. Vertical turbulent diffusivity profiles calculated in the Tyrrhenian Sea with the parameterization developed by Pacanowski and Philander 1981 *(Latitude: 39.6° N; Longitude from 9.75° E to 11° E, each 0.25°). Left panel represents the variability of the vertical turbulent diffusivity during Winter (i. e. 21/03/2019), while right panel represents a Summer case (i. e. 21/09/2019).*

Following these arguments and with the aim of obtaining a parameterization for the vertical turbulent diffusivity physically based and suitable for LSMs, in this work, the vertical turbulent diffusivity $K_z(z)$ has been described starting from the Taylor theory, as already mentioned in par. (2.3.2.2), which states that:

$$K_z(z) = \sigma_w^2(z) * T_L(z)$$

The vertical velocity variance, $\sigma_w^2(z)$, has been measured in realistic conditions and the results are reported in few studies, such as D'Asaro 2001 and Tseng and D'Asaro 2004; few other

studies approached this topic using LES simulations, such as Li, Garrett, and Skyllingstad 2005. The characteristics of these works are summarized in the Tab. (3).

Table 3. Vertical velocity variance measurements in world oceans.

Source	Domain	Period	Measurement approach
D'Asaro 2001	North Pacific Ocean	January 1995	Neutrally buoyant Lagrangian floats
Tseng and D'Asaro 2004	North Pacific Ocean	September – November 2000	Neutrally buoyant Lagrangian floats
Gargett and Grosch 2014	North Atlantic Ocean	May – October 2003	ADCP 5 beam
Scully et al. 2015	North Atlantic Ocean	October – December 2013	ADVs
Jarosz et al. 2017	North Pacific Ocean	October 2012 – March 2013	ADCPs
Wijesekera et al. 2017	North Pacific Ocean	October 2012 – March 2013	ADCP 4 beam

In Fig. (11) are represented the experimental profiles of the vertical velocity variance of the studies mentioned in the Tab. (3); specifically, the vertical velocity variance is scaled with the friction velocity and the depth with the mixed layer depth.

In this figure, two different relative maximum are visible almost in all the curves, except that of Wijesekera et al. 2017, one close to the surface and the other below the half of the mixed layer depth. It is possible to suppose that two sources act to enhance turbulence at different depths: the first could be related to shear turbulence, in fact the wind blowing on the sea surface enhance mixing in the first meters of the water column, while the other could be due to an unknown forcing.

The analysis of these profiles highlights that it is important to represent both these peaks.

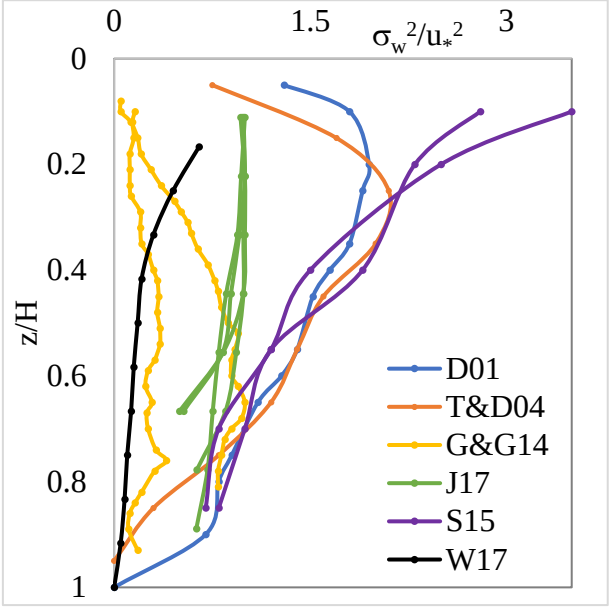

Figure 11. Vertical velocity variance, scaled with the friction velocity, profiles measured during sampling campaigns in the Atlantic (Gargett and Grosch 2014; Scully et al. 2015) *and Pacific ocean* (D'Asaro 2001; Jarosz et al. 2017; Tseng and D'Asaro 2004; Wijesekera et al. 2017).

Among these research work, in this study, the vertical velocity variance has been parameterized using the experimental data reported in Tseng and D'Asaro 2004. This work has been chosen because their measurements are Lagrangian, in fact they were performed with Lagrangian floats in the North Pacific ocean. Lagrangian floats are designed to follow accurately the three-dimensional motion of the water surrounding them in turbulent flows (D'Asaro et al. 1996).

As it is visible in the Fig. (12), these data have been well fitted with a function which results from the sum of a Gauss and Rayleigh distribution.

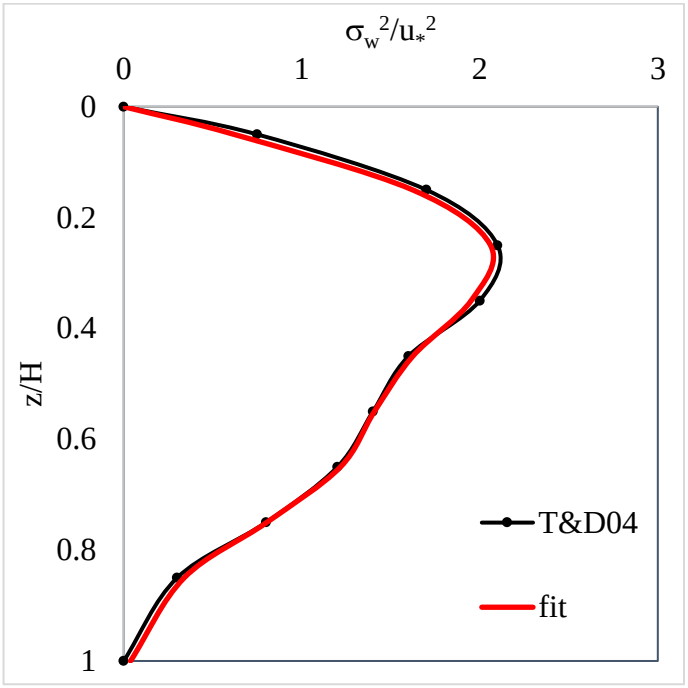

Figure 12. Vertical velocity variance profile measured by Tseng and D'Asaro 2004 *described by Eq. (65).*

In detail, it has been obtained a novel relationship:

$$\frac{\sigma_w^2}{u_*^2} = \beta_\sigma \frac{1}{\sqrt{2\pi S_G^2}} e^{-\frac{(Z-\mu)^2}{2S_G^2}} + \gamma_\sigma \frac{Z}{S_R^2} e^{-\frac{Z^2}{2S_R^2}} \tag{65}$$

In Eq. (65), $Z = z/H$; while the best fit has been obtained with these parameters: $\beta_\sigma = 0.24$, $\gamma_\sigma = 0.94, \mu = 0.66$, $S_G = \sigma_G/H = 0.12$ and $S_R = \sigma_R/H = 0.26$, where σ_G and σ_R are the standard deviation of the Gauss and Rayleigh distribution, respectively.

The sum of these two different functions allows to consider both peaks evidenced in Fig. (11).

So, the vertical velocity variance has been calculated with a similarity law based only on the mixed layer depth and the friction velocity as scaled parameters, these data are usually calculated with operational oceanography and meteorological models.

The Lagrangian integral time scale, $T_L(z)$, is the second term in the Eq. (54), it is the integral of the autocorrelation of the vertical velocity fluctuations. As it has been pointed out in paragraph (2.2), it is a key parameter in the framework of the study of the turbulent dispersion from a Lagrangian point of view. Since no field data about the spatial-temporal dimension of the vertical turbulent eddies are available, the Lagrangian integral time scale has been obtained thanks to its connection with the Eulerian integral time scale $T_E(z)$, adapting the study of the atmospheric turbulent boundary layer by Hay and Pasquill 1959 to the marine turbulence. So, $T_L(z)$ could be expressed as in the following equation:

$$T_L(z) = \beta_T T_E(z) \tag{66}$$

where $\beta_T = \gamma/i$, γ is an experimental coefficient which depends on the thermal stratification and $i = \sigma_w/\bar{u}$ is the turbulence intensity, where $\bar{u}$ is the average velocity of the sea currents.

In the frozen turbulence hypothesis, $T_E(z) = L_E(z)/\bar{u}$, where $L_E(z)$ is the Eulerian length scale, and considering that $L_E(z)$ could behave like the mixing length $l(z)$ (Li et al. 2017), the relation between the two time scales could be expressed in the following way:

$$T_L(z) = \frac{\gamma l(z)}{\sigma_w(z)} \tag{67}$$

where, in case of neutral boundary layer, $\gamma = 0.4$ (Anfossi et al. 2006).

The mixing length in the Prandtl boundary layer is $l(z) = \kappa * z$. In this work, the mixing length is described by the following bilinear law (Craig & Banner, 1994):

$$l(z) = \begin{cases} \kappa(z_0 + z), & z < H/2 \\ \kappa(z_0 - z + H), & z > H/2 \end{cases} \tag{68}$$

where $z_0 = 0.1$ m is the rugosity scale. $l(z) = 0.04$ m at the sea surface, so, this parameterization accounts for surface wave breaking turbulent mixing. Moreover, Eq. (68) assumes that $l(z)$ is minimum at the boundaries, at both the sea surface and at the bottom of the mixed layer, and maximum at the half of the mixed layer, where eddies have much more space to develop. The fact that the size of the eddies at the boundaries is smaller, is confirmed even by the fact that there the dissipation, which occurs at small scales, is maximum (Stacey, Monismith, and Burau 1999).

So, combining the Eq. (65 and 68), it has been obtained the following parameterization for the vertical turbulent diffusivity within the mixed layer:

$$K_z(z) = \gamma * \sigma_w(z) * l(z) \tag{69}$$

Hereinafter this parameterization will be called ZPL, from the surnames of the researcher that worked on that (i.e. Giovanni Leuzzi, Agnese Pini and Simone Zazzini).

In addition, the value of $K_z(z)$ at the sea surface has been set equal to the value at the second level of the water column, according to that at the sea surface the drift term in Eq. (64) should be null.

Furthermore, below the mixed layer, it has been assumed that $K_z(z) = 1.2 * 10^{-4}$ m^2/s.

As example, in Fig. (13) are represented the vertical turbulent diffusivity, the mixing length and the vertical velocity variance profiles calculated in the Tyrrhenian Sea with the ZPL parameterization. It is possible to see that within the mixed layer, the order of magnitude of $K_z(z)$ ranges between 10^{-4} and 10^{-2} m^2/s, either in Winter and in Summer. The maximum of vertical turbulence is at the half of the mixed layer due to the fact that the eddies have much more space to develop, but at this depth $K_z(z)$ could be twice higher in Winter than in Summer; also $l(z)$ has his maximum at the same depth and it could be of the order of 10 m in Winter and 3 m in Summer. On the contrary, $K_z(z)$, $l(z)$ and $\sigma_w(z)$ are minimum at the boundaries.

ZPL parameterization, due to its dependency on the friction velocity and the mixed layer depth, brings information about both shear and eddy length scale. In fact, during the warm season, the water column is stratified and the values of the friction velocity and the mixed layer depth are similar, so the profiles do not have significant differences in their form and in their order of magnitude, as it is visible in the bottom panels of Fig. (13). On the other hand, during the cold season, the mixing processes enhance the mixed layer depth and it means an higher value of the mixing length; also the vertical velocity variance have a direct proportionality with the

friction velocity, for example the blue curve in the top panels of Fig. (13) has the maximum value of the vertical velocity variance and the maximum value of u_*, i.e. $2.36 * 10^{-4}$ m/s.

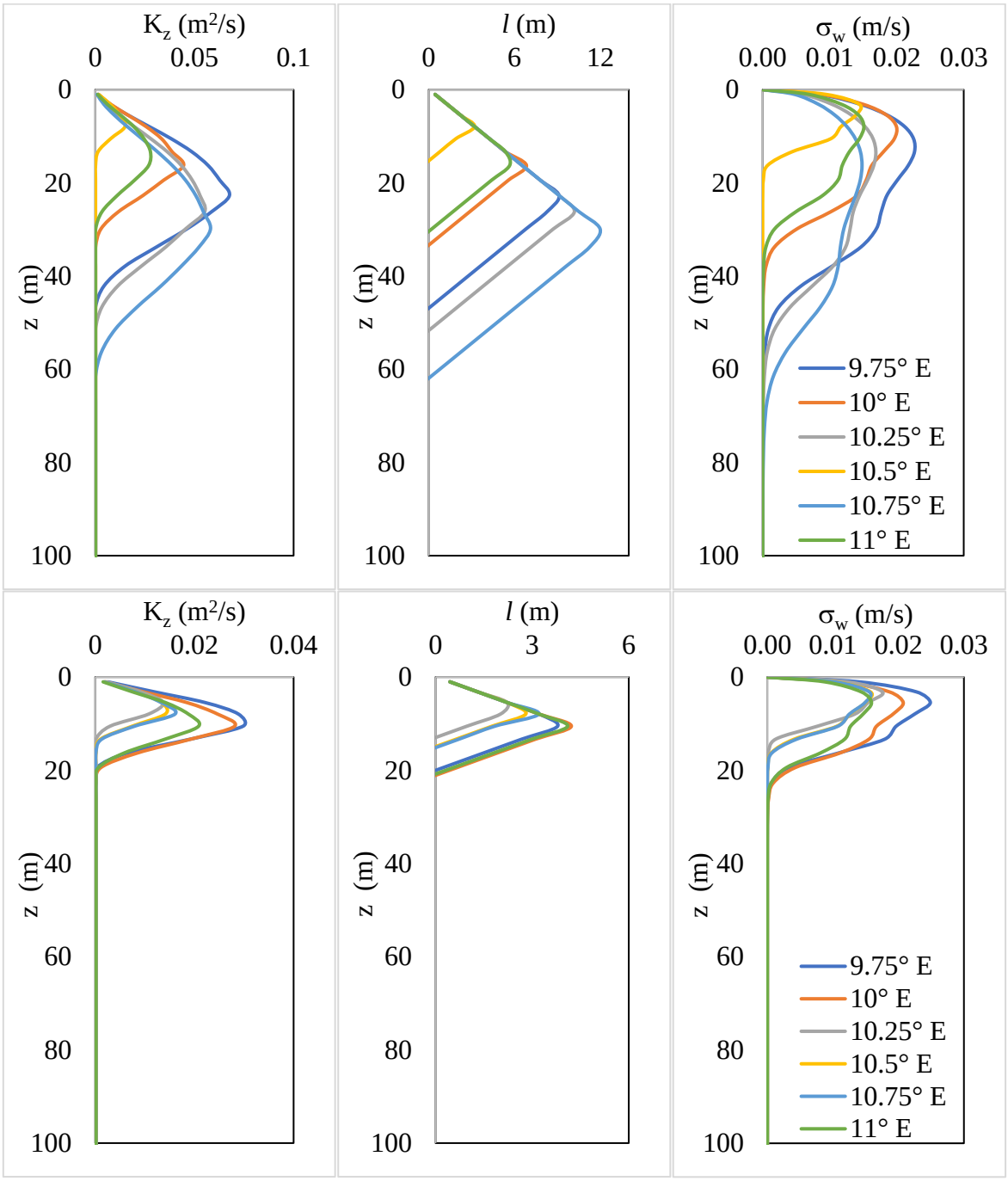

Figure 13. Vertical turbulent diffusivity, mixing length and vertical velocity standard deviation profiles calculated in the Tyrrhenian Sea with the ZPL parameterization (Latitude: 39.6° N; Longitude from 9.75° E to 11° E, each 0.25°). Top panels represent the variability of the vertical turbulent diffusivity, of the mixed layer and of the vertical velocity standard deviation during Winter (i. e. 21/03/2019), while bottom panels represent a Summer case (i. e. 21/09/2019).

3.4.2 Simulation configurations

The domain investigated during the simulations of the dispersion of MP with Wiener3D v6, described in the previous paragraph, has a 210x208 horizontal grid with spatial resolution of 1/24° (≃ 4 km) and 120 vertical levels with depth ranging from 1 m to 3710 m.

The characteristics of the simulations have been summarized in the next Table.

Table 4. Simulation configuration performed with the LSM Wiener3D v6.

	Lagrangian Stochastic Model Wiener3D v6
Domain	Tyrrhenian sea
	210x208 horizontal grid, spatial resolution: 1/24° (≃ 4 km)
	120 vertical levels with different depth (from 1 m to 3710 m)
Temporal coverage	10 year (2010-2019) (3652 days)
	Integration time step: $dt = 600$ s
Inputs	3D daily mean fields of sea currents, CMEMS (1/24°) (Escudier et al. 2020)
	2D daily fields of mixed layer depth, CMEMS (1/24°) (Escudier et al. 2020)
	2D daily mean fields of friction velocity, ECMWF (1/4°) (Hersbach et al. 2020)
Turbulent diffusivity	Horizontal turbulent diffusivity: 30 m^2/s
	Vertical turbulent diffusivity parameterized by means of Eq. (66)
MP sources	135 (70 rivers, 65 coastal cities)
	0.06 kg of MP per inhabitant per year
	$4 \cdot 10^6$ per year released particles
	Constant emission, every 10 minutes
MP characteristics	Neutrally buoyant: $w_{r,s} = 0$ m/s; $\rho_P = \rho = 1025$ kg/m^3
	Positively buoyant: $w_r = -0.0005$ m/s; $\rho_P = 900$ kg/m$^3 < \rho$
	Negatively buoyant: $w_s = 0.0005$ m/s; $\rho_P = 1040$ kg/m$^3 > \rho$
MP removal processes	Beaching
	Sedimentation on the bottom
Outputs	3D daily, monthly, seasonal and annual fields of MP concentration
	Vertical profiles of MP concentration, turbulent diffusivity and vertical velocities

Furthermore, with the aim to execute a sensitivity analysis, five different simulations have been performed with the version 3 (v3) of the LSM Wiener3D v6, investigating the role of the mean currents, the sub-grid turbulence and the rising/settling velocity in the dispersion of MP in the water column.

Wiener3D v3 is a basic version of the LSM utilized only with the purpose to study the role of the mean currents, the sub-grid turbulence and the rising/settling velocity in the dispersion of MP in the water column. In fact, in Wiener3D v3 each MP source discharge in the Tyrrhenian Sea the same number of MP particles, but with a mass proportional to its population. The release is every 20 min, with an integration time step of 1200 s. In addition, Wiener3D v3 does not model any MP removal processes.

The characteristics of the simulations with Wiener3D v3 have been summarized in the next Table.

Table 5. Simulation configuration performed with the LSM Wiener3D v3 - sensitivity analysis.

	Lagrangian Stochastic Model Wiener3D v3
Domain	Tyrrhenian sea
	210x208 horizontal grid, spatial resolution: 1/24° (≃ 4 km)
	120 vertical levels with different depth (from 1 m to 3710 m)
Temporal coverage	3 year (2019-2021) (860 days)
	Integration time step: $dt = 1200$ s
Inputs	3D daily mean fields of sea currents, CMEMS (1/24°) (Clementi et al. 2021)
	2D daily fields of mixed layer depth, CMEMS (1/24°) (Clementi et al. 2021)
	2D daily mean fields of friction velocity, ECMWF (1/4°)
Turbulent diffusivity	Constant horizontal turbulent diffusivity: 30 m^2/s
	Variable vertical turbulent diffusivity
MP vertical trajectories	$\overline{w}$, $K_z(z) = 0$, $w_{r,s} = 0$
	$\overline{w} = 0$, $K_z(z) = \gamma * \sigma_w(z) * l(z)$, $w_{r,s} = 0$
	$\overline{w}$, $K_z(z) = 1.2 * 10^{-4}$ m^2/s, $w_{r,s} = 0$
	$\overline{w}$, $K_z(z) = \gamma * \sigma_w(z) * l(z)$, $w_{r,s} = 0$
	$\overline{w}$, $K_z(z) = \gamma * \sigma_w(z) * l(z)$, $w_s = 0.0005$ m/s
MP sources	135 (70 rivers, 65 coastal cities)
	0.06 kg of MP per inhabitant per year
	$4 \cdot 10^6$ per year released particles
	Constant emission, every 20 minutes
MP removal processes	None
Outputs	3D daily, monthly, seasonal and annual fields of MP concentration
	Vertical profiles of MP concentration, turbulent diffusivity and vertical velocities

3.5 Field data

As it has been highlighted in Tab. (1), in the Mediterranean Sea the sampling campaigns were carried out almost exclusively with manta trawl, so only MP surface concentration data are available. Considering that, MP vertical concentration simulated with the 3D LSM v6 in the Tyrrhenian Sea has been compared with MP concentration profiles sampled all over the world oceans.

A dataset of vertical microplastics concentration profiles collected across the entire water column have been compiled to validate the simulated concentration profiles; it is constituted by a total of 113 profiles and 479 data points. For the sampling stations the date, the coordinates, the mixed layer depth and the MP concentration have been considered.

The main characteristics of the sampling campaigns are summarized in Tab. (6) and (7).

Table 6. Field data characteristics (I).

Source	Domain	Period	Measurement approach	Instrument mesh	Sample analysis method
Kukulka et al. 2012	North Atlantic Ocean	June - July 2010	multi-level trawl	333 μm	not reported
Bagaev et al. 2018	Baltic Sea	October 2015 - September 2016	10-l Niskin bottle	174 μm	microscope 40x
Song et al. 2018	South Korea Sea	July - August 2016-17	pump	20 μm	μFTIR imaging system
Pabortsava and Lampitt 2020	Atlantic Ocean	September - November 2016	pump	55 μm	FTIR imaging system
Egger et al. 2020	Pacific Ocean	November - December 2018	multi-level trawl	333 μm	visually
Li et al. 2020	Indian Ocean, West Pacific Ocean	November 2018 - April 2019	pump	60 μm	visually + stereomicroscope

Table 7. Field data characteristics (II).

Source	Number of sampling cruises	Number of concentration profiles	Number of sampling points	Unit	Particle size range	Average concentration
Kukulka et al. 2012	13	13	46	MP/m^3	not specified	0.1 MP/m^3
Bagaev et al. 2018	4	35	81	MP/l	0.5 - 5 mm	400 MP/m^3
Song et al. 2018	8	41	123	MP/m^3	20 μm – 5 mm	871 MP/m^3
Pabortsava and Lampitt 2020	12	12	141	MP/l	32 - 651 μm	2000 MP/m^3
Egger et al. 2020	5	6	53	MP/m^3 g/m^3	500 μm – 5 cm	0.04 MP/m^3
Li et al. 2020	6	6	35	MP/m^3	0.03 - 6.33 mm	2 MP/m^3
tot	48	113	479			

The samples were collected in the Atlantic Ocean (Kukulka et al. 2012; Pabortsava and Lampitt 2020), in the Pacific Ocean (Egger et al. 2020; Li et al. 2020; Song et al. 2018), in the Indian Ocean (Li et al. 2020) and in the Baltic Sea (Bagaev et al. 2018).

The measurements were collected with multi-stage trawls that consecutively sample fixed depths or depth ranges (Egger et al. 2020; Kukulka et al. 2012). These nets have mesh sizes of 0.33 mm and generally sample high- and medium-buoyancy particulates. Bagaev et al. 2018 filtered samples collected via Niskin bottles with a 0.8 μm filter and thus was able to filter out smaller particulates with lower rise velocities. A pump with a finer mesh size was the measurements approach of Li et al. 2020, Pabortsava and Lampitt 2020 and Song et al. 2018.

4. Results

The results of the study of the turbulent dispersion in the OSBL with the 3D LSM Wiener3D v6 will be presented in this chapter.

It is divided in two parts: the first one is devoted to the comparison of the original parameterization of the vertical turbulent diffusivity with others already used; moreover, the second part summarises the main results of the simulations of the 3D dispersion of MP in the Tyrrhenian Sea presenting MP concentration maps and profiles. A special attention was paid to the comparison of the simulated MP concentration with experimental data, with the intention to validate the LSM Wiener3D v6.

References are made to 'Summer' and 'Winter' as shorthand for the periods of heating and cooling respectively.

4.1 Physical characteristics of the sea water

In this work, the density has been calculated following the UNESCO formula (Millero and Poisson 1981), in which it depends on temperature, salinity and pressure. The data of temperature and salinity have been extracted from the MEDSEA_ANALYSISFORECAST_PHY_006_013 database (Clementi et al. 2021).

In particular, as displayed in Fig. (14), during Winter, in the Tyrrhenian Sea, the sea surface temperature could be around 14°C, the salinity 38.2 g/kg and the density 1028.7 kg/m^3. These values remain constant until a strong gradient occurs, which highlights the depth of the pycnocline. During Winter, the mixed layer could be even 100 m deep.

On the other hand, during Summer, the sea surface temperature could be 26°C or so, the salinity 38.3 g/kg and the density 1025.8 kg/m^3. In this case, the pycnocline is very shallow; during Summer, it is very common in the world oceans to have a mixed layer 10 m deep. After this depth, the water column is strongly stratified and poorly mixed.

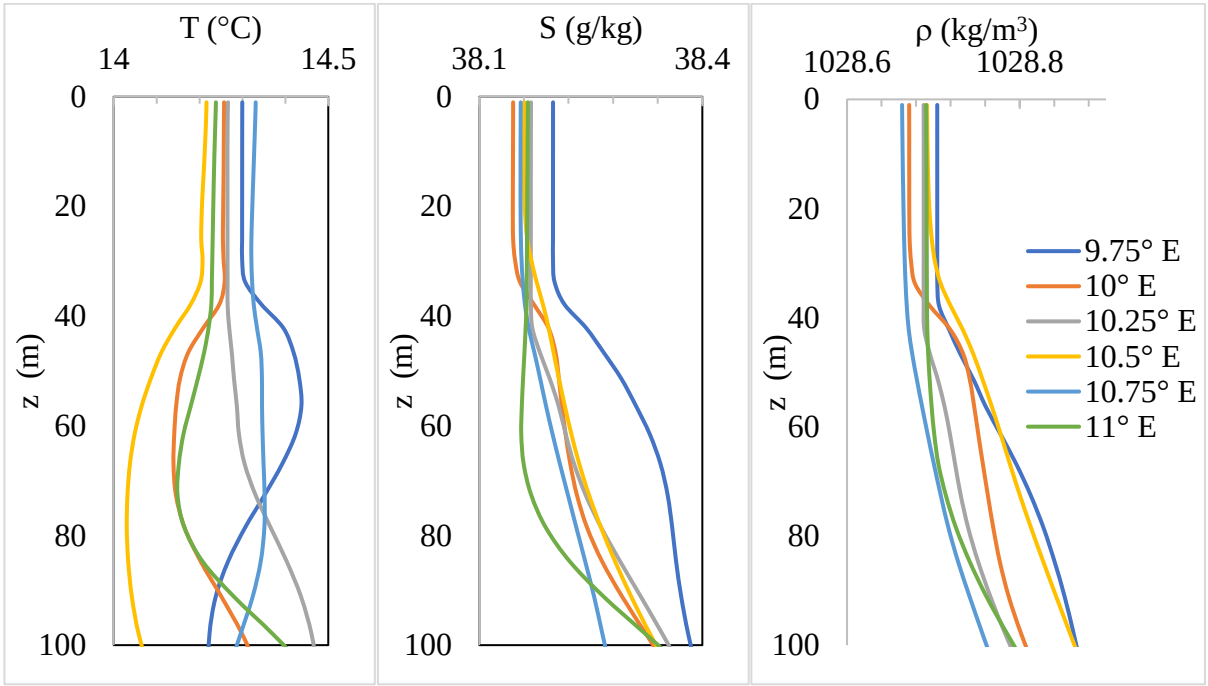

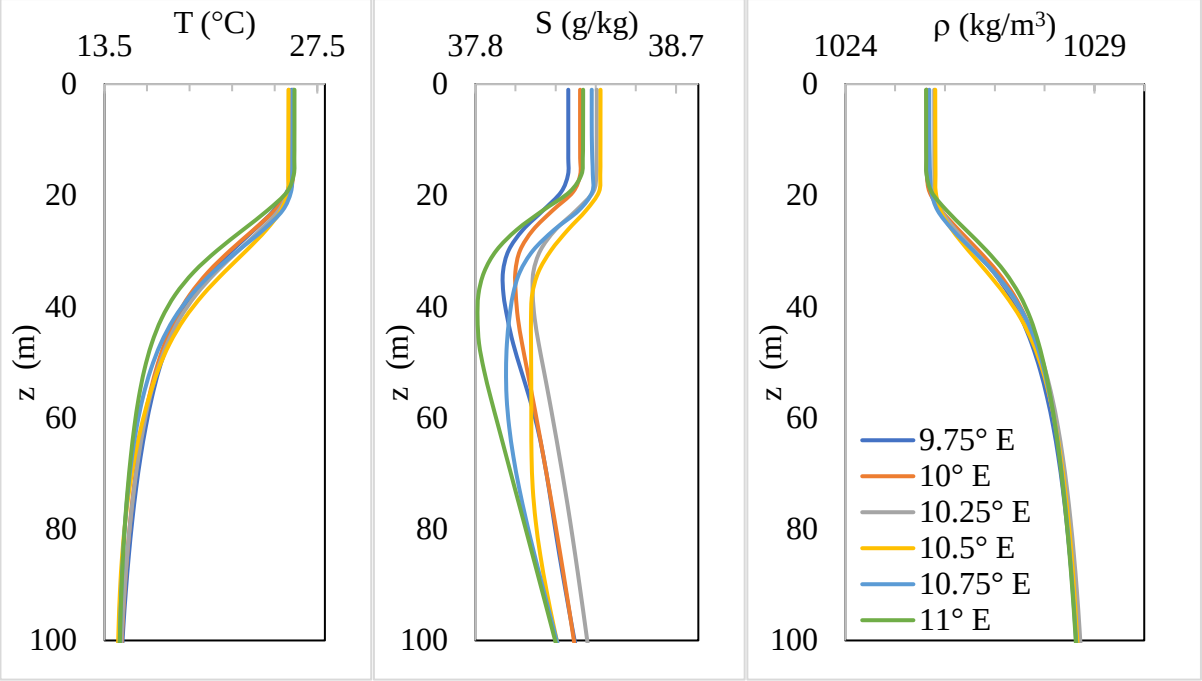

Figure 14. Temperature, salinity and density profiles calculated in the Tyrrhenian Sea (Latitude: 39.6° N; Longitude from 9.75° E to 11° E, each 0.25°). Top panels represent the physical characteristics of seawater during Winter (i. e. 21/03/2019), while bottom panels represent a Summer case (i. e. 21/09/2019).

In Fig. (15), as example, it is visible the behaviour of the mixed layer depth and its seasonality. The mixed layer depth has been calculated as the water column depth where the density increases at least by 0.01 kg/m^3 (de Boyer Montégut et al. 2004) and it has been extracted from the MEDSEA_ANALYSISFORECAST_PHY_006_013 database (Clementi et al. 2021). The mixed layer deepens each Winter, while during Summer it becomes shallower. In particular, in the Tyrrhenian Sea, it is around 10 m deep when the water column is stratified; while during Winter when the mixing phenomena happen, its depth could enhance even to 100 m.

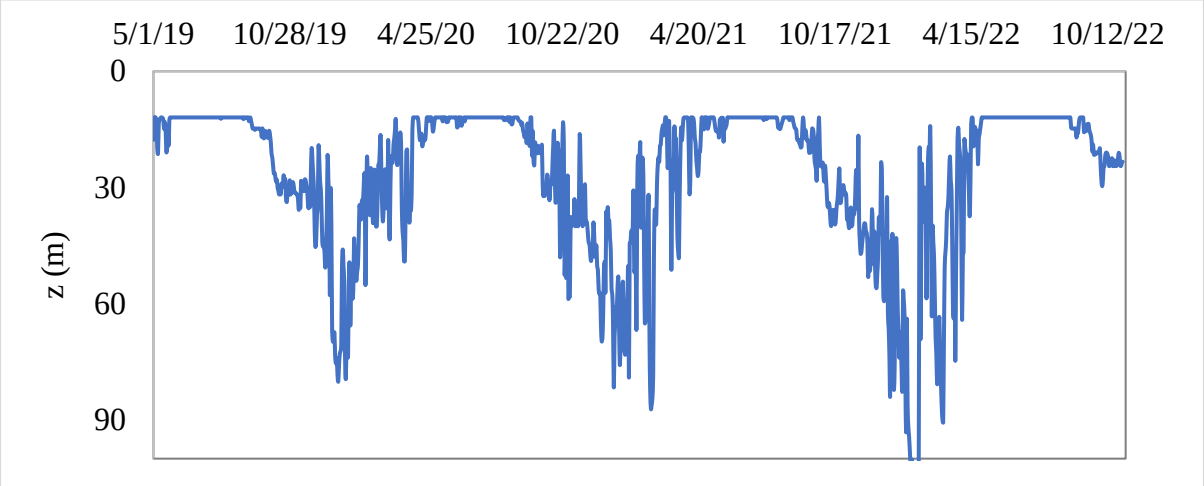

Figure 15. Mixed layer depth seasonal cycle in a point in the Tyrrhenian Sea (Latitude: 39.6° N; Longitude: 11° E).

Following these arguments, it could be useful to use a parameter which can represents the seasonal cycle of the mixed layer depth, as key parameter representing the turbulent state of the water column. Thus, the stratification of the water column is commonly represented by the Richardson number, Ri, which is a dimensionless number that expresses the ratio of the energy produced by the buoyancy term (N^2) to that produced by the flow shear term (S^2), as in Eq. (37).

As shown in Fig. (16), shear prevails over buoyancy in the mixed layer during Winter, $Ri < 0.25$ and it means that vertical turbulence could mix efficiently this layer; on the other hand, below the mixed layer depth the stratification overbears turbulence and Ri grows significatively. The value of Ri below which the seawater column becomes dynamically unstable and turbulent is usually taken as $Ri = 0.25$, although suggestions in the literature range from 0.2 to 1 (Zaron and Moum 2009).

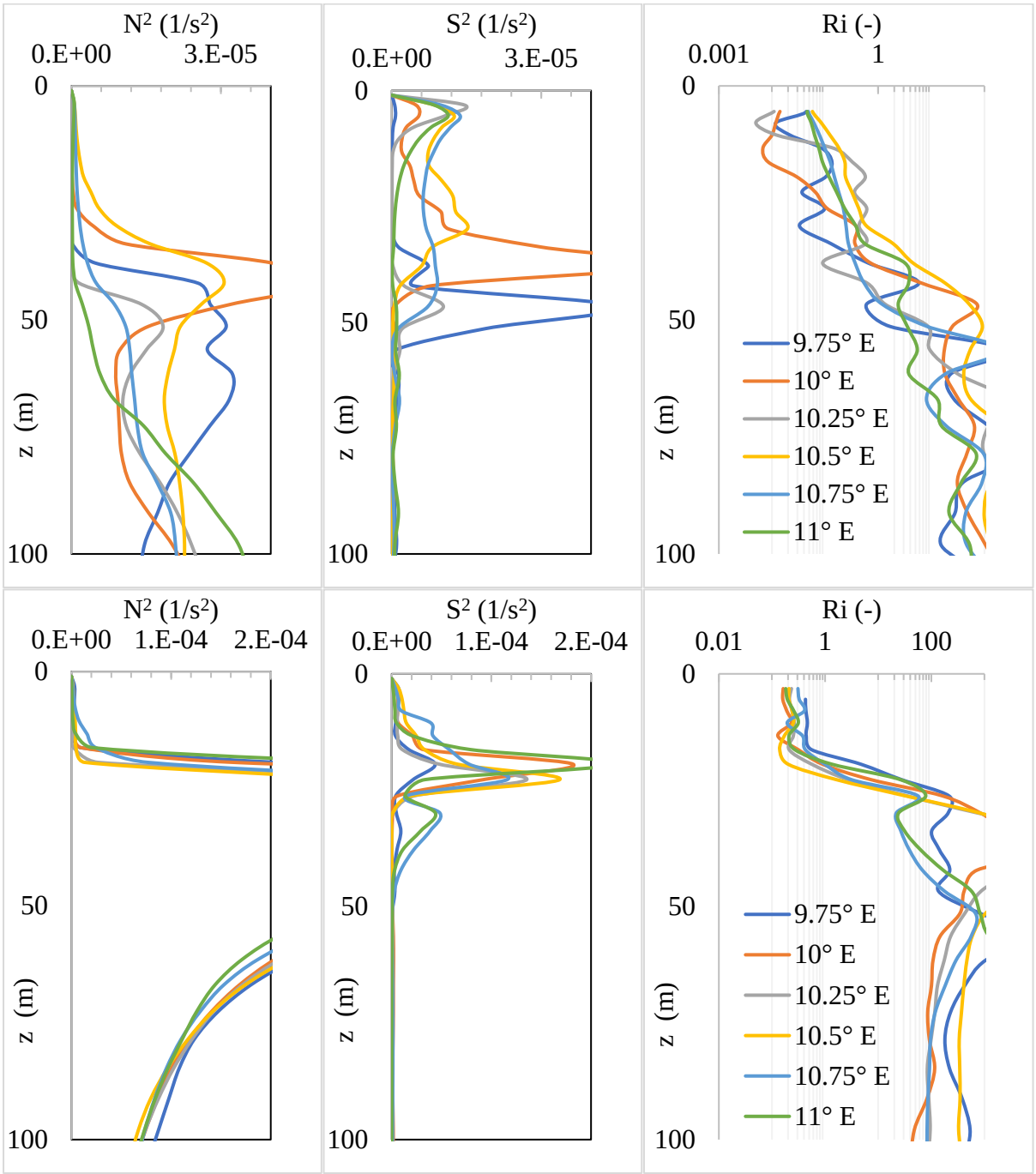

Figure 16. Buoyancy, Shear and Richardson number calculated in the Tyrrhenian Sea (Latitude: 39.6° N; Longitude from 9.75° E to 11° E, each 0.25°). Top panels represent the stratification of the water column during Winter (i. e. 21/03/2019), while bottom panels represent a Summer case (i. e. 21/09/2019).

4.2 Comparison between different vertical turbulent diffusivity parameterizations

The ZPL parameterization, developed in this work, has been compared with others already used in literature. In particular, the P&P81 (Pacanowski and Philander 1981), the KPP (Large et al. 1994) and the SWB parameterization (Kukulka et al. 2012), extended by Poulain et al. 2019, have been considered. These parameterizations have been well enough described in paragraph (2.3.1.2).

In Fig. (17-18) are displayed the $K_z(z)$ profiles calculated with the aforementioned different parameterizations, but in the same days and the same locations in the Tyrrhenian Sea.

Analysing $K_z(z)$ calculated by P&P81, it is possible to notice that it is of the order of magnitude of 10^{-4} m^2/s, it has its maximum value close to the surface, but in general $K_z(z)$ has a very low variability in the mixed layer; below the mixed layer $K_z(z) = 1.2 * 10^{-4}$ m^2/s. These characteristics are not able to represent adequately the vertical turbulence in the mixed layer: first of all, close to the surface it has been expected a non-zero value, but not the maximum value, because turbulent eddies do not have enough space to develop; furthermore, $K_z(z)$ has a very low variability within the water column.

Furthermore, $K_z(z)$ evaluated by means of KPP rises from a small non-zero value at $z = 0$ to a maximum at $z = 1/3H$, before dropping to $K_z(z) = K_B$ for $z \leq H$.

Moreover, SWB allows the estimation of the surface breaking waves turbulence defining a constant $K_z(z)$ in the first meters of the water column. On the other hand, SWB does not provide any information about the stratification of the water column, in fact it is impossible to have an estimation of the mixed layer depth from Fig. (17-18); the profile of $K_z(z)$, after the first meters, decreases as $|z|^{3/2}$.

Thus, comparing these four parameterizations, it is possible to affirm that within the mixed layer $K_z(z)$ estimated by P&P81 is two order of magnitude lower than the others. Moreover, below the mixed layer, the background value of $K_z(z)$ parameterized by P&P81 and ZPL is of the order of 10^{-4}; while KPP has a background value of the order of 10^{-5}.

The behaviour of $K_z(z)$ calculated by SWB is consistently different than the others $K_z(z)$ profiles, either because it is constant in the first meters either because it does not have any specification about the mixed layer depth, so the entire water column is treated in the same way. Moreover, as it has been mentioned earlier, $K_z(z)$ profile by P&P81 has a very low variability in the mixed layer failing to represent the heterogeneity of turbulence.

Finally, comparing these four $K_z(z)$ parameterizations is possible to say that, ZPL and KPP are both physically based and their $K_z(z)$ profiles look like similar, but the main advantage of ZPL is that is directly related to LSMs via $\sigma_w^2(z)$ and $T_L(z)$. In fact, these quantities are essential input for LSM: $\sigma_w^2(z)$ is a measure of turbulence, which can be directly obtained by means of field measurements (e.g. Tseng and D'Asaro 2004) or estimated with parameterizations; $T_L(z)$ gives information about the dimension of the eddies and, since no measures of $T_L(z)$ have been performed, it can be estimated with empirical laws. In ZPL parameterization, $\sigma_w^2(z)$ depends only on u_* and H, as in Eq. (65) and $T_L(z)$ can be estimated from the mixing length.

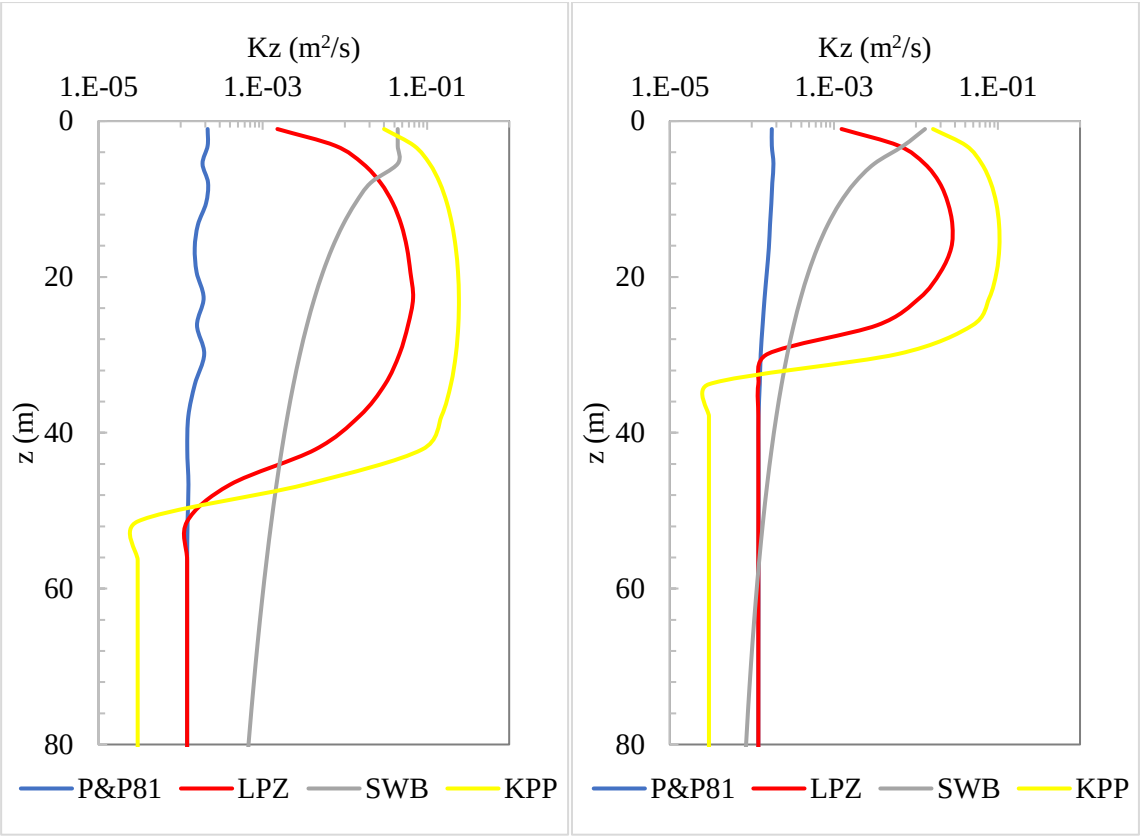

Figure 17. Vertical turbulent diffusivity profiles calculated in the TYS with the P&P81, ZPL, SWB and KPP param., during Winter (i. e. 21/03/2019). Left panel coord.: 39.6° N; 9.75° E. Right panel coord.: 39.6° N; 11° E.

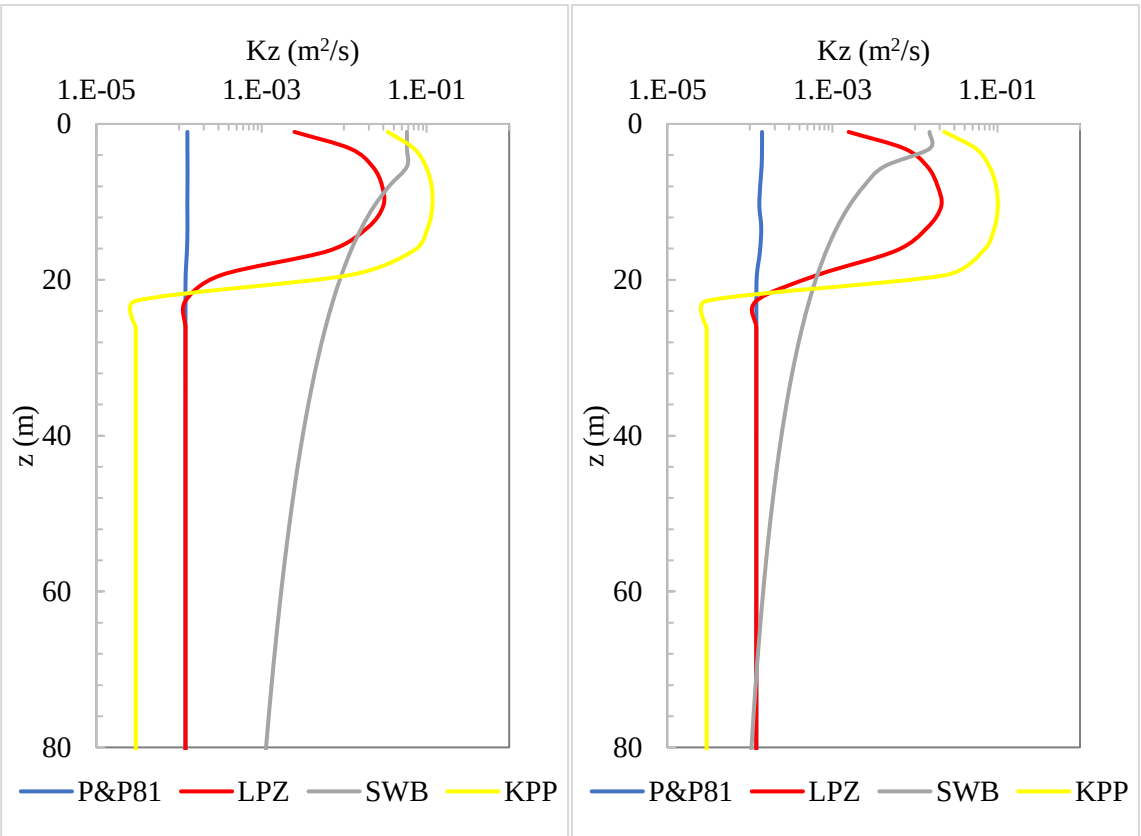

Figure 18. Vertical turbulent diffusivity profiles calculated in the TYS with the P&P81, ZPL, SWB and KPP param., during Summer (i. e. 21/09/2019). Left panel coord.: 39.6° N; 9.75° E. Right panel coord.: 39.6° N; 11° E.

4.3 3D MP dispersion in the Tyrrhenian Sea

The ZPL parameterization of $K_z(z)$ has been implemented in the 3D LSM Wiener3D v6, presented in paragraph (3.4); with this model, several simulation with different settings have been carried out, in order to investigate the 3D MP dispersion in the Tyrrhenian Sea. In this paragraph, the validation of the model, by means of a comparison with experimental data, will be presented; in addition, a detailed attention will be given to the results of the simulations investigating the role of the mean currents, the sub-grid turbulence and the physical characteristics of the particles in the dispersion of the MP within the water column.

4.3.1 3D MP dispersion testing different values of K_z

In this paragraph, the results of the sensitivity analysis with the LSM Wiener3D v3 will be presented. With the intention to simulate the 3D dispersion of MP in the Tyrrhenian Sea, MP particles have been discharged from each source with a mass proportional to its population; the releasing of MP was continuous, every $1200s$, all MP have been considered as passive tracers and neutrally buoyant (except case E). No MP removal processes have been modelled, such as beaching, sedimentation on the bottom or biofouling.

The period simulated ranges from 06/05/2019 to 11/09/2021.

Five different simulations have been performed with the aim to investigate the role of the mean currents, the sub-grid turbulence and the rising/settling velocity in the dispersion of MP within the water column. All the details of the simulations are summarized in Tab. (8).

Table 8. Simulation configuration with Wiener3D v3.

Simulation	Mean currents	Sub-grid turbulence	Rising/settling velocity
A	yes	$K_z(z) = 0$	$w_{r,s} = 0$ m/s
B	no	$K_z(z) = LPZ$	$w_{r,s} = 0$ m/s
C	yes	$K_z(z) = 1.2 * 10^{-4}$ m^2/s	$w_{r,s} = 0$ m/s
D	yes	$K_z(z) = LPZ$	$w_{r,s} = 0$ m/s
E	yes	$K_z(z) = LPZ$	$w_s = 0.0005$ m/s

In Fig. (19) are represented the statistical moments (average, standard deviation and skewness) of the depth of the all particles dispersed in the Tyrrhenian Sea. The analysis of these graphs allows to evaluate the statistics of the dispersion of the MP particles within the water column.

The common characteristics of the all different simulations are that the depth of the particles averaged over the entire Tyrrhenian Sea increases progressively during the simulation period; also the standard deviation grows and confirms that the pollutant cloud progressively widens; finally, the asymmetry coefficient, after about 200 days from the start of the simulations, remains constant, indicating that the plume during the sinking widening maintains its shape.

More in detail, considering the simulation B, where no mean vertical currents or rising/settling velocities have been considered, so, particles are vertically dispersed by means of only the sub-grid turbulence occurring on the water column (see Eq. (69)), they sink but they are unable to disperse over the entire water column and they remain confined into the first 100 m. On the other hand, in the case E where the mean currents, the sub-grid turbulence and the rising/settling velocity interact and transport the particle, they can exceed even 1000 m.

These two are borderline cases. The other cases (A, C or D), where different values of $K_z(z)$ are tested, as reported in Tab. 8, give similar results. On average terms, after some weeks, case C, where $K_z(z) = 1.2 * 10^{-4}$ m^2/s, and case D, where $K_z(z)$ is obtained by means of ZPL parameterization, behave the same. The MP dispersion in case A, in which the sinking of the

particles is due only to the vertical currents velocities, given that the diffusivity has been set equal to zero, is weaker during the first days of the simulation, but after about 200 days the particles have the same behaviour.

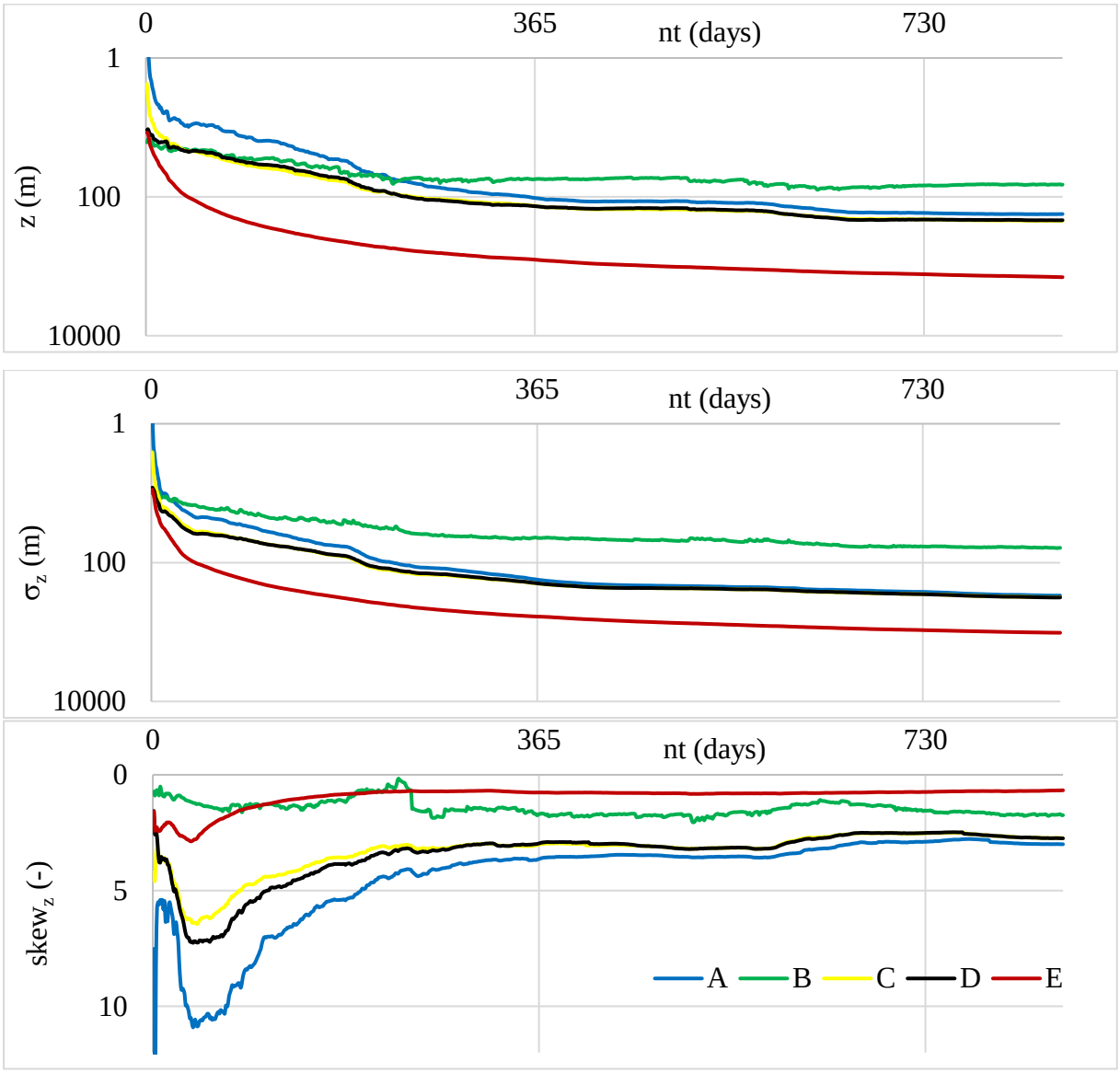

Figure 19. Statistical moments of the depth of all the particles dispersed in the Tyrrhenian Sea (the average value is represented in the top panel, the standard deviation in the centre panel and the skewness in the bottom panel). The period simulated ranges from 06/05/2019 to 11/09/2021. The different curves refer to the results of the simulations presented in Tab. 8.

Further information can be obtained from Fig. (20-21), where are shown the average MP surface concentration maps in the Tyrrhenian Sea during Winter and Summer seasons, respectively. The MP concentrations are averaged over the period from 06/05/2019 to 11/09/2021. These maps highlight the difference between the distinct simulation configuration, i.e. the different role of the vertical mean currents, the sub-grid turbulence and the rising/settling velocity in the dispersion of MP in the water column, and the features of the dispersion during different periods of the year.

In general, surface MP concentration is higher during Summer, this could be of the order of 10^{-4} g/m^3 or greater, because the water column is stratified; for the same reason the horizontal transport is enhanced, so it is possible to notice accumulations of the particles even in the middle of the basin. On the other hand, during Winter, more intense mixing processes disperse more efficiently the particles vertically, so MP surface concentration are lower than in Summer and they have their maximum close to the Italian coasts, where the sources are.

More in detail, in case A, when $K_z(z) = 0$, a great accumulation of MP could be spotted in the centre of the basin, because MP are transported in all the directions by the mean currents, but sub-grid vertical mixing processes are neglected.

Furthermore, comparing the results of the simulation C, where $K_z(z) = 1.2 * 10^{-4}$ m^2/s, and D, where vertical turbulence is parameterized as function of the mixed layer depth and the friction velocity, it is possible to see that using a constant vertical diffusivity means to underestimate vertical mixing during Winter, while to overestimate it during Summer. In fact, MP surface concentration is higher in case C than case D, either offshore either onshore, but the opposite happens during Summer. So, the parameterization used in case C is unable to represent the turbulent phenomena that mix the particles on the water column.

So, even though on average terms simulations A, C and D have similar results, a more accurate parameterization of the vertical turbulence allows to consider the variability of the turbulent phenomena that occur on the water column and therefore how differently these disperse the particles. Thus, an appropriate parameterization of the vertical turbulence gives a better description of the dispersion of the MP in the Tyrrhenian Sea.

As it has already said, in case E, where all of the particles have a settling velocity equal to 0.0005 m/s, MP sink rather quickly close to the sources and they tend to accumulate on the continental shelf, both in Summer and in Winter. Thus, MP surface concentration in the middle of the basin is lower than 10^{-6} g/m^3. This contribution to the vertical advection changes completely the behaviour of the particles and thus it will be further deepen in the next paragraph.

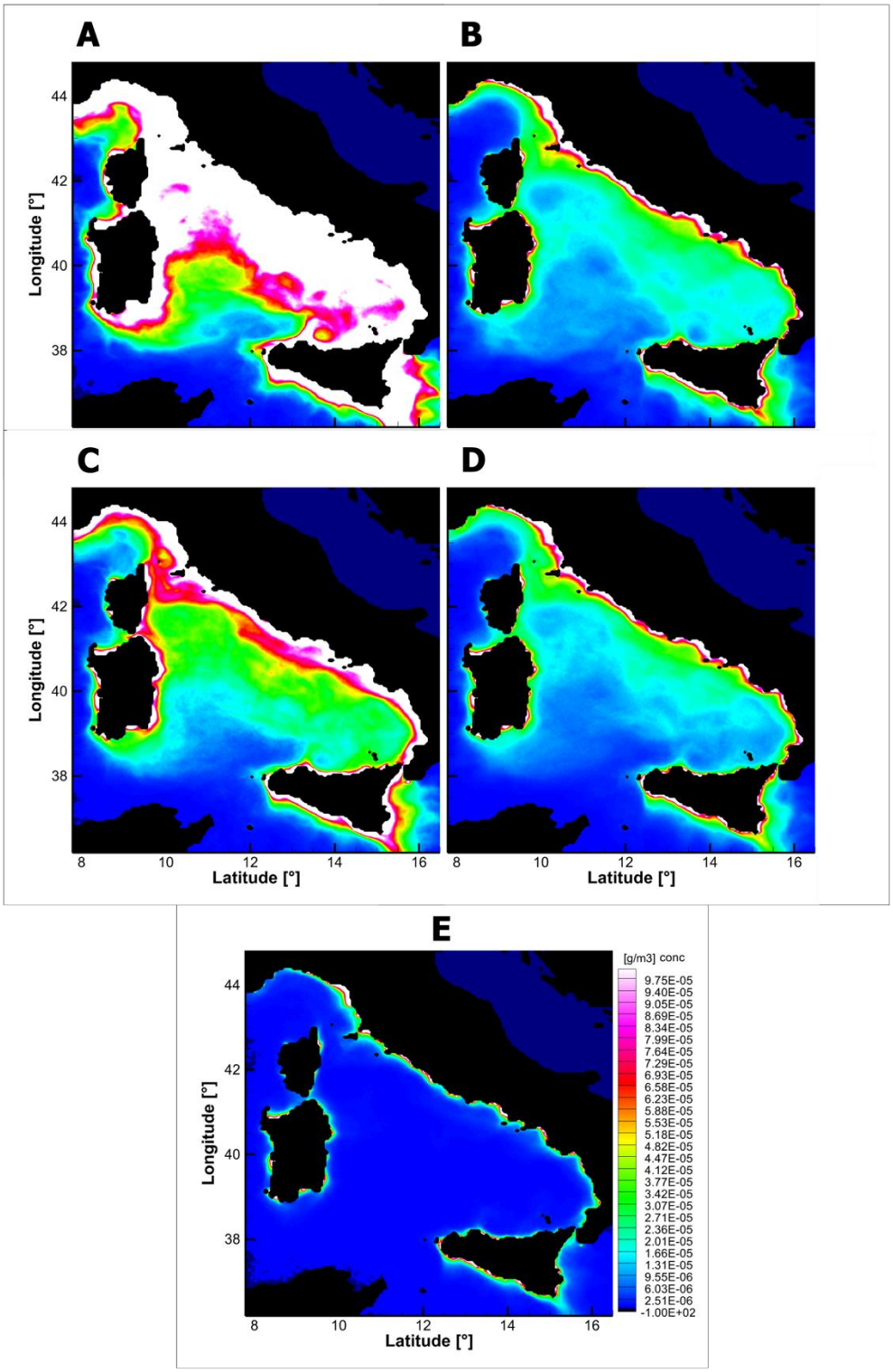

Figure 20. MP surface concentration maps of the Tyrrhenian Sea during the Winter season. The MP concentrations are averaged over the period from 06/05/2019 to 11/09/2021. The different maps refer to the results of the simulations presented in Tab. 8.

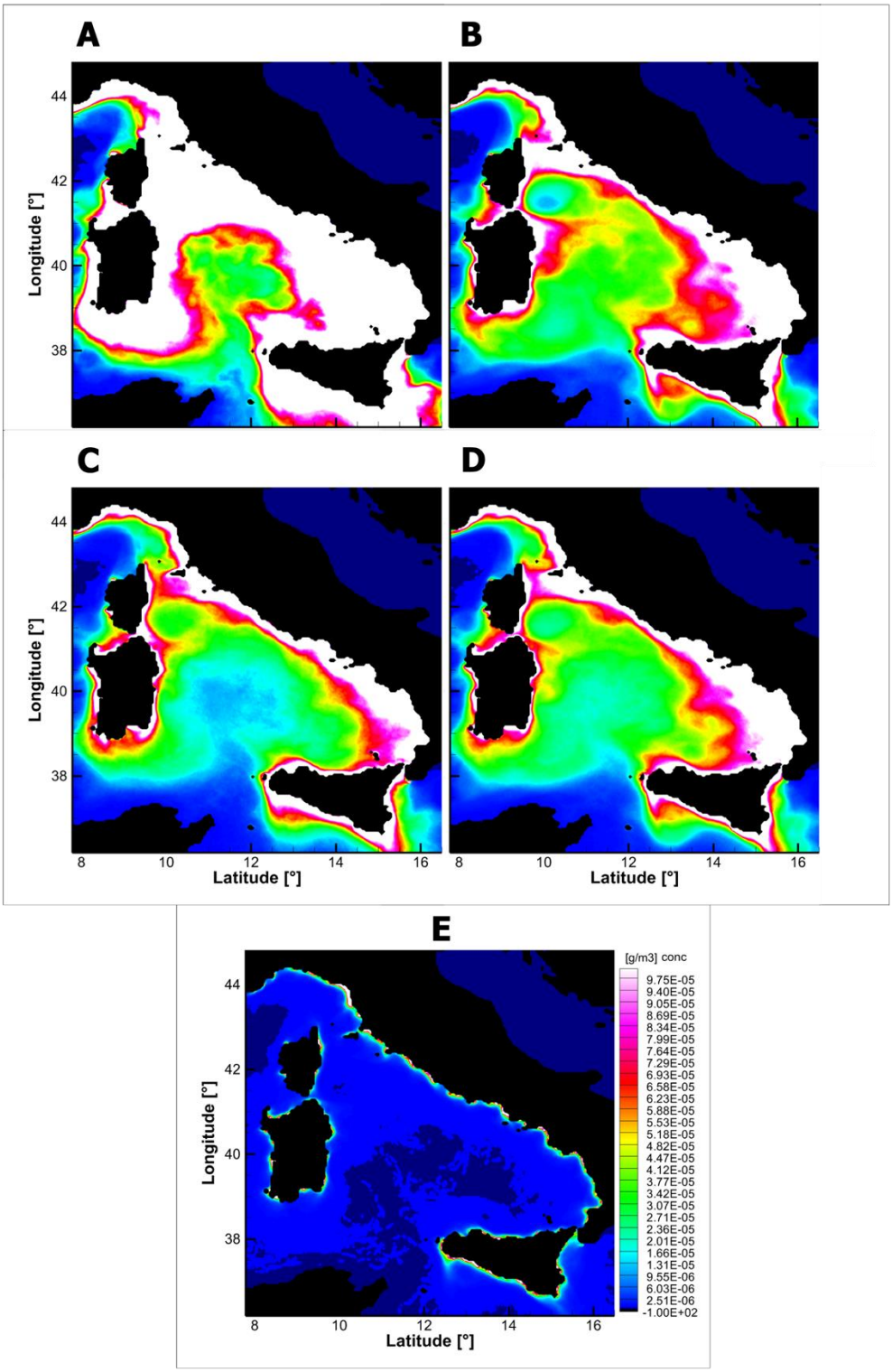

Figure 21. MP surface concentration maps of the Tyrrhenian Sea during the Summer season. The MP concentrations are averaged over the period from 06/05/2019 to 11/09/2021. The different maps refer to the results of the simulations presented in Tab. 8.

The 3D simulations allow to study what happens below the sea surface. Thus, in Fig. (22) are represented the MP vertical concentration in the Tyrrhenian Sea at Latitude 41.78°N. Comparing left and right panels, it is possible to notice the different mixing processes that transport the MP during Winter and Summer, respectively.

These vertical sections confirm what has been already said about the two borderline cases: B and E. In fact, it is worth noting that if MP are dispersed in the water column only by means of the sub-grid turbulence (case B), they remain confined in the first 200-300 m; on the other hand, if particles are negatively buoyant (case E), they sink close to the coast and accumulate on the seafloor, both during Winter and Summer.

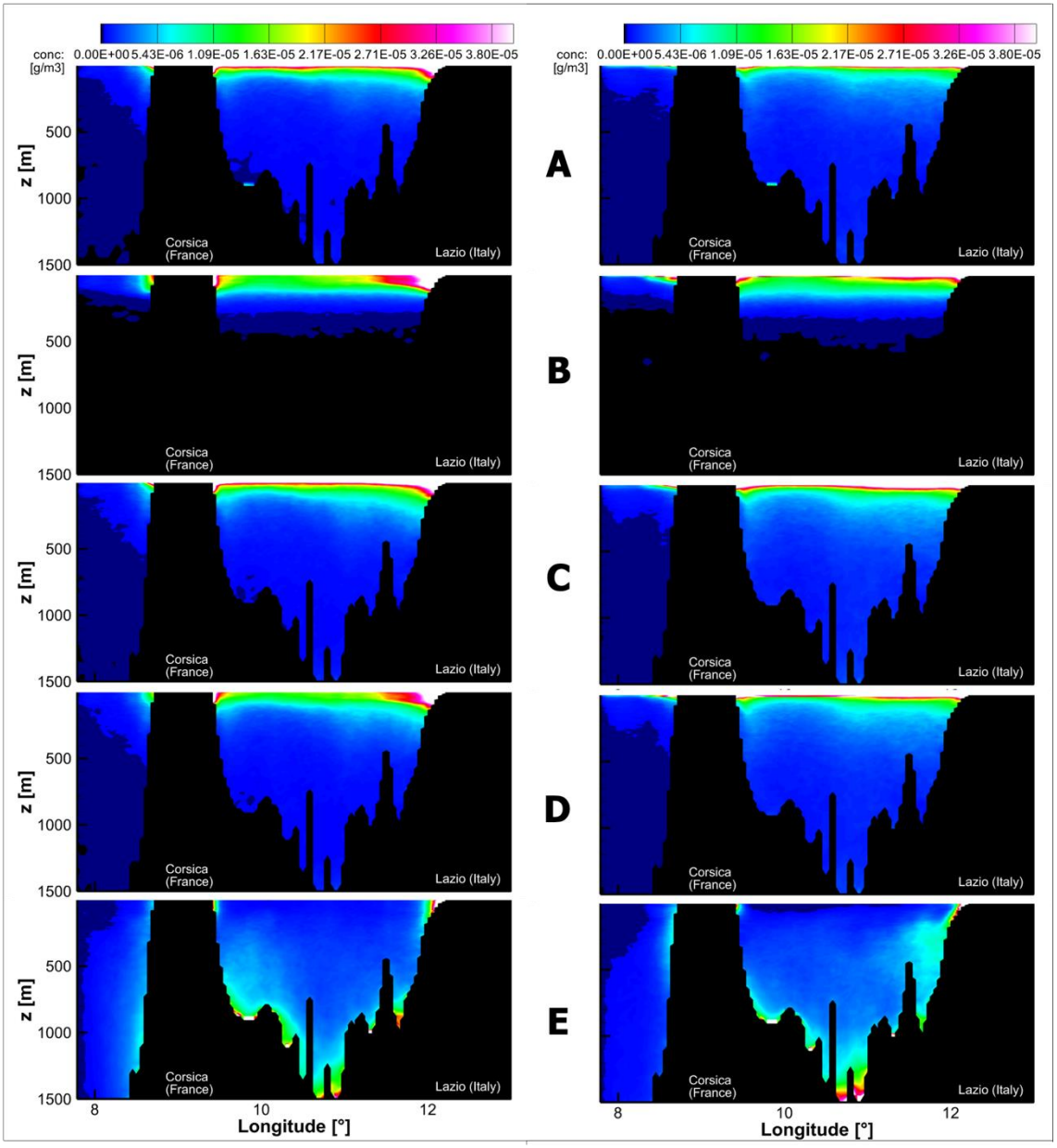

Figure 22. Vertical MP concentration in the Tyrrhenian Sea at Latitude 41.78°N. The MP concentrations are averaged over the period from 06/05/2019 to 11/09/2021. Left panels concern to the Winter period, right panels to the Summer period. The different vertical sections refer to the results of the simulations presented in Tab. 8.

Furthermore, analysing Fig. (23), the comparison between case A, C and D, where different parameterizations of vertical turbulence are considered, is more clear. In fact, for a more specific analysis of the mixed layer, Fig. (23) is focused on the first 150 m of the water column.

Again, in case D, vertical dispersion seems to be modelled more accurately compared with case A and C, where $K_z = 0$ m^2/s and $K_z(z) = 1.2 * 10^{-4}$ m^2/s, respectively. In fact, in case D, it is evident the mixed layer depth and its role on the MP vertical dispersion. It could be about 10 m deep during Summer, so particles could remain trapped in the first meters of the water column, on the contrary during Winter, it could reach 100 m, so MP are dispersed deeply with

the highest concentrations close to the coast. On the other hand, considering no vertical mixing (case A) means that MP tend to disperse horizontally rather than vertically and to accumulate in the first meters of the water column.

In addition, considering a constant $K_z(z)$, as in case C, means that MP dispersion is not influenced by different mixing processes happening in different period of the year, so MP sink far below the mixed layer depth during Summer, while in Winter anomalous accumulation of particles close to the surface occurs.

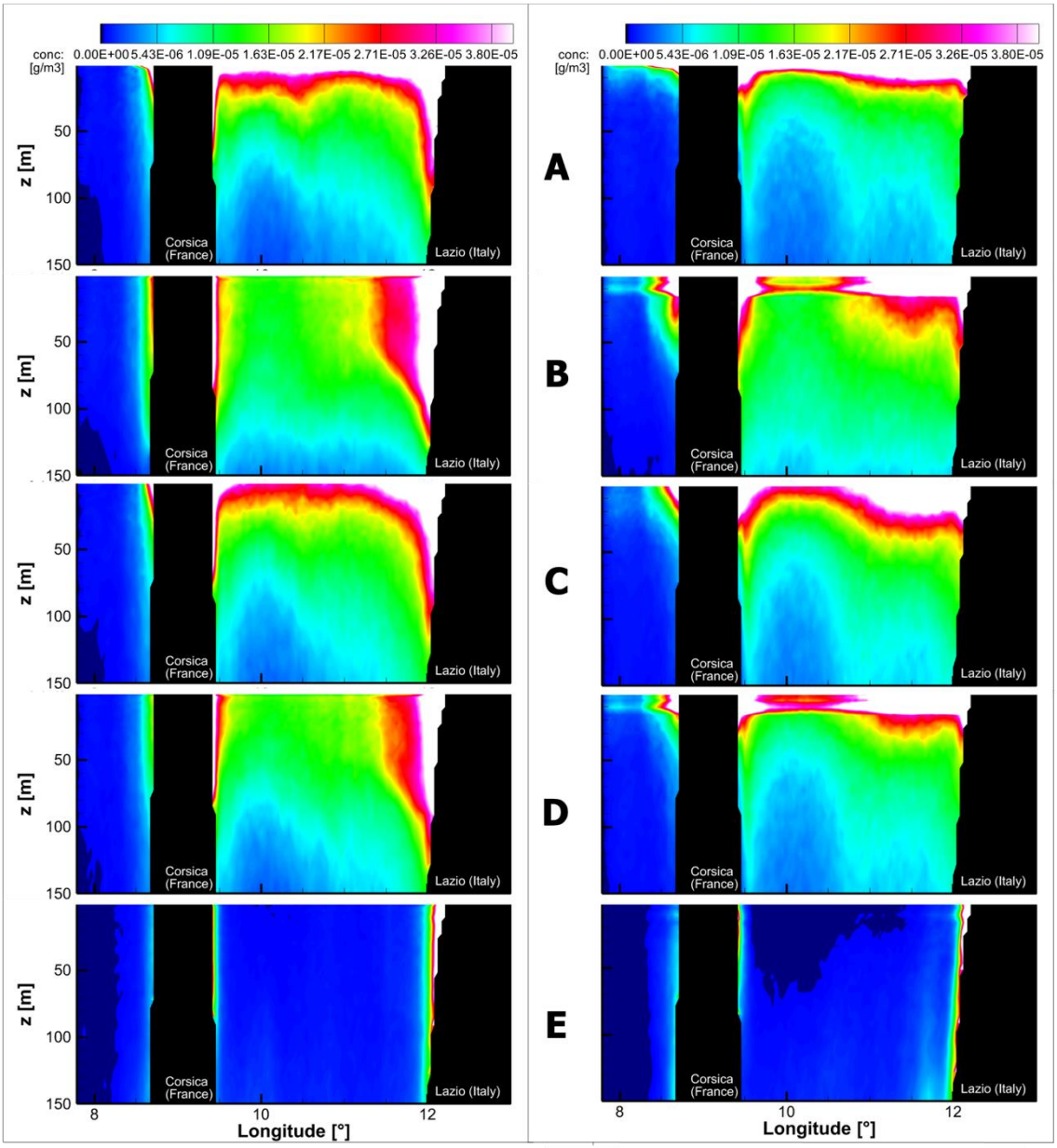

Figure 23. Vertical MP concentration in the Tyrrhenian Sea at Latitude 41.78°N, where only the first 150 m are highlighted. Left panels concern to the Winter period, right panels to the Summer period.

Finally, the analysis of the profiles, shown in Fig. (24), gives information about the order of magnitude of the MP concentration at different levels of the water column. These profiles refer to the average concentration of profiles calculated in 60 locations unevenly spaced in the Tyrrhenian Sea.

In case A (blue curve), it is noticed the highest surface concentration of the order of 10^{-4} g/m^3, but then it drops more quick than the other cases, both during Summer and Winter. Case B and

D have similar values: during Winter MP concentration is on average of the order of 10^{-5} g/m^3 with the maximum at the sea surface, during Summer MP concentration have a maximum at the bottom of the mixed layer with a value one order of magnitude higher than Winter concentration. Case C have a profile similar to case A, but with lower concentration values. Finally, in case E, MP concentration is of the order of 10^{-5} g/m^3 in the first 150 m of the water column, but higher values could be spotted at lower levels where they accumulate (even though they are not represented in Fig. (24) for graphical reasons).

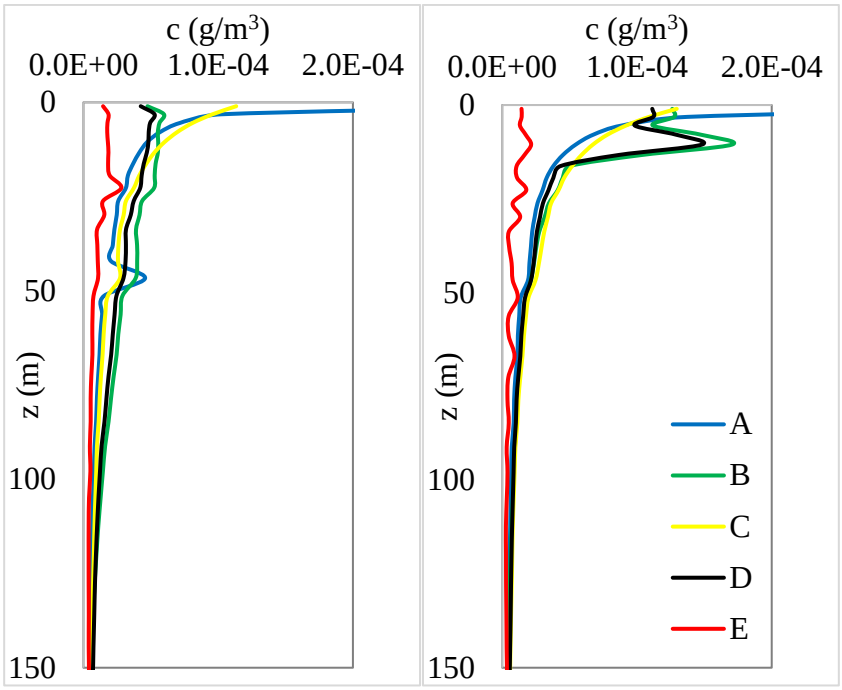

Figure 24. MP concentration profiles in the Tyrrhenian Sea. The MP concentrations are averaged over the period from 06/05/2019 to 11/09/2021. Left panel concerns to the Winter period, right panel to the Summer period. The different curves refer to the simulations presented in Tab. 8.

4.3.2 3D MP long-term dispersion of different polymers

Given the results presented in the previous paragraph, in order to have a finer representation of the 3D dispersion of MP in the marine environment, it is necessary to consider the combined contribution of the mean currents, the sub-grid turbulence and even of the rising/settling velocity characteristic of each particle. So, in this paragraph, to test the 3D dispersion of MP in the Tyrrhenian Sea of different MP polymers, long-term simulations with the Wiener3D v6 have been performed. The period analysed is: 01/01/2010 - 31/12/2019.

MP particles were released in the Tyrrhenian Sea every 10 min; all of them have the same mass, but they are released in a number proportional to the less populated source.

In these simulations, some MP removal processes have been modelled: beaching and sedimentation on the bottom; so, MP particles could remain trapped on the coasts or could lie on the sea floor. The biofouling process have not been modelled yet.

Three different simulation have been carried out, in order to study how different MP polymers behave in the water column. More details are summarized in Tab. (9).

Table 9. Simulation configuration with Wiener3D v6.

Simulation	Particle density	Rising/settling velocity
Positively buoyant particles	$\rho_P = 900$ kg/m^3 $< \rho$	$w_r = -0.0005$ m/s
Neutrally buoyant particles	$\rho_P = \rho = 1025$ kg/m^3	$w_{r,s} = 0$ m/s
Negatively buoyant particles	$\rho_P = 1040$ kg/m^3 $> \rho$	$w_s = 0.0005$ m/s

Considering the statistical moments (average, standard deviation and skewness) of the depth of the all particles dispersed in the Tyrrhenian Sea, represented in Fig. (25), it is possible to affirm that diverse polymers of MP behave in different ways.

The average depth of the neutral particles in the entire Tyrrhenian Sea increases progressively during the simulation period and it is possible to notice a seasonality of the sinking of the plume, with a period of one year; this can be explained by the fact that during Winter the mixing phenomena are more intense than in the Summer, where on the contrary the water column is stratified. Moreover, the standard deviation grows and confirms that the pollutant cloud progressively widens. Finally, the asymmetry coefficient, after about one year, oscillates around a constant value.

The seasonality of the dispersion of the plume is even more visible in the case of positively buoyant particles; in this case, during Winter there is progressively deeper mixing of the average depth of the particles with increasing wind speeds and decreasing buoyancy. On average, the particles remain confined in the first 10 m of the water column but the skewness is very high, so the plume is very asymmetric.

Finally, considering negatively buoyant particles (orange curve), it is possible to say that most of the particles sink quickly and on average in the basin the centre of the pollutant plume is at depth greater that 1000 m. The skewness seems to be constant describing a steady asymmetric cloud.

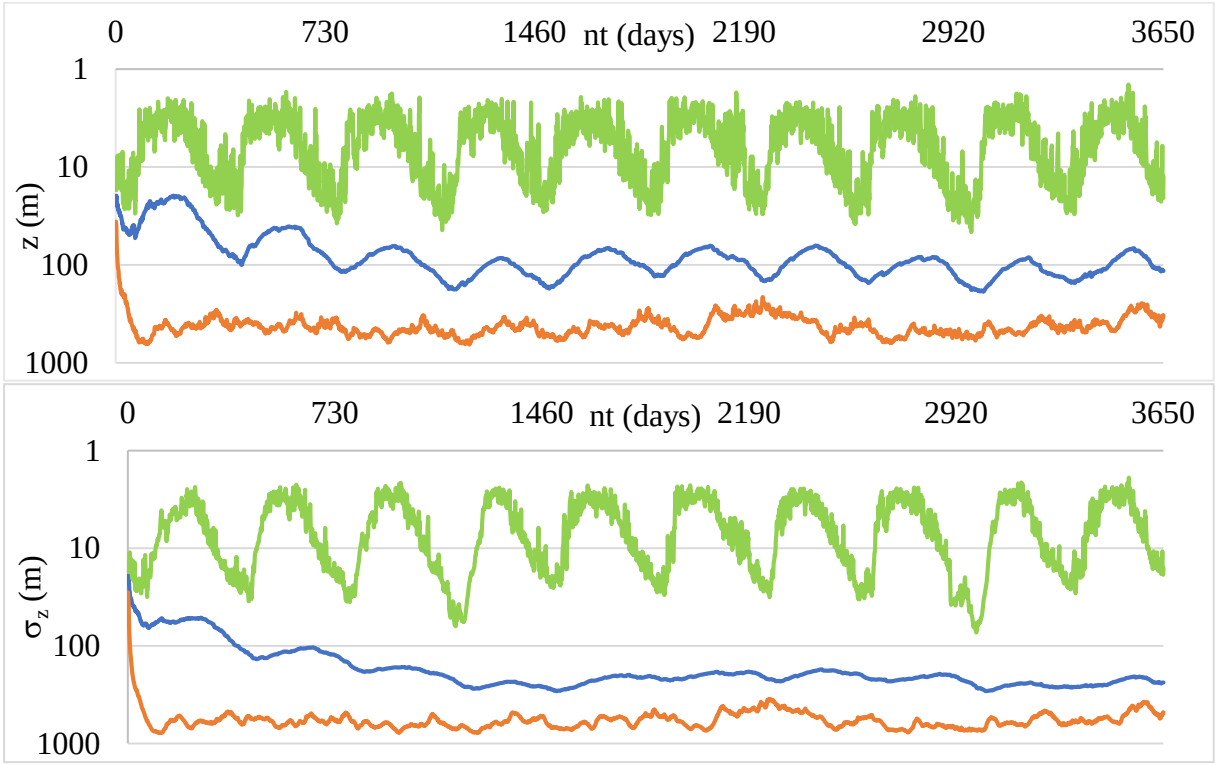

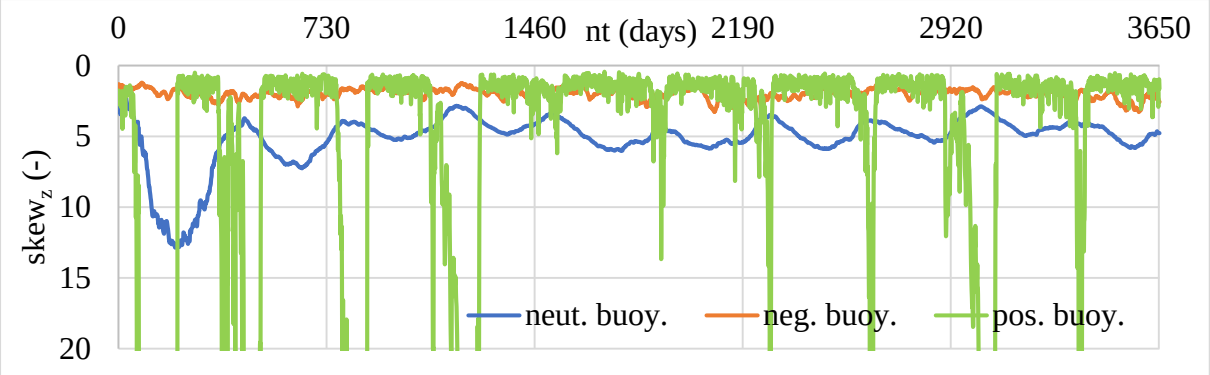

Figure 25. Statistical moments of the depth of all the particles dispersed in the Tyrrhenian Sea (the average value is represented in the top panel, the standard deviation in the centre panel and the skewness in the bottom panel). The period simulated ranges from 01/01/2010 to 31/12/2019. The different curves refer to the results of the simulations presented in Tab. 9.

The distinct characteristics of the dispersion of MP with different densities are even more clear looking at the MP surface concentration maps of the Tyrrhenian Sea, Fig. (26).

Neutral particles (Fig. 26, panels a-b) are distributed throughout the domain with an average surface concentration of the order of 10^{-6} g/m^3, but the highest concentrations are close the Italian coasts, where the anthropogenic sources are. In addition, it is possible to notice that during Summer, when the mixed layer is shallow, particles are mainly spread horizontally by the mean currents; during Winter, while the mixed layer depth could reach 100 m, vertical turbulent phenomena are more intense so they provoke a stronger vertical dispersion.

Similar considerations could be done talking about the dispersion of positively buoyant particles (Fig. 26, panels c-d), but in this case, either in Summer either in Winter, surface MP concentrations are higher than neutral particles. For instance, the highest concentrations could be spotted in the Ligurian Sea or in front of the Lazio and Campania coasts, they are of the order of 10^{-4} g/m^3.

Finally, negatively buoyant particles (Fig. 26, panels e-f) settle rather quickly and appreciable surface MP concentrations are only near the coast, while most of the MP are sedimented; these particles have a sedimentation rate of about 40 m per day, so they reach the bottom not far from the coastal source and the surface concentration is practically zero throughout the basin.

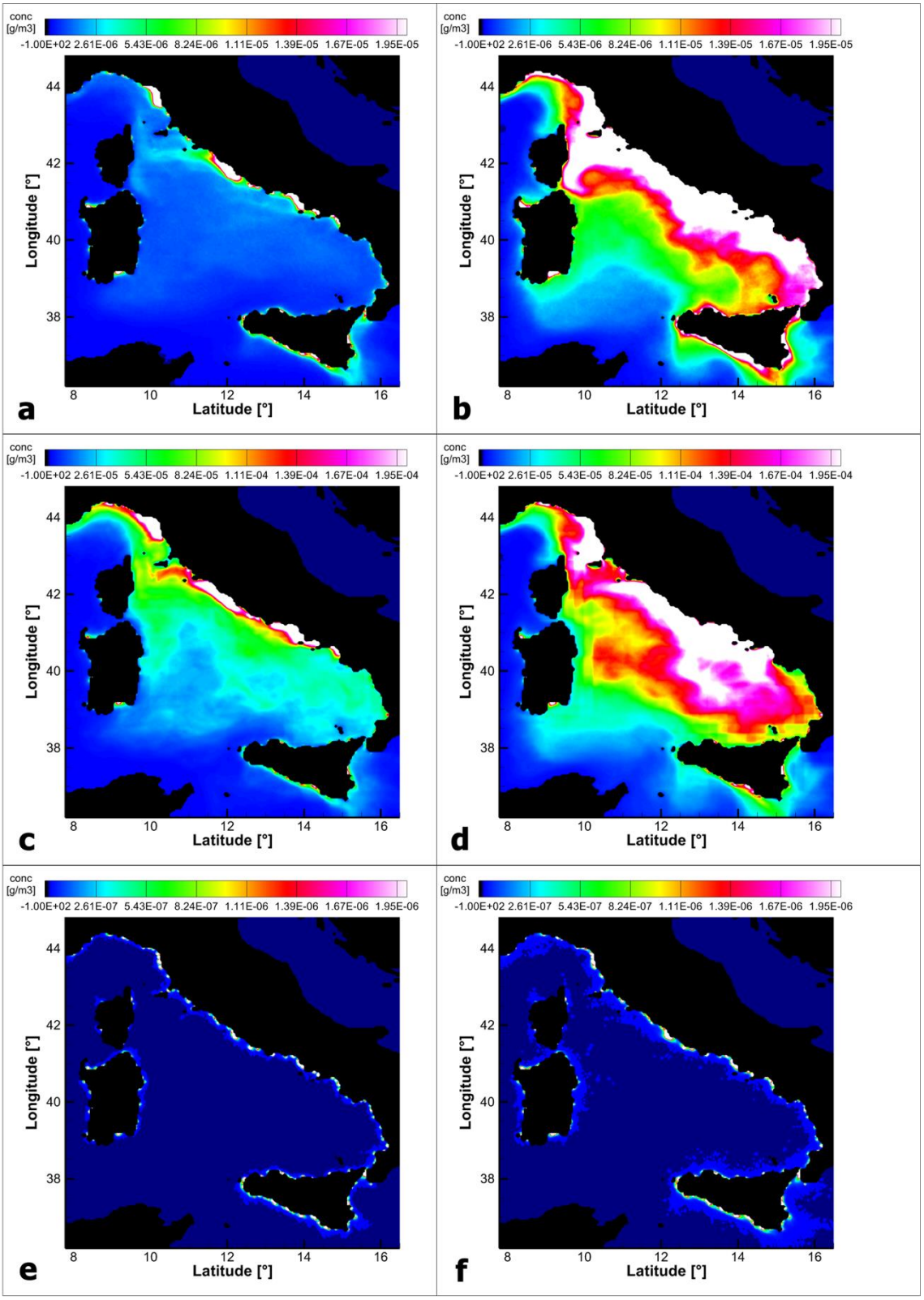

Figure 26. MP surface concentration maps of the Tyrrhenian Sea. The MP concentrations are averaged over the period from 01/01/2010 to 31/12/2019. Left panels concern to the Winter period, right panels to the Summer period. Panels (a-b) represent the surface concentration of neutrally buoyant MP, panels (c-d) positively buoyant MP and panels (e-f) negatively buoyant MP. Note: MP concentration ranges are different!

The vertical dispersion of MP is appreciable looking at the vertical sections of the Tyrrhenian Sea at latitude 41.78° N, represented in Fig. (27).

Neutral particles (Fig. 27, panels a-b) can be found at the all depths of the water column: higher concentration can be noticed in the first 100 m, MP concentration in the middle levels of the water column is an order of magnitude lower, while in the last levels it is very small.

Furthermore, positively buoyant particles (Fig. 27, panels c-d) are confined close to the sea surface. On the other hand, particles denser than seawater (Fig. 27, panels e-f) sink close to the coastal sources and they accumulate on the sea floor.

In addition, Fig. (27), especially in panels e-f, allows to appreciate the quantity of MP spilled by the Tevere river and how they spread into the water column.

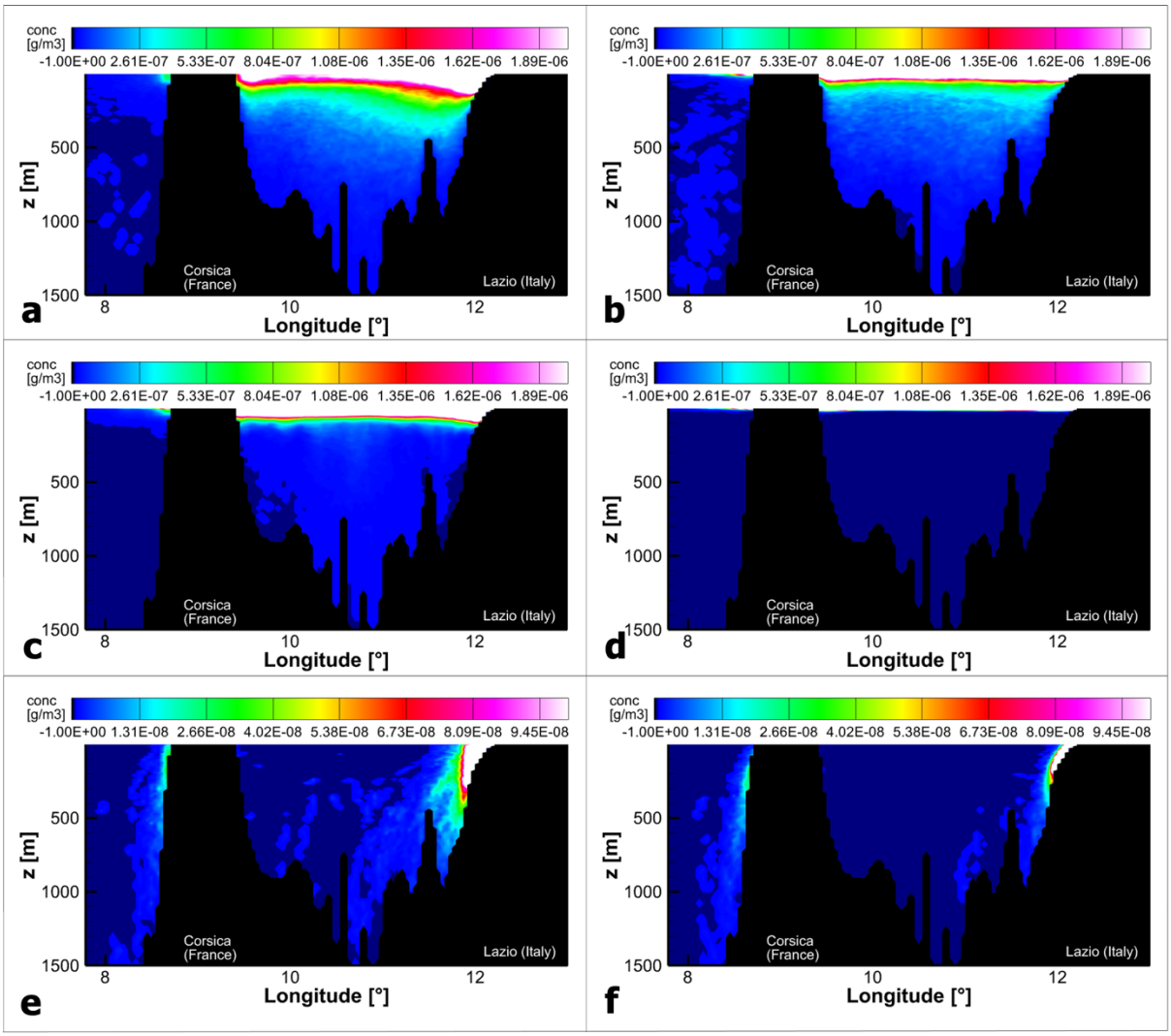

Figure 27.Vertical MP concentration in the Tyrrhenian Sea at Latitude 41.78°N. The MP concentrations are averaged over the period from 01/01/2010 to 31/12/2019. Left panels concern to the Winter period, right panels to the Summer period. Panels (a-b) represent the vertical concentration of neutrally buoyant MP, panels (c-d) positively buoyant MP and panels (e-f) negatively buoyant MP. Note: MP concentration ranges are different!

Fig. (28) confirms what has been said about Fig. (27), but a specific attention is deserved to Fig. (28, panels c-d), where is clearly visible the role of the stratification on the dispersion of positively buoyant MP in the water column, in fact, only the first 150 m of the water column are represented.

MP get mixed below the sea surface, but they remain trapped in the first layers. The mixed layer depth behaves as a boundary in same way: during Summer, particles remain confined in the first 10 m with a concentration of the order of 10^{-4} g/m^3; this layer is also abundant of flora and fauna, so fish or sea birds could ingest these particles. During Winter, the mixed layer depth could be between 60 and 80 m, MP settle within the water column, so the concentration decreases from the sea surface.

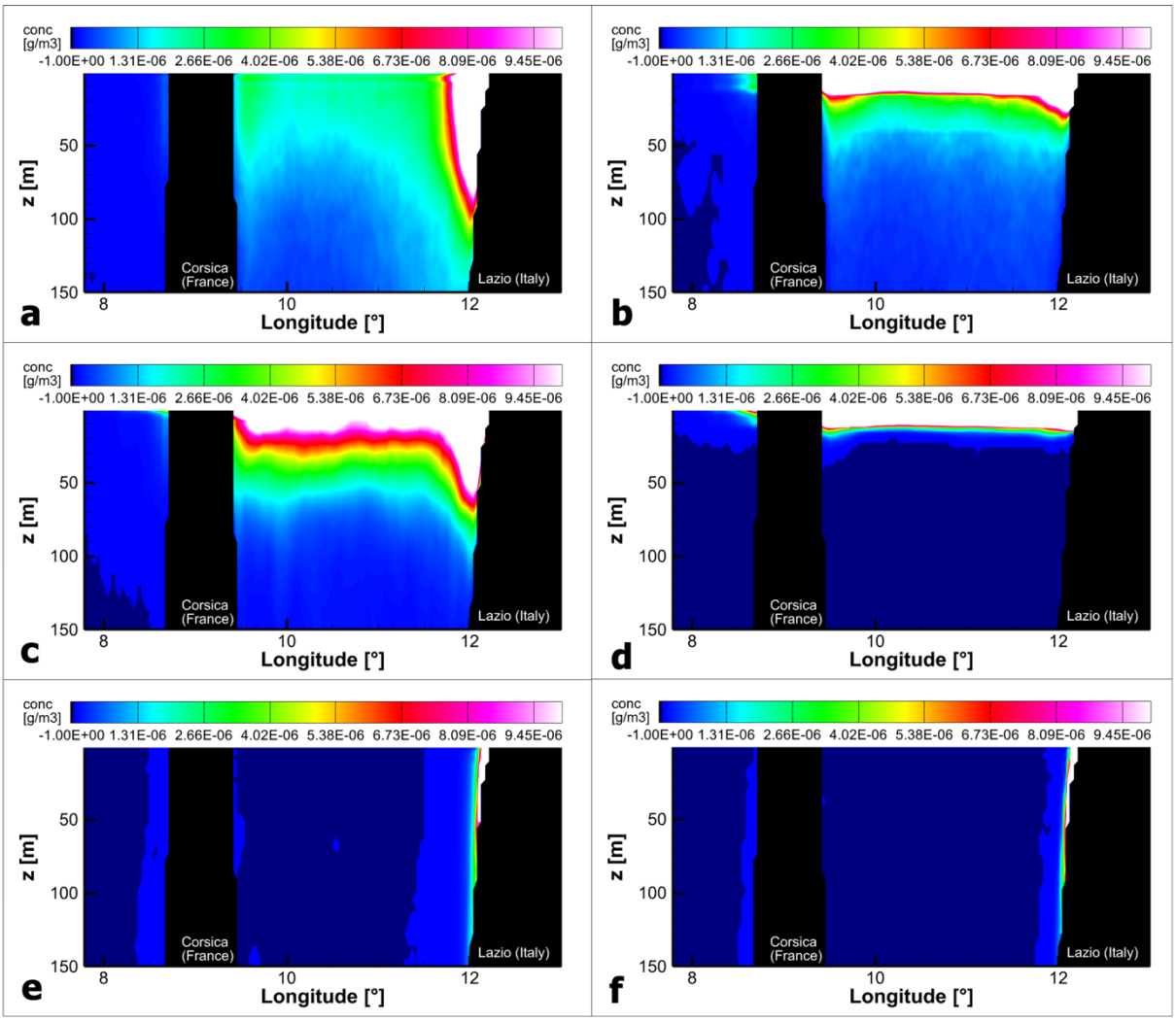

Figure 28. Vertical MP concentration in the Tyrrhenian Sea at Latitude 41.78°N, where only the first 150 m are highlighted. Left panels concern to the Winter period, right panels to the Summer period. Panels (a-b) represent the vertical concentration of neutrally buoyant MP, panels (c-d) positively buoyant MP and panels (e-f) negatively buoyant MP.

4.3.3 LSM validation: comparison with experimental data

The 3D LSM has been validated comparing the results of the simulations of the MP dispersion in the Tyrrhenian Sea with the field data presented in paragraph (3.5).

As it has already been said, the field data belongs to six different experimental campaigns with a total of 113 profiles and 479 sampling points in the water column.

These data have been a priori elaborated in order to have a more general comparison; in particular, if necessary, the concentration values have been converted in items/m^3 (i.e. MP/m^3); moreover, many profiles have few sampling points in the mixed layer, thus the missing values

on the water column have been linearly interpolated on the same vertical grid of the simulations.

Finally, these profiles have been divided in two groups with similar mixed layer depth; in fact, this could be considered a parameter which makes possible to analyse different turbulent cases. In the case of stratified water column, the mixed layer depth is on average close to 10 m; instead, during the cold season, the mixed layer is deeper, on average in the considered campaigns it is between 30 and 40 m.

Furthermore, the simulated concentrations refer to the long-term simulation presented in paragraph (3.4.2), so, the dispersion of different polymers of plastic have been analysed in 60 profiles unevenly spaced in the Tyrrhenian Sea, as in Fig. (9). The MP concentration in these 60 profiles have been studied considering two different period of the year with similar mixed layer depth; in particular, a seasonal average concentration of each profile have been calculated: during Summer, when the water column is stratified and the mixed layer depth is about 10 m, and during Winter when the mixed layer depth is on average 50 m. Then, the average concentration of different MP polymer profiles have been arranged by means of a linear combination with the weights presented in Tab. (10), reported in Bello et al. 2022, and an average profile for each location and for the two period of the year have been obtained.

Kooi and Koelmans 2019 presented three different discrete probability functions of size, density and shape of the particles based on a very large database of field and laboratory data, combining them a discrete probability function for the rising/settling velocity have been derived (Bello et al. 2022). From this function, it was obtained that approximately 15% of the particles are positively buoyant, while 67% are negatively buoyant, this result confirms that about 70 to 90% of MP are accumulated on the seafloor (Uddin et al. 2021).

Table 10. Weights considered in the linear combination of the simulated concentrations of different MP polymers in the TYS.

Simulation	Rising/settling velocity	Weight
Positively buoyant particles	$w_r = -0.0005$ m/s	15%
Neutrally buoyant particles	$w_{r,s} = 0$ m/s	18%
Negatively buoyant particles	$w_s = 0.0005$ m/s	67%

Before the comparison, in order to obtain a generalizable behaviour, both measured and simulated concentration profiles have been normalized; in detail:

- the depth of the water column has been normalized with the mixed layer depth, H;
- the MP concentration have been normalized with the average value within the mixed layer, which have been calculated in the following way:

$$cmed = \int_0^1 c(\xi) d\xi \tag{70}$$

where $\xi = z/H$. In synthesis:

- 39 experimental profiles with a relatively deep mixed layer have been compared with 60 simulated MP profiles in the Tyrrhenian Sea, where the MP concentration results from the linear combination of the average concentration of different MP polymers during the Winter season;
- 74 profiles sampled in periods with a shallow mixed layer ($H \approx 10$ m) have been confronted with 60 simulated MP profiles in the Tyrrhenian Sea, where the MP concentration results from the linear combination of the average concentration of different MP polymers during the Summer season.

The comparison between the experimental profiles of MP concentration and the simulated profiles is presented in Fig. (29). In general, in the left panel, where profiles have a relatively deep mixed layer, there is a good agreement between the data and the shape of the profiles is very similar; but, the maximum value of the simulated data seems to be shifted closer to the sea surface than the experimental maximum value. Moreover, in the right panel, where profiles have a mixed layer 10 m deep, there is an even better agreement between the field and the simulated data and the order of magnitude of the normalized MP concentration is similar at the different depths analysed.

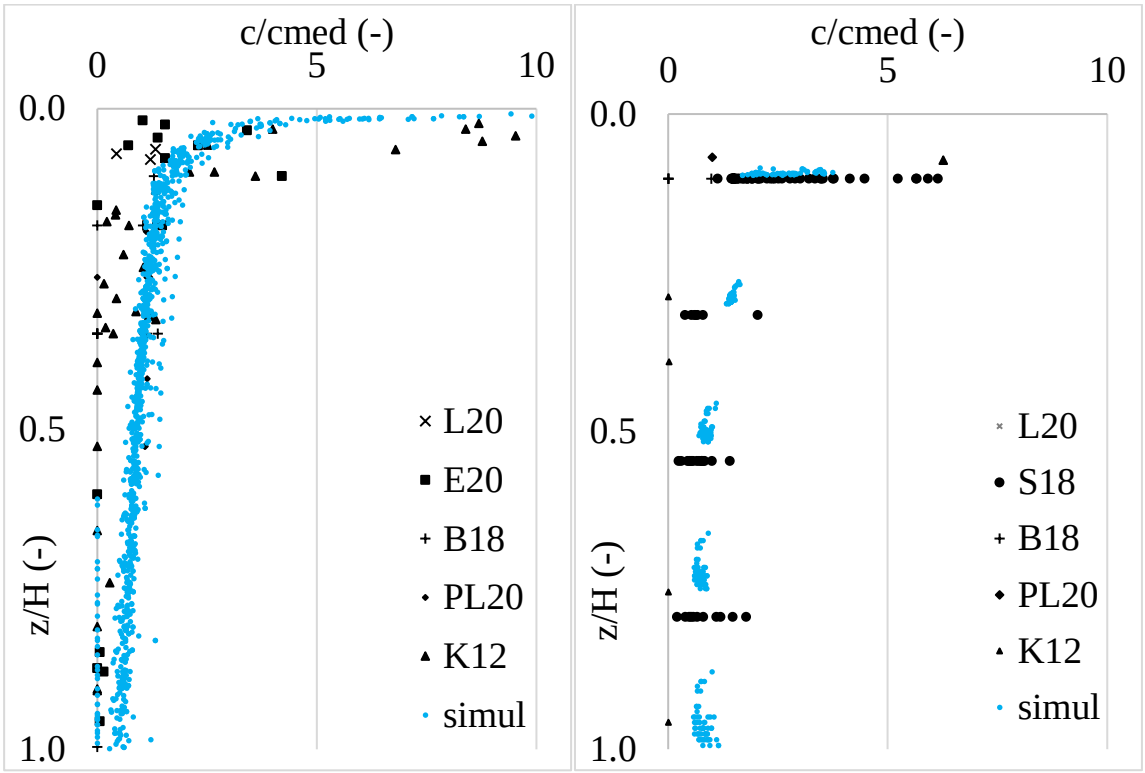

Figure 29. Comparison between the experimental profiles of MP concentration, represented in black marks where different marks belong to different sampling campaigns, and the simulated profiles, represented in light blue points. The MP concentration is scaled with the average concentration in the mixed layer, as in Eq. (70), while the depth is scaled with the mixed layer depth. Left panel refers to profiles with a relatively deep mixed layer; while in the right panel, profiles have a mixed layer 10 m deep.

With the intention to obtain a more precise analysis, the simulated data have been compared with the better detailed sampling campaigns. In fact, in some campaigns few points are provided in the mixed layer depth and the linear interpolation adopted could alter the experimental results and therefore also the comparison. Thus, in Fig. (30-31) the simulated MP concentration profiles have been compared separately with the sampling campaigns of Egger et al. 2020, Kukulka et al. 2012 and Song et al. 2018.

In the left panel of Fig. (30), 60 simulated MP profiles are compared with 6 profiles sampled in the North Pacific ocean by Egger et al. 2020; in the right panel of Fig. (30), 60 simulated MP profiles are compared with 11 profiles sampled in the North Atlantic ocean by Kukulka et al. 2012. As it is possible to notice in Fig. (30), during the cold season, the simulated concentrations fit pretty well the experimental data, especially considering the second part of the mixed layer, on the contrary the simulated concentrations overestimate the field data at the sea surface and underestimate the field data at the level just below.

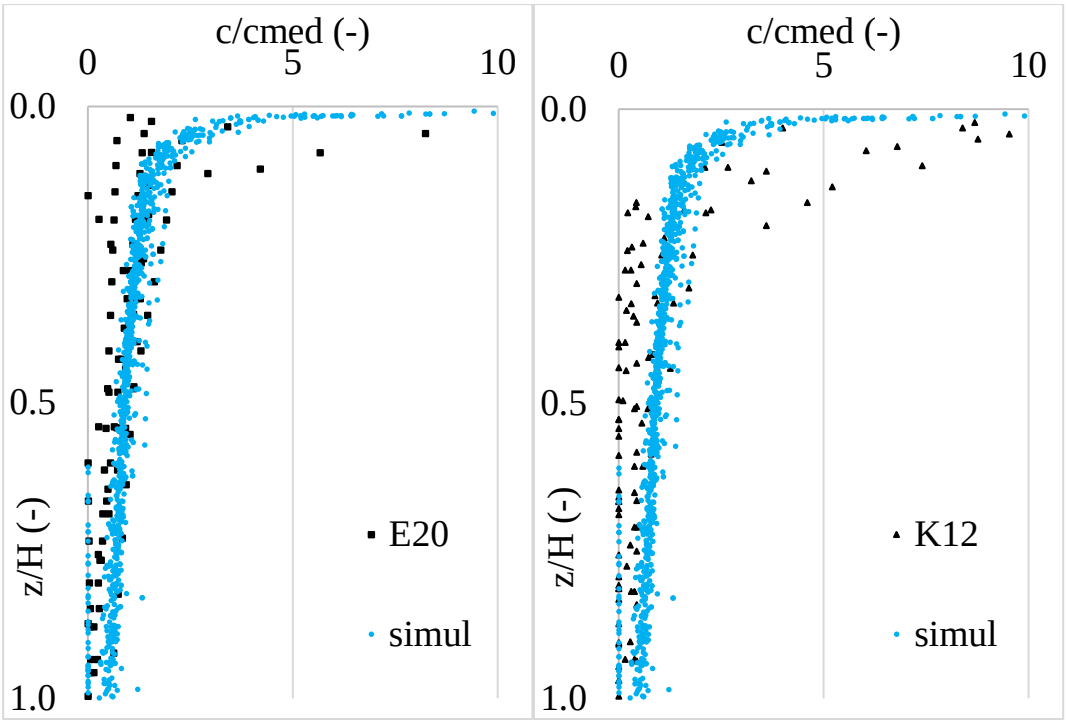

Figure 30. Comparison between the experimental profiles of MP concentration and the simulated profiles, represented in light blue points, during the cold season. In the left panel the experimental profiles, represented in black squares, belong to Egger et al. 2020 *campaign in the Pacific Ocean; in the right panel, the experimental profiles, represented in black triangles, belong to* Kukulka et al. 2012 *campaign in the Atlantic Ocean.*

Furthermore, as it is possible to notice in Fig. (31), when the mixed layer is shallow, there is a nice agreement between the simulated concentrations and the experimental data of Song et al. 2018, which sampled 41 MP concentration profiles in the Pacific ocean. This confirms what has been said about the right panel of Fig. (29).

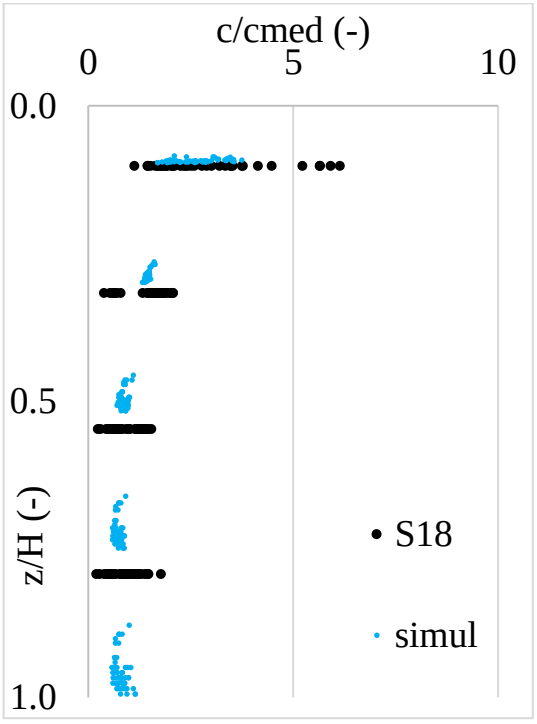

Figure 31. Comparison between the experimental profiles of MP concentration sampled during the Song et al. 2018 *campaign in the Pacific Ocean close to the Korean shores, represented in black points, and the simulated profiles, represented in light blue points, during the warm season.*

Finally, it has been developed a similarity law which could describe the profile of the normalized concentration of MP in the mixed layer. Considering that MP concentration is maximum at the sea surface, then it decreases exponentially in the mixed layer, the experimental data have been fitted, by means of the least square method, with a negative exponential function, which could describe the MP concentration profiles of the two different cases presented previously, at the same time. The result is visible in Fig. (32).

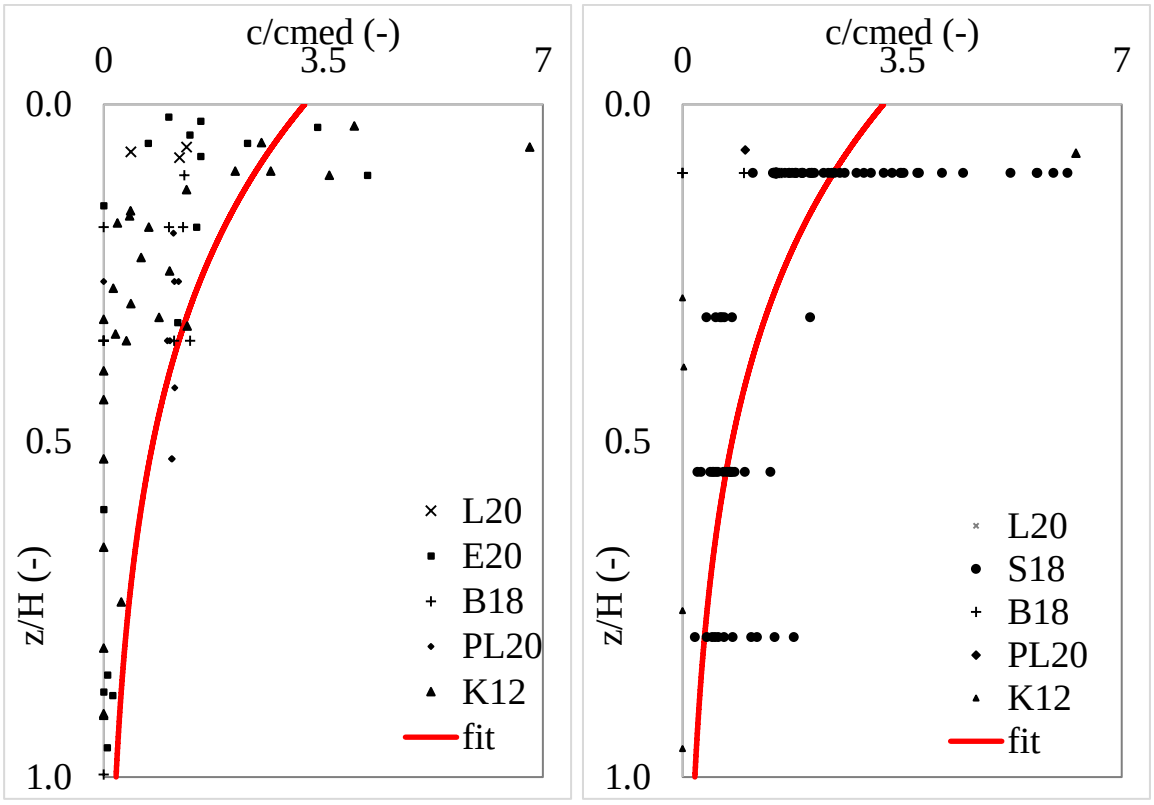

Figure 32. Experimental profiles of MP concentration, represented in black marks, described by Eq. (71), represented with a red curve. Left panel refers to profiles with a relatively deep mixed layer; while in the right panel, the profiles have a mixed layer 10 m deep.

Besides, the similarity law obtained is:

$$c(z) = cmed[3.2 * \exp(-2.8 * z/H)] \quad (71)$$

As presented in paragraph (2.4.2.1), other similarity laws which describe the MP vertical distribution have been obtained in a similar way (e.g. Egger et al. 2020; Kukulka et al. 2012). Kukulka et al. 2012 developed a one-dimensional model where $c(z)$ depends on the surface concentration, the rise velocity of plastic pieces and the near-surface vertical diffusivity. Egger et al. 2020 proposed a law where the vertical MP concentration is calculated as a function of the water depth.

The similarity law presented in this work, Eq. (71), depends only on two scale parameters: $cmed$ and H. Since most of the sampling data have been collected on the sea surface, $cmed$ could be obtained with Eq. (71) using the $c(0)$ value coming from sampling campaigns; while, the mixed layer depth is commonly calculated with operational oceanographic models.

In addition, the agreement between the simulated profiles and Eq. (71) has been tested.

In general, as it is visible in Fig. (33), the accordance is good: the profile shape behaves nearly the same and the order of magnitude of the MP concentration is similar. But in particular, as it has already been said, during the cold season, the simulated data are described pretty well by

this function especially when $z/H > 0.25$; while at the sea surface, the simulated concentrations are higher than the experimental MP concentrations. On the contrary, when the mixed layer is shallow, there is a good agreement between the simulated concentrations and Eq. (71), especially in the first half of the mixed layer depth.

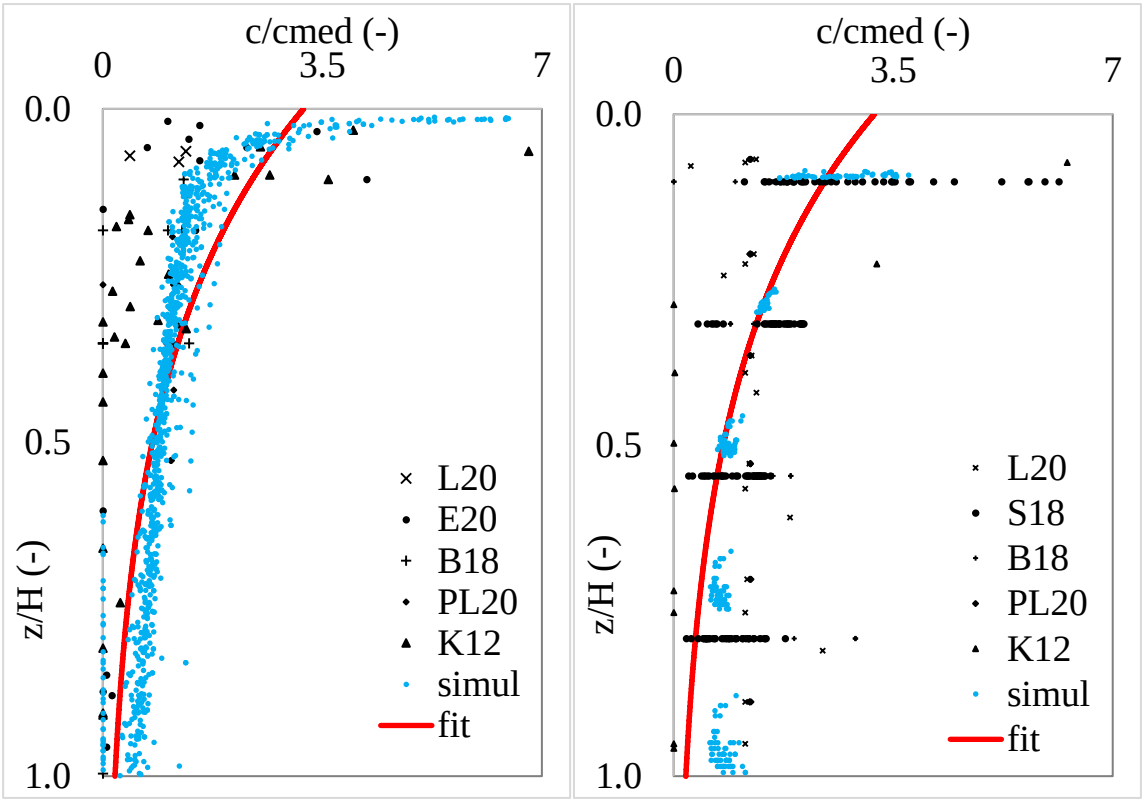

Figure 33. Simulated (blue marks) and experimental (black marks) MP concentration profiles described by Eq. (71), represented with a red curve. Left panel refers to profiles with a relatively deep mixed layer; while in the right panel, the profiles have a mixed layer 10 m deep.

5. Conclusions

This work is focused on the study of the 3D turbulent dispersion of MP in the marine environment, with a specific attention to the OSBL. An innovative parameterization of the vertical turbulent diffusivity has been developed and it has been implemented in a LSM specifically devoted to the study of the 3D dispersion of MP.

More in detail, the study of the turbulent mixing in the OSBL and the intention to model it produced an original vertical turbulence parameterization. This is based on the Taylor 1921 theory and the vertical turbulent diffusivity has been derived evaluating other turbulent quantities: the vertical velocity variance and the Lagrangian integral time scale.

Compared with other parameterizations, the main advantage of ZPL parameterization is that is based on Lagrangian quantities: the vertical velocity variance is a measure of the turbulence and the Lagrangian time scale is an indicator of the dimension of the eddies, so this turbulence parameterization is directly related to Lagrangian model parameters. In addition, it allows to have an estimation of turbulent diffusivity by means of similarity laws that can be easily generalized because they are mainly based on two parameters: the friction velocity and the mixed layer depth.

A further development of the ZPL parameterization could concern the study of the horizontal variability of the vertical turbulent diffusivity; in addition, a detailed analysis on the important role of LC and how the ZPL parameterisation behaves under strongly convective forcing without wind stress will be carried out.

The validity of ZPL parameterization in modelling turbulent dispersion in the OSBL have been evaluated through several simulation of the 3D MP dispersion with the LSM Wiener3D v6. The domain analysed was a sub-basin of the Mediterranean Sea, i.e. the Tyrrhenian Sea, which is a semi-closed and densely populated basin.

Different simulations have been performed with the intention to test the role of the mean currents, the sub-grid turbulence and the rising/settling velocity in the 3D dispersion of MP in the marine environment.

The results have shown that, on average, it is possible to point out that the role of the mean currents is predominant over sub-grid turbulence, even in the vertical direction, as it happens on the horizontal plane; in fact, it seems that the vertical dispersion is not conditioned by different vertical turbulence diffusivity values. More in detail, analysing the surface MP concentration maps and the vertical section of the Tyrrhenian Sea, it caught the eye that MP disperse differently in the basin, considering diverse simulation with different vertical turbulence diffusivity schemes. In particular, if K_z is null, anomalous surface accumulations of MP could be spotted in the centre of the basin. Furthermore, if K_z is constant, MP concentration are affected by the fact that this assumption underestimates vertical mixing during Winter, while overestimates it during Summer. So, if vertical dispersion is not modelled, and it is neglected in many LSM, a partial representation of the mixing in the OSBL could be obtained. So, even though on average terms different parameterizations of the vertical turbulent diffusivity give similar results, a more accurate parameterization of the vertical turbulence leads to a better description of the sea surface dispersion.

Furthermore, it has been shown that the MP physical characteristics can determine how they disperse; in fact, if a settling velocity is assigned to the particles, they sink rather quickly and they tend to accumulate on the continental shelf, both in the warm and in the cold season. This contribution to the vertical dispersion cannot be neglected and this result gave rise to the need to simulate the dispersion of different plastic polymers.

In particular, analysing the vertical dispersion of MP with a density similar to the seawater, it has been found that they are spread throughout the water column: higher concentrations can be noticed in the first 100 m, MP concentration in the middle levels of the water column is an order of magnitude lower, while in the last levels it is very small. Furthermore, it has been found that positively buoyant particles are mainly confined close to the sea surface; on the other hand, particles denser than seawater sink soon after their release from the coastal sources and they accumulate on the sea floor.

The analysis of the results of these simulations have also highlighted how mixing phenomena happening in different period of the year influence the MP dispersion in the marine environment. In fact, during Winter the vertical mixing is more intense than in the Summer, so MP tend to disperse and sink at greater depths; on the contrary, when the water column is stratified, during the warm season, MP remain confined in the first 10 m or so, and they are transported mainly on the horizontal plane.

The LSM Wiener3D v6 has been validated comparing the simulated MP concentrations profiles with field data. Considering that in the Mediterranean Sea only MP surface concentrations have been sampled, the comparison has been carried out with MP concentration profiles obtained during campaigns in the world oceans. This comparison has been possible because the data are representative of the MP distribution through the water column. In general, when profiles have a relatively deep mixed layer, there is a good agreement between the data and the shape of the profiles is very similar; but the maximum value of the simulated data seems to be shifted closer to the sea surface than the experimental maximum value. Moreover, when profiles have a mixed layer 10 m deep, there is an even better agreement between the experimental and the simulated data and the order of magnitude of the normalized MP concentration is similar at the different depths analysed.

Furthermore, the comparison with these experimental data gives the opportunity to develop a similarity law which describe the MP vertical distribution. It allows an estimation of the MP profile by means of the average concentration on the mixed layer and the mixed layer depth, as scale parameters. Thus, in the cases of lack of experimental data on the vertical direction, this could be a useful tool for the study of the turbulent dispersion of MP in the marine environment, in particular within the water column.

References

Adamopoulou, Argyro, Christina Zeri, Francesca Garaventa, Chiara Gambardella, Christos Ioakeimidis, and Elli Pitta. 2021. "Distribution Patterns of Floating Microplastics in Open and Coastal Waters of the Eastern Mediterranean Sea (Ionian, Aegean, and Levantine Seas)." *Frontiers in Marine Science* 8(September):1–15.

Andrady, Anthony L. 2011. "Microplastics in the Marine Environment." *Marine Pollution Bulletin* 62(8):1596–1605.

Anfossi, D., U. Rizza, C. Mangia, G. A. Degrazia, and E. Pereira Marques Filho. 2006. "Estimation of the Ratio between the Lagrangian and Eulerian Time Scales in an Atmospheric Boundary Layer Generated by Large Eddy Simulation." *Atmospheric Environment* 40(2):326–37.

Arcangeli, Antonella, Ilaria Campana, Dario Angeletti, Fabrizio Atzori, Marta Azzolin, Lara Carosso, Valentina Di Miccoli, Antonio Giacoletti, Martina Gregorietti, Cristina Luperini, Miriam Paraboschi, Giuliana Pellegrino, Martina Ramazio, Gianluca Sarà, and Roberto Crosti. 2018. "Amount, Composition, and Spatial Distribution of Floating Macro Litter along Fixed Trans-Border Transects in the Mediterranean Basin." *Marine Pollution Bulletin* 129(2):545–54.

Bagaev, Andrei, Liliya Khatmullina, and Irina Chubarenko. 2018. "Anthropogenic Microlitter in the Baltic Sea Water Column." *Marine Pollution Bulletin* 129(2):918–23.

Baini, Matteo, Maria Cristina Fossi, Matteo Galli, Ilaria Caliani, Tommaso Campani, Maria Grazia Finoia, and Cristina Panti. 2018. "Abundance and Characterization of Microplastics in the Coastal Waters of Tuscany (Italy): The Application of the MSFD Monitoring Protocol in the Mediterranean Sea." *Marine Pollution Bulletin* 133(June):543–52.

Baudena, Alberto, Enrico Ser-Giacomi, Isabel Jalón-Rojas, François Galgani, and Maria Luiza Pedrotti. 2022. "The Streaming of Plastic in the Mediterranean Sea." *Nature Communications* 13(1):2981.

Belcher, Stephen E., Alan L. M. Grant, Kirsty E. Hanley, Baylor Fox-Kemper, Luke P. Van Roekel, Peter P. Sullivan, William G. Large, Andy Brown, Adrian Hines, Daley Calvert, Anna Rutgersson, Heidi Pettersson, Jean Raymond Bidlot, Peter A. E. M. Janssen, and Jeff A. Polton. 2012. "A Global Perspective on Langmuir Turbulence in the Ocean Surface Boundary Layer." *Geophysical Research Letters* 39(17):1–9.

Bello, Paolo, Agnese Pini, Simone Zazzini, Paolo Monti, and Giovanni Leuzzi. 2022. "Discrete Multivariate Probability Distributions of Microplastic Settling/Rising Velocity in the Marine Environment." Pp. 358–62 in *2022 IEEE International Workshop on Metrology for the Sea*.

Di Bernardino, Annalisa, Paolo Monti, Giovanni Leuzzi, and Giorgio Querzoli. 2020. "Eulerian and Lagrangian Time Scales of the Turbulence above Staggered Arrays of Cubical Obstacles." *Environmental Fluid Mechanics* 20(4):987–1005.

Blanke, Bruno and Stéphane Raynaud. 1997. "Kinematics of the Pacific Equatorial Undercurrent: An Eulerian and Lagrangian Approach from GCM Results." *Journal of Physical Oceanography* 27(6):1038–53.

Boccaletti, Giulio, Raffaele Ferrari, and Baylor Fox-Kemper. 2007. "Mixed Layer Instabilities and Restratification." *Journal of Physical Oceanography* 37(9):2228–50.

Boucher, Julien and Guillaume Billard. 2020. *The Mediterranean: Mare Plasticum*. Gland, Switzerland.

Boucher, Julien, Guillaume Billard, Eleonora Simeone, and Joao Sousa. 2020. *The Marine Plastic Footprint*. Gland, Switzerland.

Boucher, Julien and Damien Friot. 2017. *Primary Microplastics in the Oceans: A Global Evaluation of Sources*. edited by I. João Matos de Sousa, Marine Project Officer. IUCN, Gland, Switzerland ©.

Boufadel, Michel C., Ruixue Liu, Lin Zhao, Youyu Lu, Tamay M. Özgökmen, Timothy Nedwed, and Kenneth Lee. 2020. "Transport of Oil Droplets in the Upper Ocean: Impact of the Eddy Diffusivity." *Journal of Geophysical Research: Oceans* 125(2):1–16.

de Boyer Montégut, Clément, Gurvan Madec, Albert S. Fischer, Alban Lazar, and Daniele Iudicone. 2004. "Mixed Layer Depth over the Global Ocean: An Examination of Profile Data and a Profile-Based Climatology." *Journal of Geophysical Research: Oceans* 109(12):1–20.

Brunner, K., Tobias Kukulka, Giora Proskurowski, and Kara Lavender Law. 2015. "Passive Buoyant Tracers in the Ocean Surface Boundary Layer: 2. Observations and Simulations of Microplastic Marine Debris." *Journal of Geophysical Research: Oceans* 120:7759–7573.

Burchard, Hans, Peter D. Craig, Johannes R. Gemmrich, Hans van Haren, Pierre Philippe Mathieu, H. E. Marku. Meier, W. Alex M. Nimmo Smith, Hartmut Prandke, Tom P. Rippeth, Eric D. Skyllingstad, William D. Smyth, David J. S. Welsh, and Hemantha W. Wijesekera. 2008. "Observational and Numerical Modeling Methods for Quantifying Coastal Ocean Turbulence and Mixing." *Progress in Oceanography* 76(4):399–442.

Caldwell, Jessica, Alke Petri-Fink, Barbara Rothen-Rutishauser, and Roman Lehner. 2019. "Assessing Meso- and Microplastic Pollution in the Ligurian and Tyrrhenian Seas." *Marine Pollution Bulletin* 149(October):110572.

Carlson, Daniel F., Giuseppe Suaria, Stefano Aliani, Erick Fredj, Tomaso Fortibuoni, Annalisa Griffa, Aniello Russo, and Valentina Melli. 2017. "Combining Litter Observations with a Regional Ocean Model to Identify Sources and Sinks of Floating Debris in a Semi-Enclosed Basin: The Adriatic Sea." *Frontiers in Marine Science* 4(APR):1–17.

Carr, Mary Elena. 2001. "Estimation of Potential Productivity in Eastern Boundary Currents Using Remote Sensing." *Deep-Sea Research Part II: Topical Studies in Oceanography* 49(1–3):59–80.

Chrysagi, Evridiki, Lars Umlauf, Peter Holtermann, Knut Klingbeil, and Hans Burchard. 2021. "High-Resolution Simulations of Submesoscale Processes in the Baltic Sea: The Role of Storm Events." *Journal of Geophysical Research: Oceans* 126(3).

Clementi, Emanuela, A. Aydogdu, A. C. Goglio, Jenny Pistoia, Romain Escudier, Massimiliano Drudi, Alessandro Grandi, A. Mariani, V. Lyubartsev, Rita Lecci, S. Cretí, Giovanni Coppini, S. Masina, and Nadia Pinardi. 2021. "Mediterranean Sea Analysis and Forecast (CMEMS MED-Currents, EAS6 System) (Version 1) [Data Set]. Copernicus Monitoring Environment Marine Service (CMEMS)."

Collignon, Amandine, Jean Henri Hecq, François Galgani, France Collard, and Anne Goffart. 2014. "Annual Variation in Neustonic Micro- and Meso-Plastic Particles and Zooplankton in the Bay of Calvi (Mediterranean-Corsica)." *Marine Pollution Bulletin* 79(1–2):293–98.

Collignon, Amandine, Jean Henri Hecq, François Glagani, Pierre Voisin, France Collard, and Anne Goffart. 2012. "Neustonic Microplastic and Zooplankton in the North Western Mediterranean Sea." *Marine Pollution Bulletin* 64(4):861–64.

Coppini, Giovanni, Svitlana Liubartseva, Rita Lecci, Sergio Cretì, Giorgia Verri, Emanuela Clementi, and Nadia Pinardi. 2018. "Toward 3D Modeling the Plastic Marine Debris in the Mediterranean." Pp. 159–65 in *Proceedings of the International Conference on Microplastic Pollution in the Mediterranean Sea*.

Cózar, Andrés, Fidel Echevarría, J. Ignacio González-Gordillo, Xabier Irigoien, Bárbara Úbeda, Santiago Hernández-León, Álvaro T. Palma, Sandra Navarro, Juan García-de-Lomas, Andrea Ruiz, María L. Fernández-de-Puelles, and Carlos M. Duarte. 2014. "Plastic Debris in the Open Ocean." Pp. 10239–44 in *Proceedings of the National Academy of Sciences of the United States of America*. Vol. 111.

Cózar, Andrés, Marina Sanz-Martín, Elisa Martí, J. Ignacio González-Gordillo, Bárbara Ubeda, José A. Gálvez, Xabier Irigoien, and Carlos M. Duarte. 2015. "Plastic Accumulation in the Mediterranean Sea." *PLoS ONE* 10(4):1–12.

Craig, Peter D. and Michael L. Banner. 1994. "Modelling Wave-Enhanced Turbulence in the Ocean Surface Layer." *Journal of Physical Oceanography* 24:2546–59.

Craik, A. D. D. and S. Leibovich. 1976. "A Rational Model for Langmuir Circulations." *Journal of Fluid Mechanics* 73(3):401–26.

D'Asaro, Eric A. 2001. "Turbulent Vertical Kinetic Energy in the Ocean Mixed Layer." *Journal of Physical Oceanography* 31(12):3530–37.

D'Asaro, Eric A., David M. Farmer, James T. Osse, and Geoffrey T. Dairiki. 1996. "A Lagrangian Float." *Journal of Atmospheric and Oceanic Technology* 13(December):1230–46.

Dagestad, Knut Frode, Johannes Röhrs, Øyvind Breivik, and Bjørn Ådlandsvik. 2018. "OpenDrift v1.0: A Generic Framework for Trajectory Modelling." *Geoscientific Model Development* 11(4):1405–20.

Damerell, Gillian M., Karen J. Heywood, Daley Calvert, Alan L. M. Grant, Michael J. Bell, and Stephen E. Belcher. 2020. "A Comparison of Five Surface Mixed Layer Models with a Year of Observations in the North Atlantic." *Progress in Oceanography* 187(May):102316.

Delandmeter, Philippe and Erik van Sebille. 2019. "The Parcels v2.0 Lagrangian Framework: New Field Interpolation Schemes." *Geoscientific Model Development* 12(8):3571–84.

Di-Méglio, Nathalie and Ilaria Campana. 2017. "Floating Macro-Litter along the Mediterranean French Coast: Composition, Density, Distribution and Overlap with Cetacean Range." *Marine Pollution Bulletin* 118(1–2):155–66.

Dobricic, Srdjan and Nadia Pinardi. 2008. "An Oceanographic Three-Dimensional Variational Data Assimilation Scheme." *Ocean Modelling* 22(3–4):89–105.

Döös, Kristofer, Bror Jönsson, and Joakim Kjellsson. 2017. "Evaluation of Oceanic and Atmospheric Trajectory Schemes in the TRACMASS Trajectory Model v6.0." *Geoscientific Model Development* 10(4):1733–49.

Durgadoo, Jonathan V., Arne Biastoch, Adrian L. New, Siren Rühs, A. J. George Nurser, Yann Drillet, and Jean Raymond Bidlot. 2019. "Strategies for Simulating the Drift of Marine Debris." *Journal of Operational Oceanography* 0(0):1–12.

Egger, Matthias, Fatimah Sulu-Gambari, and Laurent C. M. Lebreton. 2020. "First Evidence of Plastic Fallout from the Great Pacific Garbage Patch." *Scientific Reports* 10:1–10.

Eriksen, Marcus, Laurent C. M. Lebreton, Henry S. Carson, Martin Thiel, Charles J. Moore, Jose C. Borrero, François Galgani, Peter G. Ryan, and Julia Reisser. 2014. "Plastic Pollution in the World's Oceans: More than 5 Trillion Plastic Pieces Weighing over 250,000 Tons Afloat at Sea." *PLoS ONE* 9(12):1–15.

Erni-Cassola, Gabriel, Vinko Zadjelovic, Matthew I. Gibson, and Joseph A. Christie-Oleza. 2019. "Distribution

of Plastic Polymer Types in the Marine Environment; A Meta-Analysis." *Journal of Hazardous Materials* 369(November 2018):691–98.
Escudier, Romain, Emanuela Clementi, M. Omar, A. Cipollone, Jenny Pistoia, A. Ydogdu, Massimiliano Drudi, Alessandro Grandi, V. Lyubartsev, Rita Lecci, S. Cretí, S. Masina, Giovanni Coppini, and Nadia Pinardi. 2020. "Mediterranean Sea Physical Reanalysis (CMEMS MED-Currents) (Version 1) [Data Set]. Copernicus Monitoring Environment Marine Service (CMEMS)."
Fagiano, V., Carme Alomar, Montserrat Compa, Javier Soto-Navarro, Gabriel Jordá, and Salud Deudero. 2022. "Neustonic Microplastics and Zooplankton in Coastal Waters of Cabrera Marine Protected Area (Western Mediterranean Sea)." *Science of the Total Environment* 804:150120.
Faure, Florian, Camille Saini, Gaël Potter, François Galgani, Luiz Felippe de Alencastro, and Pascal Hagmann. 2015. "An Evaluation of Surface Micro- and Mesoplastic Pollution in Pelagic Ecosystems of the Western Mediterranean Sea." *Environmental Science and Pollution Research* 22(16):190–97.
Fossi, Maria Cristina, Cristina Panti, Cristiana Guerranti, Daniele Coppola, Matteo Giannetti, Letizia Marsili, and Roberta Minutoli. 2012. "Are Baleen Whales Exposed to the Threat of Microplastics? A Case Study of the Mediterranean Fin Whale (Balaenoptera Physalus)." *Marine Pollution Bulletin* 64(11):2374–79.
Fossi, Maria Cristina, Teresa Romeo, Matteo Baini, Cristina Panti, Letizia Marsili, Tommaso Campani, Simonepietro Canese, François Galgani, Jean Noël Druon, Sabina Airoldi, Stefano Taddei, Maria Fattorini, Carlo Brandini, and Chiara Lapucci. 2017. "Plastic Debris Occurrence, Convergence Areas and Fin Whales Feeding Ground in the Mediterranean Marine Protected Area Pelagos Sanctuary: A Modeling Approach." *Frontiers in Marine Science* 4:1–15.
Gajšt, Tamara, Tine Bizjak, Andreja Palatinus, Svitlana Liubartseva, and Andrej Kržan. 2016. "Sea Surface Microplastics in Slovenian Part of the Northern Adriatic." *Marine Pollution Bulletin* 113(1–2):392–99.
Galperin, B., L. H. Kantha, S. Hassid, and A. Rosati. 1988. "A Quasi-Equilibrium Turbulent Energy Model for Geophysical Flows." *Journal of the Atmospheric Siences* 45(1):55–62.
Gargett, A. E. and C. E. Grosch. 2014. "Turbulence Process Domination under the Combined Forcings of Wind Stress, the Langmuir Vortex Force, and Surface Cooling." *Journal of Physical Oceanography* 44(1):44–67.
Gaspar, Philippe. 1988. "Modeling the Seasonal Cycle of the Upper Ocean." *Journal of Physical Oceanography* 18:161–80.
Gaspar, Philippe, Yves Grégoris, and Jean-Michel Lefevre. 1990. "A Simple Eddy Kinetic Energy Model for Simulations of the Oceanic Vertical Mixing: Tests at Station Papa and Long-Term Upper Ocean Study Site." *Journal of Geophysical Research* 95(C9):16,179-16,193.
van Gennip, Simon Jan, Boris Dewitte, Véronique Garçon, Martin Thiel, Ekaterina Popova, Yann Drillet, Marcel Ramos, Beatriz Yannicelli, Luis Bravo, Nicolas Ory, Guillermo Luna-Jorquera, and Carlos F. Gaymer. 2019. "In Search for the Sources of Plastic Marine Litter That Contaminates the Easter Island Ecoregion." *Scientific Reports* 9(1):1–13.
Gent, Peter R. and James C. McWilliams. 1990. "Isopycnal Mixing in Ocean Circulation Models." *Journal of Physical Oceanography* 20:150–55.
Griffa, Annalisa. 1996. "Applications of Stochastic Particle Models to Oceanographic Problems." *Stochastic Modelling in Physical Oceanography* 113–40.
Guerrini, Federica, Lorenzo Mari, and Renato Casagrandi. 2019. "Modeling Plastics Exposure for the Marine Biota: Risk Maps for Fin Whales in the Pelagos Sanctuary (North-Western Mediterranean)." *Frontiers in Marine Science* 6(JUN):1–10.
Guerrini, Federica, Lorenzo Mari, and Renato Casagrandi. 2021. "The Dynamics of Microplastics and Associated Contaminants: Data-Driven Lagrangian and Eulerian Modelling Approaches in the Mediterranean Sea." *Science of the Total Environment* 777:145944.
Gula, J., J. Taylor, A. Shcherbina, and A. Mahadevan. 2022. *Submesoscale Processes and Mixing*. edited by M. Meredith and A. N. Garabato. Elsevier.
Gündoğdu, Sedat. 2017. "High Level of Micro-Plastic Pollution in the Iskenderun Bay NE Levantine Coast of Turkey." *Ege Journal of Fisheries and Aquatic Sciences* 34(4):401–8.
Gündoğdu, Sedat and Cem Çevik. 2017. "Micro- and Mesoplastics in Northeast Levantine Coast of Turkey: The Preliminary Results from Surface Samples." *Marine Pollution Bulletin* 118(1–2):341–47.
Güven, Olgaç, Kerem Gökdağ, Boris Jovanović, and Ahmet Erkan Kıdeyş. 2017. "Microplastic Litter Composition of the Turkish Territorial Waters of the Mediterranean Sea, and Its Occurrence in the Gastrointestinal Tract of Fish." *Environmental Pollution* 223:286–94.
de Haan, William P., Anna Sanchez-Vidal, and Miquel Canals. 2019. "Floating Microplastics and Aggregate Formation in the Western Mediterranean Sea." *Marine Pollution Bulletin* 140(December 2018):523–35.
van der Hal, Noam, Asaf Ariel, and Dror L. Angel. 2017. "Exceptionally High Abundances of Microplastics in the Oligotrophic Israeli Mediterranean Coastal Waters." *Marine Pollution Bulletin* 116(1–2):151–55.
Hay, J. S. and F. Pasquill. 1959. "Diffusion from a Continuous Source in Relation to the Spectrum and Scale of Turbulence." *Advances in Geophysics* 6(C):345–65.

Hersbach, Hans, Bill Bell, Paul Berrisford, Shoji Hirahara, András Horányi, Joaquín Muñoz-Sabater, Julien Nicolas, Carole Peubey, Raluca Radu, Dinand Schepers, Adrian Simmons, Cornel Soci, Saleh Abdalla, Xavier Abellan, Gianpaolo Balsamo, Peter Bechtold, Gionata Biavati, Jean Bidlot, Massimo Bonavita, Giovanna De Chiara, Per Dahlgren, Dick Dee, Michail Diamantakis, Rossana Dragani, Johannes Flemming, Richard Forbes, Manuel Fuentes, Alan Geer, Leo Haimberger, Sean Healy, Robin J. Hogan, Elías Hólm, Marta Janisková, Sarah Keeley, Patrick Laloyaux, Philippe Lopez, Cristina Lupu, Gabor Radnoti, Patricia de Rosnay, Iryna Rozum, Freja Vamborg, Sebastien Villaume, and Jean Noël Thépaut. 2020. "The ERA5 Global Reanalysis." *Quarterly Journal of the Royal Meteorological Society* 146(730):1999–2049.

Iacono, Roberto, Ernesto Napolitano, Massimiliano Palma, and Gianmaria Sannino. 2021. "The Tyrrhenian Sea Circulation: A Review of Recent Work." *Sustainability* 13(11):6371.

IOC and IAPSO. 2010. "The International Thermodynamic Equation of Seawater – 2010: Calculation and Use of Thermodynamic Properties." *Manuals and Guides. UNESCO* (June):196.

Jambeck, Jenna, Roland Geyer, Chris Wilcox, Theodore R. Siegler, Miriam Perryman, Anthony L. Andrady, Ramani Narayan, and Kara Lavender Law. 2015. "Plastic Waste Inputs from Land into the Ocean." *Science* 347(6223).

Jarosz, E., David Wang, Hemantha W. Wijesekera, W. S. Pegau, and James N. Moum. 2017. "Flow Variability within the Alaska Coastal Current in Winter." *Journal of Geophysical Research: Oceans* 122:3884–3906.

Jemaa, Sharif, Celine Mahfouz, Maria Kazour, Myriam Lteif, Abed El Rahman Hassoun, Myriam Ghsoub, Rachid Amara, Gaby Khalaf, and Milad Fakhri. 2021. "Floating Marine Litter in Eastern Mediterranean From Macro to Microplastics: The Lebanese Coastal Area as a Case Study." *Frontiers in Environmental Science* 9(July):1–15.

Jones, W. P. and B. E. Launder. 1972. "The Prediction of Laminarization with a Two-Equation Model of Turbulence." *International Journal of Heat and Mass Transfer* 15(2):301–14.

Kaandorp, Mikael L. A., Henk A. Dijkstra, and Erik van Sebille. 2020. "Closing the Mediterranean Marine Floating Plastic Mass Budget: Inverse Modeling of Sources and Sinks." *Environmental Science and Technology* 54(19):11980–89.

Kaandorp, Mikael L. A., Henk A. Dijkstra, and Erik van Sebille. 2021. "Modelling Size Distributions of Marine Plastics under the Influence of Continuous Cascading Fragmentation." *Environmental Research Letters* 16(5).

Kara, A. Birol, Peter A. Rochford, and Harley E. Hurlburt. 2000. "An Optimal Definition for Ocean Mixed Layer Depth." *Journal of Geophysical Research* 105:16803–21.

Klemas, Victor. 2012. "Remote Sensing of Ocean Internal Waves: An Overview." *Journal of Coastal Research* 28(3):540–46.

Kooi, Merel and Albert A. Koelmans. 2019. "Simplifying Microplastic via Continuous Probability Distributions for Size, Shape,and Density." *Environmental Science and Technology Letters* 6(9):551–57.

Koszalka, Inga Monika and Lothar Stramma. 2019. *Current Systems in the Atlantic Ocean.* 3rd ed. Elsevier Ltd.

Kraus, E. B. and J. S. Turner. 1967. "A One-Dimensional Model of the Seasonal Thermocline II. The General Theory and Its Consequences." *Tellus* 19(1):98–106.

Kukulka, Tobias and K. Brunner. 2015. "Passive Buoyant Tracers in the Ocean Surface Boundary Layer: 1. Influence of Equilibrium Wind-Waves on Vertical Distributions." *Journal of Geophysical Research: Oceans* 120:3837–58.

Kukulka, Tobias, Giora Proskurowski, Skye Morét-Ferguson, D. W. Meyer, and Kara Lavender Law. 2012. "The Effect of Wind Mixing on the Vertical Distribution of Buoyant Plastic Debris." *Geophysical Research Letters* 39(7):1–6.

Kundu, P. K. and I. M. Cohen. 2008. *Fluids Mechanics*. Vol. 1. Academic Press.

De La Fuente, Rebeca, Gábor Drótos, Emilio Hernández-García, Cristóbal López, and Erik Van Sebille. 2021. "Sinking Microplastics in the Water Column: Simulations in the Mediterranean Sea." *Ocean Science* 17(2):431–53.

Lange, Michael and Erik van Sebille. 2017. "Parcels v0.9: Prototyping a Lagrangian Ocean Analysis Framework for the Petascale Age." *Geoscientific Model Development* 10(11):4175–86.

Large, William G., James C. McWilliams, and S. C. Doney. 1994. "Oceanic Vertical Mixing: A Review and a Model with a Nonlocal Boundary Layer Parameterization." *Reviews of Geophysics* 32(4):363–403.

Lebreton, Laurent C. M., S. D. Greer, and Jose C. Borrero. 2012. "Numerical Modelling of Floating Debris in the World's Oceans." *Marine Pollution Bulletin* 64(3):653–61.

van Leer, B. 1979. "Towards the Ultimate Conservative Difference Scheme. V. A Second-Order Sequel to Godunov's Method." *Journal of Computational Physics* 32(1):101–36.

Li, Daoji, Kai Liu, Changjun Li, Guyu Peng, Anthony L. Andrady, Tianning Wu, Zhiwei Zhang, Xiaohui Wang, Zhangyu Song, Changxing Zong, Feng Zhang, Nian Wei, Mengyu Bai, Lixin Zhu, Jiayi Xu, Hui Wu, Lu Wang, Siyuan Chang, and Wenxi Zhu. 2020. "Profiling the Vertical Transport of Microplastics in the West Pacific Ocean and the East Indian Ocean with a Novel in Situ Filtration Technique." *Environmental Science*

and Technology 54(20):12979–88.
Li, Ming, Chris Garrett, and Eric D. Skyllingstad. 2005. "A Regime Diagram for Classifying Turbulent Large Eddies in the Upper Ocean." *Deep-Sea Research Part I: Oceanographic Research Papers* 52(2):259–78.
Li, Qing, Brandon G. Reichl, Baylor Fox-Kemper, Alistair J. Adcroft, Stephen E. Belcher, Gokhan Danabasoglu, Alan L. M. Grant, Stephen M. Griffies, Robert W. Hallberg, Tetsu Hara, Ramsey R. Harcourt, Tobias Kukulka, William G. Large, James C. McWilliams, Brodie Pearson, Peter P. Sullivan, Luke P. Van Roekel, Peng Wang, and Zhihua Zheng. 2019. "Comparing Ocean Surface Boundary Vertical Mixing Schemes Including Langmuir Turbulence." *Journal of Advances in Modeling Earth Systems* 11(11):3545–92.
Li, S. W., Z. Z. Hu, P. W. Chan, and Gang Hu. 2017. "A Study on the Profile of the Turbulence Length Scale in the Near-Neutral Atmospheric Boundary for Sea (Homogeneous) and Hilly Land (Inhomogeneous) Fetches." *Journal of Wind Engineering and Industrial Aerodynamics* 168:200–210.
Liu, Yonggang, Robert H. Weisberg, Chuanmin Hu, and Lianyuan Zheng. 2011. "Tracking the Deepwater Horizon Oil Spill: A Modeling Perspective." *Eos* 92(6):45–46.
Liubartseva, Svitlana, Giovanni Coppini, Rita Lecci, and Emanuela Clementi. 2018. "Tracking Plastics in the Mediterranean: 2D Lagrangian Model." *Marine Pollution Bulletin* 129(1):151–62.
Lobelle, Delphine, Merel Kooi, Albert A. Koelmans, Charlotte Laufkötter, Cleo E. Jongedijk, Christian Kehl, and Erik van Sebille. 2021. "Global Modeled Sinking Characteristics of Biofouled Microplastic." *Journal of Geophysical Research: Oceans* 126(4):1–15.
de Lucia, Giuseppe Andrea, Ilaria Caliani, Stefano Marra, Andrea Camedda, Stefania Coppa, Luigi Alcaro, Tommaso Campani, Matteo Giannetti, Daniele Coppola, Anna Maria Cicero, Cristina Panti, Matteo Baini, Cristiana Guerranti, Letizia Marsili, Giorgio Massaro, Maria Cristina Fossi, and Marco Matiddi. 2014. "Amount and Distribution of Neustonic Micro-Plastic off the Western Sardinian Coast (Central-Western Mediterranean Sea)." *Marine Environmental Research* 100:10–16.
de Lucia, Giuseppe Andrea, Alvise Vianello, Andrea Camedda, Danilo Vani, Paolo Tomassetti, Stefania Coppa, Luca Palazzo, Marina Amici, Giulia Romanelli, Giorgio Zampetti, Anna Maria Cicero, Serena Carpentieri, Stefania Di Vito, and Marco Matiddi. 2018. "Sea Water Contamination in the Vicinity of the Italian Minor Islands Caused by Microplastic Pollution." *Water (Switzerland)* 10(8):1–13.
Lumpkin, Rick and Gregory C. Johnson. 2013. "Global Ocean Surface Velocities from Drifters: Mean, Variance, El Niño-Southern Oscillation Response, and Seasonal Cycle." *Journal of Geophysical Research: Oceans* 118(6):2992–3006.
Lutjeharms, J. R. E. 2007. "Three Decades of Research on the Greater Agulhas Current." *Ocean Science* 3(1):129–47.
Macias, D., Andrés Cózar, E. Garcia-Gorriz, D. González-Fernández, and A. Stips. 2019. "Surface Water Circulation Develops Seasonally Changing Patterns of Floating Litter Accumulation in the Mediterranean Sea. A Modelling Approach." *Marine Pollution Bulletin* 149(July):110619.
Madec, Gurvan, Romain Bourdallé-Badie, Mike Bell, Jérôme Chanut, Emanuela Clementi, Andrew Coward, Massimiliano Drudi, Christian Ethé, Doroteaciro Iovino, Dan Lea, Claire Lévy, Nicolas Martin, Sébastien Masson, Pierre Mathiot, Silvia Mocavero, Simon Müeller, A. J. George Nurser, Guillaume Samson, and Dave Storkey. 2019. "NEMO Ocean Engine." *Notes Du Pôle de Modélisation de l'Institut Pierre-Simon Laplace (IPSL)* (27).
Maes, Christophe and Bruno Blanke. 2015. "Tracking the Origins of Plastic Debris across the Coral Sea: A Case Study from the Ouvéa Island, New Caledonia." *Marine Pollution Bulletin* 97(1–2):160–68.
Mansui, J., G. Darmon, T. Ballerini, O. van Canneyt, Y. Ourmières, and C. Miaud. 2020. "Predicting Marine Litter Accumulation Patterns in the Mediterranean Basin: Spatio-Temporal Variability and Comparison with Empirical Data." *Progress in Oceanography* 182(October 2019):102268.
Mansui, J., A. Molcard, and Y. Ourmières. 2015. "Modelling the Transport and Accumulation of Floating Marine Debris in the Mediterranean Basin." *Marine Pollution Bulletin* 91(1):249–57.
McWilliams, James C. and Peter P. Sullivan. 2000. "Vertical Mixing by Langmuir Circulations." *Spill Science and Technology Bulletin* 6(3–4):225–37.
McWilliams, James C., Peter P. Sullivan, and Chin Hoh Moeng. 1997. "Langmuir Turbulence in the Ocean." *Journal of Fluid Mechanics* 334:1–30.
Mellor, George L. and Tetsuji Yamada. 1982. "Development of a Turbulence Closure Model for Geophysical Fluid Problems." *Reviews of Geophysics and Space Physics* 20(4):851–75.
Mendler de Suarez, Janot, Biliana Cicin-Sain, Kateryna Wowk, Rolph Payet, and Ove Hoegh-Guldberg. 2014. "Ensuring Survival: Oceans, Climate and Security." *Ocean and Coastal Management* 90:27–37.
Millero, Frank J. and Alain Poisson. 1981. "International One-Atmosphere Equation of State of Seawater." *Deep Sea Research Part A, Oceanographic Research Papers* 28(6):625–29.
Monti, Paolo and Giovanni Leuzzi. 2010. "Lagrangian Models of Dispersion in Marine Environment." *Environmental Fluid Mechanics* 10(6):637–56.
Moum, James N. and William D. Smyth. 2001. "Upper Ocean Mixing Processes." *Encyclopedia of Ocean*

Sciences bf 6:3093–3100.
Onink, Victor, Erik van Sebille, and Charlotte Laufkötter. 2022. "Empirical Lagrangian Parametrization for Wind-Driven Mixing of Buoyant Particles at the Ocean Surface." *Geoscientific Model Development* 15(5):1995–2012.
Onink, Victor, David Wichmann, Philippe Delandmeter, and Erik van Sebille. 2019. "The Role of Ekman Currents, Geostrophy, and Stokes Drift in the Accumulation of Floating Microplastic." *Journal of Geophysical Research: Oceans* 124(3):1474–90.
Osborn, T. R. 1980. "Estimates of the Local Rate of Vertical Diffusion from Dissipation Measurements." *Journal of Physical Oceanography* 10:83–89.
Pabortsava, Katsiaryna and Richard S. Lampitt. 2020. "High Concentrations of Plastic Hidden beneath the Surface of the Atlantic Ocean." *Nature Communications* 11(1):1–11.
Pacanowski, R. C. and S. G. H. Philander. 1981. "Parameterization of Vertical Mixing in Numerical Models of Tropical Oceans." *Journal of Physical Oceanography* 11:1443–51.
Palatinus, Andreja, Manca Kovač Viršek, Uroš Robič, Mateja Grego, Oliver Bajt, Jasna Šiljić, Giuseppe Suaria, Svitlana Liubartseva, Giovanni Coppini, and Monika Peterlin. 2019. "Marine Litter in the Croatian Part of the Middle Adriatic Sea: Simultaneous Assessment of Floating and Seabed Macro and Micro Litter Abundance and Composition." *Marine Pollution Bulletin* 139(December 2018):427–39.
Panti, Cristina, Matteo Giannetti, Matteo Baini, Fabrizio Rubegni, Roberta Minutoli, and Maria Cristina Fossi. 2015. "Occurrence, Relative Abundance and Spatial Distribution of Microplastics and Zooplankton NW of Sardinia in the Pelagos Sanctuary Protected Area, Mediterranean Sea." *Environmental Chemistry* 12(5):618–26.
Paris, Claire B., Judith Helgers, Erik van Sebille, and Ashwanth Srinivasan. 2013. "Connectivity Modeling System: A Probabilistic Modeling Tool for the Multi-Scale Tracking of Biotic and Abiotic Variability in the Ocean." *Environmental Modelling and Software* 42:47–54.
Pedrotti, Maria Luiza, Fabien Lombard, Alberto Baudena, François Galgani, Amanda Elineau, Stéphanie Petit, Maryvonne Henry, Romain Troublé, Gilles Reverdin, Enrico Ser-Giacomi, Mikaël Kedzierski, Emmanuel Boss, and Gabriel Gorsky. 2022. "An Integrative Assessment of the Plastic Debris Load in the Mediterranean Sea." *Science of the Total Environment* 838(May):155958.
Pedrotti, Maria Luiza, Stéphanie Petit, Amanda Elineau, Stéphane Bruzaud, Jean-Claude Crebassa, Bruno Dumontet, Elisa Martí, Gabriel Gorsky, and Andrés Cózar. 2016. "Changes in the Floating Plastic Pollution of the Mediterranean Sea in Relation to the Distance to Land." *PLoS ONE* 11(8):1–14.
Pini, Agnese, Giovanni Leuzzi, Paolo Monti, and Matteo Manfredi. 2018. "Modelling of Short-Term Dispersion in the Sea Surface Layer." *2018 IEEE International Workshop on Metrology for the Sea; Learning to Measure Sea Health Parameters, MetroSea 2018 - Proceedings* 50–54.
Pini, Agnese, Paolo Tomassetti, Marco Matiddi, Giuseppe Andrea de Lucia, Paolo Bello, Simone Zazzini, Giovanni Leuzzi, and Paolo Monti. 2020. "Microplastic Detection and Lagrangian Modelling in the Tyrrhenian Sea." Pp. 17–21 in *2019 IMEKO TC19 International Workshop on Metrology for the Sea: Learning to Measure Sea Health Parameters, MetroSea 2019*. Genova.
Pini, Agnese, Paolo Tomassetti, Marco Matiddi, Giuseppe Andrea de Lucia, Andrea Camedda, Giorgio Zampetti, Chiara Lattanzi, Giovanni Leuzzi, and Paolo Monti. 2019. "Microplastic Samplings and Inverse Trajectory Recognition in the Mediterranean Sea." Pp. 115–19 in *2018 IEEE International Workshop on Metrology for the Sea; Learning to Measure Sea Health Parameters, MetroSea 2018 - Proceedings*. IEEE.
Poje, Andrew C., Tamay M. Özgökmen, Bruce L. Lipphardt, Brian K. Haus, Edward H. Ryan, Angelique C. Haza, Gregg A. Jacobs, A. J. H. M. Reniers, María J. Olascoaga, Guillaume Novelli, Annalisa Griffa, Francisco J. Beron-Vera, Shuyi S. Chen, Emanuel Coelho, Patrick J. Hogan, Albert D. Kirwan, Helga S. Huntley, and Arthur J. Mariano. 2014. "Submesoscale Dispersion in the Vicinity of the Deepwater Horizon Spill." *Proceedings of the National Academy of Sciences of the United States of America* 111(35):12693–98.
Politikos, D. V., Kostas Tsiaras, G. Papatheodorou, and A. Anastasopoulou. 2020. "Modeling of Floating Marine Litter Originated from the Eastern Ionian Sea: Transport, Residence Time and Connectivity." *Marine Pollution Bulletin* 150(October 2019):110727.
Poulain, Marie, Matthieu J. Mercier, Laurent Brach, Marion Martignac, Corinne Routaboul, Emile Perez, Marie Christine Desjean, and Alexandra Ter Halle. 2019. "Small Microplastics As a Main Contributor to Plastic Mass Balance in the North Atlantic Subtropical Gyre." *Environmental Science and Technology* 53(3):1157–64.
Reichl, Brandon G. and Robert W. Hallberg. 2018. "A Simplified Energetics Based Planetary Boundary Layer (EPBL) Approach for Ocean Climate Simulations." *Ocean Modelling* 132(September):112–29.
Reijnders, Daan, Eric Deleersnijder, and Erik van Sebille. 2022. "Simulating Lagrangian Subgrid-Scale Dispersion on Neutral Surfaces in the Ocean." *Journal of Advances in Modeling Earth Systems* 14(2):1–25.
Rodi, Wolfgang. 1987. "Examples of Calculation Methods for Flow and Mixing in Stratified Fluids." *Journal of Geophysical Research: Oceans* 92(6):5305–28.

Röhrs, Johannes, Knut Frode Dagestad, Helene Asbjørnsen, Tor Nordam, Jørgen Skancke, Cathleen E. Jones, and Camilla Brekke. 2018. "The Effect of Vertical Mixing on the Horizontal Drift of Oil Spills." *Ocean Science* 14(6):1581–1601.

Ruiz-Orejón, Luis F., Rafael Sardá, and Juan Ramis-Pujol. 2018. "Now, You See Me: High Concentrations of Floating Plastic Debris in the Coastal Waters of the Balearic Islands (Spain)." *Marine Pollution Bulletin* 133(June):636–46.

Sayed, Alaa El Din H., Mohamed Hamed, Ahmed E. A. Badrey, Rania F. Ismail, Yassein A. A. Osman, Alaa G. M. Osman, and Hamdy A. M. Soliman. 2021. "Microplastic Distribution, Abundance, and Composition in the Sediments, Water, and Fishes of the Red and Mediterranean Seas, Egypt." *Marine Pollution Bulletin* 173(PA):112966.

Schmidt, Natascha, Delphine Thibault, François Galgani, Andrea Paluselli, and Richard Sempéré. 2018. "Occurrence of Microplastics in Surface Waters of the Gulf of Lion (NW Mediterranean Sea)." *Progress in Oceanography* 163(November 2017):214–20.

Schmitz, William J. and Michael S. McCartney. 1993. "On the North Atlantic Circulation." *Reviews of Geophysics* 31(1):29–49.

Schumann, U. and T. Gerz. 1995. "Turbulent Mixing in Stably Stratified Shear Flows." *Journal of Applied Meteorology* 34(1):33–48.

Scully, Malcolm E., Alexander W. Fisher, Steven E. Suttles, Lawrence P. Sanford, and William C. Boicourt. 2015. "Characterization and Modulation of Langmuir Circulation in Chesapeake Bay." *Journal of Physical Oceanography* 45(10):2621–39.

van Sebille, Erik, Stefano Aliani, Kara Lavender Law, Nikolai A. Maximenko, José M. Alsina, Andrei Bagaev, Melanie Bergmann, Bertrand Chapron, Irina Chubarenko, Andrés Cózar, Philippe Delandmeter, Matthias Egger, Baylor Fox-Kemper, Shungudzemwoyo P. Garaba, Lonneke Goddijn-Murphy, Britta Denise Hardesty, Matthew J. Hoffman, Atsuhiko Isobe, Cleo E. Jongedijk, Mikael L. A. Kaandorp, Liliya Khatmullina, Albert A. Koelmans, Tobias Kukulka, Charlotte Laufkötter, Laurent C. M. Lebreton, Delphine Lobelle, Christophe Maes, Victor Martinez-Vicente, Miguel Angel Morales Maqueda, Marie Poulain-Zarcos, Ernesto Rodríguez, Peter G. Ryan, Alan L. Shanks, Won Joon Shim, Giuseppe Suaria, Martin Thiel, Ton S. Van Den Bremer, and David Wichmann. 2020. "The Physical Oceanography of the Transport of Floating Marine Debris." *Environmental Research Letters* 15(2):23003.

van Sebille, Erik, Stephen M. Griffies, Ryan Abernathey, Thomas P. Adams, Pavel Berloff, Arne Biastoch, Bruno Blanke, Eric P. Chassignet, Yu Cheng, Colin J. Cotter, Eric Deleersnijder, Kristofer Döös, Henri F. Drake, Sybren Drijfhout, Stefan F. Gary, Arnold W. Heemink, Joakim Kjellsson, Inga Monika Koszalka, Michael Lange, Camille Lique, Graeme A. MacGilchrist, Robert Marsh, C. Gabriela Mayorga Adame, Ronan McAdam, Francesco Nencioli, Claire B. Paris, Matthew D. Piggott, Jeff A. Polton, Siren Rühs, Syed Hyder Ali Muttaqi Shah, Matthew D. Thomas, Jinbo Wang, Phillip J. Wolfram, Laure Zanna, and Jan D. Zika. 2018. "Lagrangian Ocean Analysis: Fundamentals and Practices." *Ocean Modelling* 121(October 2017):49–75.

Shchekinova, E. Y. and Y. Kumkar. 2018. "Modeling of Small Sea Floaters in the Central Mediterranean Sea: Seasonality of At--Sea Distributions." *Oceanography & Fisheries Open Access Journal* 7(4):5–8.

Sloyan, Bernadette M. 2005. "Spatial Variability of Mixing in the Southern Ocean." *Geophysical Research Letters* 32(18):1–5.

Smyth, William D., Eric D. Skyllingstad, Gregory B. Crawford, and Hemantha W. Wijesekera. 2002. "Nonlocal Fluxes and Stokes Drift Effects in the K-Profile Parameterization." *Ocean Dynamics* 52(3):104–15.

Song, Young Kyoung, Sang Hee Hong, Soeun Eo, Mi Jang, Gi Myung Han, Atsuhiko Isobe, and Won Joon Shim. 2018. "Horizontal and Vertical Distribution of Microplastics in Korean Coastal Waters." *Environmental Science and Technology* 52(21):12188–97.

Soto-Navarro, Javier, Gabriel Jordá, Salud Deudero, Carme Alomar, Ángel Amores, and Montserrat Compa. 2020. "3D Hotspots of Marine Litter in the Mediterranean: A Modeling Study." *Marine Pollution Bulletin* 155(February):111159.

Stacey, Mark T., Stephen G. Monismith, and Jon R. Burau. 1999. "Measurements of Reynolds Stress Profiles in Unstratified Tidal Flow." *Journal of Geophysical Research: Oceans* 104(C5):10933–49.

Storto, Andrea, Simona Masina, and Antonio Navarra. 2016. "Evaluation of the CMCC Eddy-Permitting Global Ocean Physical Reanalysis System (C-GLORS, 1982-2012) and Its Assimilation Components." *Quarterly Journal of the Royal Meteorological Society* 142(695):738–58.

Suaria, Giuseppe and Stefano Aliani. 2014. "Floating Debris in the Mediterranean Sea." *Marine Pollution Bulletin* 86(1–2):494–504.

Suaria, Giuseppe, Carlo G. Avio, Annabella Mineo, Gwendolyn L. Lattin, Marcello G. Magaldi, Genuario Belmonte, Charles J. Moore, Francesco Regoli, and Stefano Aliani. 2016. "The Mediterranean Plastic Soup: Synthetic Polymers in Mediterranean Surface Waters." *Scientific Reports* 6:1–10.

Sullivan, Peter P. and James C. McWilliams. 2010. "Dynamics of Winds and Currents Coupled to Surface

Waves." *Annual Review of Fluid Mechanics* 42(1):19–42.
Taylor, G. I. 1915. "Eddy Motion in the Atmosphere." *Society* 215:1–26.
Taylor, G. I. 1921. "Diffusion by Continuous Movements." *Proceedings of the London Mathematical Society* 20:196–211.
Todd, Robert E., Francisco P. Chavez, Sophie Clayton, Sophie E. CRAVATTE, Marlos P. Goes, Michelle I. Graco, Xiaopei Lin, Janet Sprintall, Nathalie V. Zilberman, Matthew Archer, Javier Arístegui, Magdalena A. Balmaseda, John M. Bane, Molly O. Baringer, John A. Barth, Lisa M. Beal, Peter Brandt, Paulo H. Calil, Edmo Campos, Luca R. Centurioni, Maria Paz Chidichimo, Mauro Cirano, Meghan F. Cronin, Enrique N. Curchitser, Russ E. Davis, Marcus Dengler, Brad DeYoung, Shenfu Dong, Ruben Escribano, Andrea J. Fassbender, Sarah E. Fawcett, Ming Feng, Gustavo J. Goni, Alison R. Gray, Dimitri Gutiérrez, Dave Hebert, Rebecca Hummels, Shin Ichi Ito, Marjolaine Krug, François Lacan, Lucas Laurindo, Alban Lazar, Craig M. Lee, Matthieu Lengaigne, Naomi Levine, John Middleton, Ivonne Montes, Mike Muglia, Takeyoshi Nagai, Hilary I. Palevsky, Jaime B. Palter, Helen E. Phillips, Alberto R. Piola, Albert J. Plueddemann, Bo Qiu, Regina R. Rodrigues, Thomas Rossby, Moninya Roughan, Daniel L. Rudnick, Ryan R. Rykaczewski, Martin Saraceno, Harvey Seim, Alex Sen Gupta, Lynne Shannon, Bernadette M. Sloyan, Adrienne J. Sutton, Lu Anne Thompson, Anja K. van der Plas, Denis Volkov, John Wilkin, Dongxiao Zhang, and Linlin Zhang. 2019. "Global Perspectives on Observing Ocean Boundary Current Systems." *Frontiers in Marine Science* 6:1–38.
Tolman, H. L. 2009. "User Manual and System Documentation of WAVEWATCH-IIITM Version 3.14." *Analysis* 166.
Tseng, Ruo Shan and Eric A. D'Asaro. 2004. "Measurements of Turbulent Vertical Kinetic Energy in the Ocean Mixed Layer from Lagrangian Floats." *Journal of Physical Oceanography* 34(9):1984–90.
Tsiaras, Kostas, Yannis Hatzonikolakis, Sofia Kalaroni, Annika Pollani, and George Triantafyllou. 2021. "Modeling the Pathways and Accumulation Patterns of Micro- and Macro-Plastics in the Mediterranean." *Frontiers in Marine Science* 8(October).
Uddin, Saif, Scott W. Fowler, Mohd Faiz Uddin, Montaha Behbehani, and Abolfazl Naji. 2021. "A Review of Microplastic Distribution in Sediment Profiles." *Marine Pollution Bulletin* 163(November 2020):111973.
Umlauf, Lars, Hans Burchard, and K. Hutter. 2003. "Extending the K-ω Turbulence Model towards Oceanic Applications." *Ocean Modelling* 5(3):195–218.
Vianello, Alvise, Luisa Da Ros, Alfredo Boldrin, Tihana Marceta, and Vanessa Moschino. 2018. "First Evaluation of Floating Microplastics in the Northwestern Adriatic Sea." *Environmental Science and Pollution Research* 25(28):28546–61.
Visser, André W. 1997. "Using Random Walk Models to Simulate the Vertical Distribution of Particles in a Turbulent Water Column." *Marine Ecology Progress Series* 158(1):275–81.
Wang, D. W., H. W. Wijesekera, E. Jarosz, W. J. Teague, and W. S. Pegau. 2016. "Turbulent Diffusivity under High Winds from Acoustic Measurements of Bubbles." *Journal of Physical Oceanography* 46(5):1593–1613.
Wijesekera, Hemantha W., D. W. Wang, E. Jarosz, W. J. Teague, W. S. Pegau, and James N. Moum. 2017. "Turbulent Large-Eddy Momentum Flux Divergence during High-Wind Events." *Journal of Physical Oceanography* 47(6):1493–1517.
Wilcox, David C. 1988. "Reassessment of the Scale-Determining Equation for Advanced Turbulence Models." *AIAA Journal* 26(11):1299–1310.
Wunsch, Carl. 2002. "What Is the Thermohaline Circulation?" *Science* 298(November):1179–80.
Yamazaki, Hidekatsu and Daniel Kamykowski. 1991. "The Vertical Trajectories of Motile Phytoplankton in a Wind-Mixed Water Column." *Deep Sea Research Part A, Oceanographic Research Papers* 38(2):219–41.
Yang, Zhaoqing, Taiping Wang, and Andrea E. Copping. 2013. "Modeling Tidal Stream Energy Extraction and Its Effects on Transport Processes in a Tidal Channel and Bay System Using a Three-Dimensional Coastal Ocean Model." *Renewable Energy* 50:605–13.
Zambianchi, Enrico, Marilisa Trani, and Pierpaolo Falco. 2017. "Lagrangian Transport of Marine Litter in the Mediterranean Sea." *Frontiers in Environmental Science* 5(FEB):1–16.
Zaron, Edward D. and James N. Moum. 2009. "A New Look at Richardson Number Mixing Schemes for Equatorial Ocean Modeling." *Journal of Physical Oceanography* 39(10):2652–64.
Zeri, Christina, Argyro Adamopoulou, D. Bojanić Varezić, Tomaso Fortibuoni, Manca Kovač Viršek, Andrej Kržan, M. Mandic, C. Mazziotti, Andreja Palatinus, M. Peterlin, M. Prvan, F. Ronchi, J. Siljic, P. Tutman, and Th Vlachogianni. 2018. "Floating Plastics in Adriatic Waters (Mediterranean Sea): From the Macro- to the Micro-Scale." *Marine Pollution Bulletin* 136(July):341–50.